SYNTHESIS AND FUNCTIONALIZATION OF GRAPHENE OXIDE NANOCOMPOSITES FOR ANTICANCER DRUG DELIVERY

A THESIS SUBMITTED TO
THE GRADUATE SCHOOL OF NATURAL AND APPLIED SCIENCES
OF
MIDDLE EAST TECHNICAL UNIVERSITY

BY

HEBA KAMAL MOHAMMED AHMED HASSAN

IN PARTIAL FULFILLMENT OF THE REQUIREMENTS
FOR
THE DEGREE OF MASTER OF SCIENCE
IN
BIOMEDICAL ENGINEERING

JUNE 2022

Approval of the thesis:

SYNTHESIS AND FUNCTIONALIZATION OF GRAPHENE OXIDE NANOCOMPOSITES FOR ANTICANCER DRUG DELIVERY

Submitted by **HEBA KAMAL MOHAMMED AHMED HASSAN** in partial fulfillment of the requirements for the degree of **Master of Science in Biomedical Engineering, Middle East Technical University** by,

Prof. Dr. Halil Kalıpçılar
Dean, Graduate School of **Natural and Applied Sciences** _____

Prof. Dr. Vilda Purutçuoğlu Gazi
Head of the Department, **Biomedical Engineering** _____

Prof. Dr. Zafer Evis
Supervisor, **Engineering Sciences, METU** _____

Prof. Dr. Ayşen Tezcaner
Co-Supervisor, **Engineering Sciences, METU** _____

Examining Committee Members:

Prof. Dr. Dilek Keskin
Engineering Sciences, METU _____

Prof. Dr. Zafer Evis
Engineering Sciences, METU _____

Prof. Dr. Ayşen Tezcaner
Engineering Sciences, METU _____

Prof. Dr. Fatih Akkurt
Chemical Engineering, Gazi University _____

Assoc. Prof. Sedat Sürdem
Environmental Sciences, Gazi University _____

Date: 27.06.2022

I hereby declare that all information in this document has been obtained and presented in accordance with academic rules and ethical conduct. I also declare that, as required by these rules and conduct, I have fully cited and referenced all material and results that are not original to this work.

Name Last name :

Heba Kamal Mohammed Ahmed Hassan

Signature :

ABSTRACT

SYNTHESIS AND FUNCTIONALIZATION OF GRAPHENE OXIDE NANOCOMPOSITES FOR ANTICANCER DRUG DELIVERY

Kamal Mohammed Ahmed Hassan, Heba
Master of Science, Biomedical Engineering
Supervisor: Prof. Dr. Zafer Evis
Co-Supervisor: Prof. Dr. Ayşen Tezcaner

June 2022, 105 pages

Graphene, graphene quantum dots (GQDs) their derivatives and gold nanoparticles (AuNPs), all have a wide range of applications in biomedical applications, particularly anticancer drug delivery, due to their large surface area, chemical and mechanical stability, and good biocompatibility. The first goal of this research is to improve the chemistry and solubility of rGO by doping it with boron and decorating it with AuNPs (Au-B-rGO), as well as to improve the loading efficiency of the anticancer drug doxorubicin (DOX). The second goal is to investigate the effect of boric acid (BA) on anticancer drug delivery when it is combined with graphene oxide quantum dots conjugated with glucosamine (GOQDs-GlcN-BA). FTIR, XPS, XRD, SEM, EDS, and zeta potential analysis were used for characterization of the nanocomposites. The hydrophobic nanocomposites were functionalized with chitosan oligosaccharide to lower the aggregation. However, high functionalization reduced the drug's loading percentage. Replacing chitosan with glucosamine GOQDs-GlcN-DOX, resulted in (57% drug loading) compared to the drug loaded after boric acid addition GOQDs-GlcN-BA-DOX (90%). Only 8% of DOX release occured from GOQDs-GlcN-DOX, in an acidic environment, after 96 h whereas BA addition in the nanocomposite increased DOX release of up to 20%. The morphology

and nanosize of the nanoassembly were confirmed by TEM. The nontoxicity of the synthesized bare nanocomposites determined by MTT assay, with cell viability more than 100% at high concentrations, while GOQD-GlcN-BA-DOX exhibited more cytotoxicity against MCF-7 cells compared to GOQD-GlcN-DOX. GOQD-GlcN-BA-DOX shows stronger fluorescence through fluorescence microscopy owing to higher MCF-7 cellular internalization via sialic acid and BA interaction. This thesis shows the addition of BA enhanced the loading and release of anticancer drug, nontoxicity of the system with higher cellular internalization thus superior potential for anticancer drug delivery.

Keywords: Graphene oxide, Gold nanoparticles, Boric acid, Anticancer drug delivery.

.

ÖZ

ANTİKANSER İLAÇ SAĞLANMASI İÇİN GRAFEN OKSİT NANOKOMPOZİTLERİN SENTEZİ VE İŞLEVSELLEŞTİRİLMESİ

Kamal Mohammed Ahmed Hassan, Heba
Yüksek Lisans, Biyomedikal Mühendisliği
Tez Yöneticisi: Prof. Dr. Zafer Evis
Ortak Tez Yöneticisi: Prof. Dr. Ayşen Tezcaner

Haziran 2022, 105 sayfa

Grafen, Grafen kuantum noktaları (GQD) ve bunların türevleri ile Altın nanoparçacıkları (AuNP), geniş yüzey alanları, kimyasal ve mekanik stabiliteleri ve iyi biyouyumlulukları nedeniyle biyomedikal uygulamalarda, özellikle antikanser ilaç iletiminde geniş bir uygulama alanına sahiptir. Bu araştırmanın ilk amacı, İndirgenmiş Grafen Oksitin Bor ile katkılanarak ve Altın nanoparçacıklar (Au-B-rGO) ile dekore edilmesi yoluyla İndirgenmiş Grafen Oksitin (rGO) kimyasını ve çözünürlüğünü iyileştirmenin yanı sıra antikanser ilacı doksorubisinin (DOX) yükleme verimliliğini artırmaktır. İkinci amaç ise, Borik asidin (BA) Glukozamin ile birleştirilmiş Grafen Oksit kuantum noktaları (GOQDs-GlcN) ile birleştirildiğinde antikanser ilaç iletimi üzerindeki etkisini araştırmaktır. Nanokompozitlerin Karakterizasyon işlemi için FTIR, XPS, XRD, SEM, EDS ve Zeta-Potansiyel'i analizleri kullanılmıştır. Ayrıca hidrofobik nanokompozitlerin, agregasyonu azaltmak için Kitosan Oligosakkarit ile işlevselleştirilmiştir. Ancak yüksek işlevsellik, ilacın yükleme yüzdesini azaltmıştır. Öte yandan, Kitosanın, glukozamin GOQDs-GlcN-DOX ile değiştirilmesi, (%57 ilaç yüklemesi) ile sonuçlanırkan, Borik Asit GOQDs-GlcN-BA-DOX ilavesinden sonra yüklenen ilacla karşılaştırıldığında bu yüzde (%90)'a yükseilmiştir. 96 saat sonra asidik bir ortamda GOQDs-GlcN-DOX'tan DOX salınımının sadece %8'i meydana gelirken,

nanokompozite BA ilavesi; DOX salınımını %20'ye kadar arttırmıştır. Nano düzeneğin morfolojisi ve nano boyutu TEM ile teyit edilmiştir. Sentezlenen yalın nanokompozitlerin yüksek konsantrasyonlarda %100'den fazla hücre canlılığı ile toksik olmaması durmunu MTT tahlili ile belirlenirken, GOQD-GlcN-BA-DOX ise; GOQD-GlcN-DOX'a kıyasla MCF-7 hücrelerine karşı daha fazla sitotoksisite sergilemiştir. GOQD-GlcN-BA-DOX, sialik asit ve BA etkileşimi aracılığıyla daha yüksek MCF-7 hücresel içselleştirmesi sayesinde floresan mikroskopisi yoluyla daha güçlü floresan göstermiştir. Bu tez, BA ilavesinin antikanser ilacının yüklenmesini ve salınımını arttırdığını, daha yüksek hücresel içselleştirme ile sistemin toksik olmamasını ve dolayısıyla antikanser ilaç iletimi için üstün bir potansiyel olduğunu göstermektedir.

Anahtar Kelimeler: Grafen oksit, Altın nanopartiküller, Borik asit, Antikanser ilaç iletimi.

To my Country, Family, Fiancé and Friends …

ACKNOWLEDGMENTS

My deepest gratitude to my supervisors, Prof. Dr. Zafer Evis and Prof. Dr. Ayşen Tezcaner, for their invaluable assistance and insights in writing this thesis. Also, their understanding and patience during my experiments that went into the creation of this work.

Furthermore, I would like to thank Mustafa Nakipoglu for his invaluable assistance in shaping my experiment methods and critiquing my results.

I appreciate my lab members Engin Pazarceviren and Hossein Jodati for their help in my daily lab work.

I would also like to thank BIOMATEN for giving technical support and the Turkish Scholarship Program for providing me with the opportunity to embark on this journey.

I am grateful to my family for their unwavering love and support, which keep me motivated and confident. My accomplishments and success are the result of their faith in me. My heartfelt gratitude goes to my fiancé, Agieb Elnazeir who has provided me with tremendous support and hope. This thesis would not have been possible without that hope.

TABLE OF CONTENTS

LIST OF TABLES

TABLES

LIST OF FIGURES

FIGURES

ABBREVIATIONS

AuNPs:	Gold nanoparticles
BBB:	Blood-brain barrier
CT:	Computed tomography
COS:	Chitosan oligosaccharide
DOX:	Doxorubicin
DEX:	Dexamethasone
DMSO:	Dimethyl sulfoxide
EDS:	Energy dispersive x-ray spectroscopy
EDC:	N-(3-dimethylaminopropyl)-N′-ethylcarbodiimide hydrochloride
FTIR:	Fourier transform infrared spectroscopy
FA:	Folic acid
GO:	Graphene oxide
GQDs:	Graphene quantum dots
GOQD:	Graphene oxide quantum dots
GOQD-GlcN:	Graphene oxide quantum dots-glucosamine
GOQD-GlcN-BA:	Graphene oxide quantum dots-glucosamine-boric acid
HEC:	Hydroxyethyl cellulose
HA:	Hyaluronic acid
ICP-MS:	Inductively coupled plasma-mass spectrometry

MES:	2-(N-Morpholino)ethanesulfonic acid
MTT:	3-(4,5-dimethylthiazol-2-yl)-2,5-diphenyltetrazolium bromide
NPs:	Nanoparticles
NHS:	N-hydroxysuccinimide
OH:	Hydroxyl
PEG:	Poly(ethylene glycol)
PDT:	Photodynamic therapy
PPT:	Photothermal therapy
PGA:	Poly-L-glutamic acid
PEI:	Polyethyleneimine
rGO:	Reduced graphene oxide
ROS:	Reactive oxygen species
RES:	Reticuloendothelial system
SEM:	Scanning electron microscopy
SPR:	Surface plasmon resonance
TEM:	Transmission electron microscopy
XPS:	X-ray photoelectron spectroscopy
XRD:	X-ray diffraction
UV:	Ultraviolet

CHAPTER 1

INTRODUCTION

1.1 Cancer

Cancer is a disease when cells begin to divide uncontrollably due to changes in the genes that control cell function. In normal lifecycle, cells grow and divide to form new cells and after they become old they die and new cells take their place. Whereas, cancerous cells after growing and becoming old they do not die hence extra cells will form tumor. There are two types of tumors, which are malignant and benign tumors. Malignant tumors are the tumors that break off to distant places through blood or lymph system. Benign tumors do not spread into nearby tissues and do not grow back ("Understanding Cancer," 2007).

There are several stages before the appearance of cancer, which are initiation, promotion, and progression as seen in Figure 1.1. Changes occur at cellular, genetic, and epigenetic levels and abnormal cell division during this long period. Thus, a benign or precancerous tumor transforms into a malignant tumor at the third stage where the triggering of cell transformation developed at the first two stages (Eskiizmir et al., 2018).

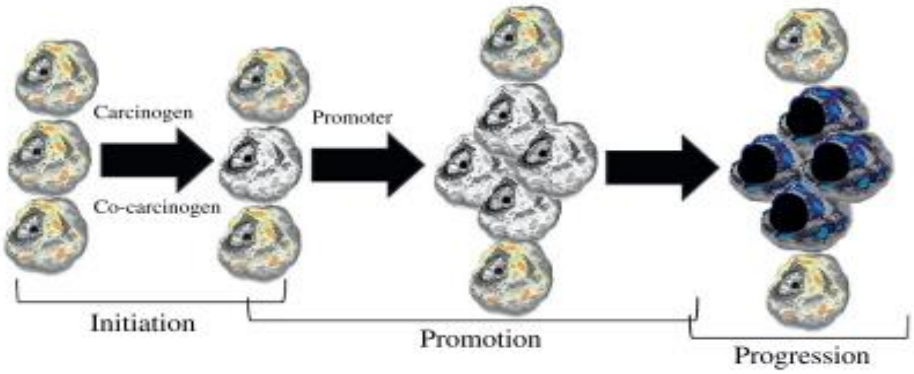

Figure 1.1 Stages of cancer progression (Eskiizmir et al., 2018).

The first aim of any cancer treatment is to kill or remove the cancerous cells without affecting the normal cells. Moreover, the clinical practices have three basic methods for cancer treatments: chemotherapy, surgery, radiotherapy, hormonal and targeted therapy that applied either in combination or alone (Damyanov et al., 2018; Eskiizmir et al., 2018; C. Y. Huang et al., 2017). However, the type of selected treatment depends on location and differentiation stage of tumor, histopathological type and patient's status (Eskiizmir et al., 2018).

In the surgeries, the removal of the cancerous tissue takes place. Successful surgical treatment increases in the early stages of the diseases whereas 60% of the cases are discovered in the advanced stages. High-quality operation depends on the skills of the surgeon. The reason behind future progress of the disease after surgery is micrometastases, which cannot be discovered by modern diagnostic methods. Other side effects the infections, suppression of the immune system, anesthesia complications, and distribution of cancer cells in the blood flow (Damyanov et al., 2018). In some cases, surgery is applied before or after chemo- or radiotherapy as a combination treatment. Moreover, the symptoms such as vessel compression that is related to cancer, are controlled by a surgery called "palliative surgical treatment" (Eskiizmir et al., 2018).

Another treatment method is radiotherapy, where an ionizing radiation is used. Radiotherapy proved its efficiency as a primary treatment method to treat cancer. It

treats from 30% to 40% of the patients who have a solid tumor. However, radiotherapy has the problem of damaging the surrounding healthy tissues (Damyanov et al., 2018). The genetic material is damaged, and oxygen species will be reactive by ionizing radiation, which will destroy the cancer cell. The radiation dose is determined according to tissue type, histopathologic type, and cell cycle. Because some of the organs are radiosensitive such as lymphoid organs and others are fairly radiosensitive such as bone. Besides, some cancer cells have a high rate of division and highly radiosensitive (Eskiizmir et al., 2018).

The third conventional treatment of cancer is chemotherapy, where chemicals or drugs are applied to inhibit rapid dividing cells. Depending on the mechanism of actions, there are several classes of anticancer drugs with different side effects (C. Y. Huang et al., 2017). Chemotherapeutic agents will affect rapidly dividing healthy cells and such treatment results with serious side effects because cancerous and healthy cells are sharing the same DNA in addition to the major metabolic pathways (Shewash, 2009). Fortunately, after chemotherapy, they can repair themselves such as intestinal mucosa and blood cells. In the treatment protocol of "combination chemotherapy", more than one chemotherapeutic agent is used to overcome multidrug resistance (Eskiizmir et al., 2018).

Photodynamic therapy (PDT), is the administration of photosensitizer (is a light-sensitive molecule (JG, 1994), in a form of non-toxic drug or dye), is another choice. After administration the lesion will be illuminated with laser or infrared, which results in cell death and tissue destruction with reactive oxygen species (ROS) formed. PDT is characterized by specificity and selectivity, hence as a cancer treatment method, many pieces of research are conducted for treatment of different forms of cancer (Robertson et al., 2009). PDT was tested against MCF-7 cancer cells using graphene quantum dots doped with nitrogen and (FA) and conjugated with zinc tetramorpholine porphyrin (complex 2) and its quaternized derivative (complex 3) and low cell viability of 28% was obtained (Magaela et al., 2022). In immunotherapy, the immortality of cancer facilitated by genetic and epigenetic changes will create neo-antigens "foreign antigens" which makes cancer cells

detected by the immune system and target them for destruction. However, multiple resistance mechanisms such as local immune evasion and systemic disruption of T cell signaling by neoplastic cells, hence will not recognize them and they will be destructed by the immune system (Farkona et al., 2016). Cancer immunotherapy is the design of therapeutic agents that will drive the immune system of the patient to kill the cancer cell (Eskiizmir et al., 2018).

The hormonal therapy is applied to patients with locally advanced or metastatic disease to reduce the size of primary cancer before applying surgery or radiotherapy. It is for oestrogen and progesterone receptor-positive breast cancer and prostate cancer (Abraham & Staffurth, 2016). It is an effective and non-toxic therapy applied to cancers triggered by a hormone. Therefore, supplying antihormones or blockage of these hormones can be very efficient (Eskiizmir et al., 2018).

The new avenue for chemotherapy are nanoparticles, with the ability to deliver the drug to specific target without affecting healthy cells.

1.2 Nanotechnology

Materials or devices in nanotechnology are designed, synthesized, and characterized to have at least one dimension on the nanometer scale and to interact with cells and tissues at the molecular level (Saini et al., 2010). It is a multidisciplinary field that has resulted in the development of new tools and capabilities as a result of the advancement of various sciences such as biology, chemistry, physics, engineering, electronics, and medicine. Humans have been dealing with nanotechnology for a long time without realizing it. Faraday created colloidal gold in 1856, which was used to color glasses and vases (Kandru, 2020). Furthermore, Richard Feynman believed that nanotechnology would have a significant impact in the future, and since his famous lecture sentence, "*There's Plenty of Room at the Bottom*," the field of nanotechnology has undergone numerous revolutions (Feynman, 1960).

Nanoparticles (NPs) range in size from 1 nm to 100 nm and come in a variety of shapes, including hollow spheres, quantum dots, nanotubes, nanobelts, NPs, nanoribbons, and nanorods (Kargozar & Mozafari, 2018) having different dimensions 0D, 1D, 2D, or 3D. Furthermore, they are classified based on the material used, such as carbon NPs, metal NPs, ceramic NPs, semiconductor NPs, polymeric NPs, and lipid-based NPs (I. Khan et al., 2019 ; Ealias & M P, 2017). Proteins, cholesterol particles, and viruses are all nanometer in size and can interact with cells; engineered nano-sized materials are similar in this respect. Furthermore, natural nanomaterials are internalized by cell endocytic machinery via specific cell receptors at the plasma membrane (Francia et al., 2020). These NPs are distinguished by their physicochemical properties, which include surface area, surface charge, degree of agglomeration, particle morphology, and surface coating (Turan et al., 2019). The physiochemical properties of nanometer-sized materials differ from those of bulk materials. It may provide new properties or specific performance at the nanoscale (Nasrollahzadeh et al., 2019). Gold in nanoscale is considered reactive, whereas gold in bulk is considered inert (Friedersdorf & Spadola, 2020). There is an inverse relationship between particle size and surface area; as the particle becomes smaller, the surface area increases, making the nanoparticle more reactive and affecting its transportation. In their cellular uptake, different sized silica NPs compete for the uptake. Small particles inhibit the uptake of large particles, whereas large particles promote the uptake of small particles by the cell (Li et al., 2019). AuNPs with sizes of 10, 30, and 60 nm were tested *in vivo* and *in vitro* to study the effect of size on cells. AuNPs with diameters of 10 and 30 nm were able to cross the cell membrane, causing DNA damage. Furthermore, the larger the size, the different excretion route; 30 and 60 nm AuNPs tend to accumulate in the spleen, whereas 10 nm AuNPs accumulate in the intestine (Lopez-Chaves et al., 2018).

Furthermore, the surface charge is important in controlling nanoparticle stability and thus agglomeration and toxicity (Turan et al., 2019). Positively charged and hydrophobic NPs obstruct extracellular membrane diffusion. It is, however,

extremely useful for modifying the surface of NPs by grafting polymer coronas (Goas et al., 2020).

1.2.1 Nanoparticles as a delivery system

NPs are well-known for their diverse applications in electronics, energy, biomedical applications, and the environment, among others. NPs in the nanomedicine field are the subject of extensive research, including drug delivery, gene delivery, and use as a contrast agent. This favorable use of NPs is due to their effectiveness at specific therapeutic targeting (Maleki & Fotouhi, 2019).

Because of their small size, which increases intracellular uptake and accurate biodistribution, and large surface area, which increases the drug's loading capacity, NPs are very efficient in drug delivery applications. Some NPs have the ability to cross the blood-brain barrier (BBB), are soluble, and can be absorbed through skin endothelial cell tight junctions (Rizvi & Saleh, 2018). Furthermore, structurally stable NPs deliver the drug for an extended period of time without degradation. NPs have the ability to transport drugs to a specific site, reducing the toxicity caused by conventional drugs that are off-target (DS et al., 2016). NPs help to reduce systemic toxicity and improve chemotherapeutic drug efficiency, and they can reverse chemotherapy resistance in tumors through active targeting and activation of alternative mechanisms of cellular uptake (Barkalina et al., 2014). Keratin NPs were used to deliver the anticancer drug doxorubicin (DOX). They were biocompatible, low immunogenic, and redox responsive. The NPs are pH sensitive and releases the drug in acidic pH. Furthermore, keratin NPs exhibited cytotoxicity against A549 cells and demonstrated more effective therapy than free DOX (P. Liu et al., 2019). Moreover, because of their ability to deliver DNA, RNA, and other molecules, NPs have been the subject of numerous studies in order to synthesize, characterize, and functionalize them for use in targeted gene delivery. Despite the fact that using NPs to deliver genes is a very promising way to cure inherited diseases (Kargozar & Mozafari, 2018).

1.3 Graphene and its derivatives

Graphene is an ultra-thin two-dimensional structure composed of sp^2-bonded carbon atoms that forms a honeycomb crystal lattice (Shao et al., 2010). It is made up of a single atom and a thick planar sheet (Eskiizmir et al., 2018). It was discovered by Geim et al.in 2004 (Geim & Novoselov, 2009). Since then, the interest of the researchers has piqued and has been studied in various fields such as chemistry, physics, and materials (T. He et al., 2018). Furthermore, due to its diverse properties, it has been found to be applicable in electronic, mechanical, biological, and medical applications (Al-Ani et al., 2017). Graphene have many derivatives due to the six membered carbon ring structure (Sun & Du, 2019). Graphene and its derivatives have high thermal conductivity, chemical stability, flexibility, a large surface area, superior mechanical strength, a large carrying capacity, and optical absorption in the near-infrared region, which makes them ideal for biomedical applications (Al-Ani et al., 2017; Toh et al., 2014). Graphene-based nanomaterials are less toxic than carbon nanotubes (Eskiizmir et al., 2018). Graphene and its derivatives have the ability to form π-π conjugation with unsaturated and aromatic biomolecules and have the potential to treat cancer by using them as drug delivery, gene transfection, photothermal therapy (PPT), and biomarker sensor as shown in Table 1 (T. He et al., 2018).

Table 1.1 Graphene and its derivatives in biomedical applications.

	Graphene	Graphene oxide	Reduced graphene oxide	Graphene quantum dots
Biosensors	3D-printed graphene/polylactic (PLA) electrode for hydrogen peroxide detection (López Marzo et al., 2020)	Glucose detection by GO- AuNPs decorated with Cu-nanoflower (Baek et al., 2020).	Detection of phenylketonuria-associated with DNA mutation by rGO-AuNPs (Seifati et al., 2018).	Detection of circulating tumor by magnetic fluorescence graphene quantum dots (Cui et al., 2019).
	Detection of nucleic acid by deformed monolayer graphene channel (Hwang et al., 2020)	Electrochemical biosensor of GO-AuNPs for detection of prostate cancer biomarker (Akbari Jonous et al., 2019).	Detection of *Salmonella* by modified polypyrrole-rGO (Ye et al., 2019).	Fast detection of antibodies based on molecularly ımprinted polymers coated on graphene quantum dots .

Table 1.1 (continued)

	Graphene	Graphene oxide	Reduced graphene oxide	Graphene quantum dots
Theranostic application	Functionalized graphene nano-flakes for anticancer drug delivery and imaging application (Lamb et al., 2019)	AuNPs decorated GO for drug delivery and chemo-photothermal therapy (Samadian et al., 2020)	Gold and silver were decorating rGO for diagnostic and therapeutics application (Darabdhara et al., 2019).	
		Iron oxide-AuNPs decorating GO for photo/radiotherapy (Beik et al., 2021)	rGO hybridized hydrogel for chemo-photothermal therpay (W. Liu et al., 2019)	

Table 1.1 (continued)

	Graphene	Graphene oxide	Reduced graphene oxide	Graphene quantum dots
Theranostic application		Chitosan grafted GO, forming a drug carrier system with enhancing MRI imaging (Baktash et al., 2021)	Iron oxide-rGO for drug delivery and hyperthermia treatment (Gupta et al., 2018)	
Drug delivery		Magnetic GO with brush polymer as DOX drug carrier (Pooresmaeil & Namazi, 2021)	rGO as drug carrier for Wound Healing (Ur Rehman et al., 2019).	chitosan modified graphene quantum dots for anticancer drug delivery (Sheng et al., 2020).

Table 1.1 (continued)

	Graphene	Graphene oxide	Reduced graphene oxide	Graphene quantum dots
Drug delivery		GO hydrogel as anticancer carrier (Ghawanmeh et al., 2019)	rGO for delivering of curcumin anticancer drug (Mostafavi & Imani, 2021)	Fe_3O_4@PEG decorated GQD's for DOX anticancer drug delivery (Javadian et al., 2021)

Oxidation occurs when oxygen functional groups are added to graphite, resulting in graphite oxide. Furthermore, GO is a single layer of graphite oxide. GO is a graphene derivative with a single atomic layered material, and its surface is functionalized with a large number of residual epoxide (-O-), hydroxide (-OH), and carboxylic acid (-COOH) groups attached on the basal planes and edges (Toh et al., 2014). GO is created by oxidizing graphite powder with strong acids and oxidants (Eskiizmir et al., 2018). The synthesis of GO is accomplished in two steps. First, oxygen functional groups such as epoxy (C-O-C), hydroxyl (OH), carbonyl (C=O), and carboxyl (R-COOH) are introduced into the basal plane and edges of the GO sheet, and graphite oxide is produced by oxidizing graphite flakes. Second, graphite oxide suspension is created by easily exfoliating graphite oxide in water through sonication or shearing (Sali et al., 2019). Brodie, Staudenmaier, Hofmann, Hummers, and Tour's methods are all used to synthesize GO. To begin developing these methods, acids such as HCl, H_2SO_4, and HNO_3 are chemically reacted with graphite powder. The graphite layers will then be intercalated with alkali metal compounds such as $KClO_3$, $KMnO_4$, $NaNO_3$, and so on. This step makes it easier to cut graphitic layers into small pieces

(Singh et al., 2016). GO is hydrophilic, meaning it has a higher chemical reactivity and surface energy. The amount of oxygen, on the other hand, determines the properties of GO. Furthermore, GO has defects in its crystalline network, making it nonconductive in comparison to graphene. Fortunately, graphene-like properties can be restored by performing additional reduction treatments on GO to produce rGO (Tarcan et al., 2020; Sengupta et al., 2018). Figure 1.2 illustrates the difference between graphite and graphite oxide, graphene and GO and rGO. Each derivative has its own property such as GO solubility, stability, and uniform dispersion, whereas rGO derivative has structure and physicochemical properties between pristine graphene and GO (S. Chen et al., 2020).

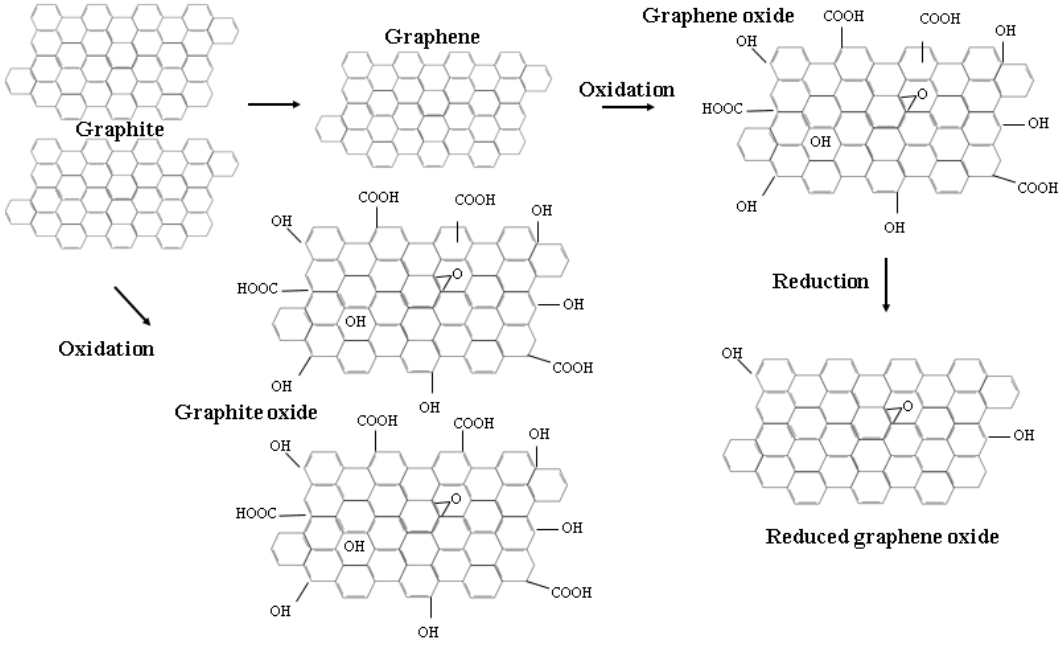

Figure 1.2 Structure of graphite, graphite oxide, graphene and its derivatives.

1.3.1 Reduced graphene oxide

The second derivative of graphene is reduced graphene oxide (rGO). Pristine graphene is conductive and can be easily prepared in the required quantities (Toh et al., 2014), using any of the chemical, thermal, electrochemical, or multi-step combined methods listed below (Tarcan et al., 2020; Toh et al., 2014). By reducing GO, this could repair GO defects and remove oxygen groups (Ahammad et al., 2019). rGO is more efficient in preparation than graphene (Q. Wang et al., 2017). Graphene is made up of one or a few layers of graphite, with no more than ten layers. Two methods for obtaining graphene are top-down and bottom-up. By overcoming van der Waals forces and thus breaking the stacked layers of graphite, a top-down strategy is used to obtain individual graphene sheets. The bottom-up approach is a substrate that is used to grow carbon molecules (Eskiizmir et al., 2018). Mechanical exfoliation, a top-down strategy, was used earlier to produce single or few layers of graphene, but it was only suitable for laboratory research due to the small-scale production (T. He et al., 2018) and an external force of around 300 N/um^2 is required to separate a single layer from graphite (Yih et al., 2018). Chemical and thermal GO reduction is another top-down technique (Toh et al., 2014) by removing functional groups, particularly OH and epoxy groups (Sengupta et al., 2018). Chemical reduction of GO is a simple and low-cost process that can be carried out at room temperature using chemical reagents such as hydrazine (Zhu et al., 2011; Tarcan et al., 2020; Toh et al., 2014). However, due to hydrazine's toxicity, it is replaced with the non-toxic, low-cost organic acid ascorbic acid (J. Zhang et al., 2010; De Silva et al., 2017), glucose (Tang et al., 2013), hydroxylamine (Zhou et al., 2011) and much more. Chun et al. used hydrazine as a reducing agent (Chun et al., 2016). However, it was unable to easily remove OH and carboxylic groups. Furthermore, hydrazine reacted with carbonyl groups to form hydrazone complexes (Chun et al., 2016), Another study discovered that hydrazine completely removed the epoxy and OH groups. In addition, the basal plane repaired the sp^2 network (Park et al., 2012). In another study, a green reduction by ascorbic acid was monitored for 1 h to control

the reduction process. After 50 minutes, XRD was used to determine the complete removal of the GO peak. In contrast, XPS demonstrates the removal of OH and epoxy groups (K Kanishka H De Silva et al., 2018). Green reducers, such as Amaranthus hybrids (Chang et al., 2015) and ascorbic acid (K. Kanishka H. De Silva et al., 2018), are superior reducing agents for GO when compared to hydrazine. The removal of oxygen-containing groups was indicated by highly ordered corrugate at green reducers (Fasakin et al., 2019). Chemically reduced graphene has a low C:O ratio and residual functional groups. Furthermore, because of the strong π-π stacking of the rGO sheets, the chemical method was used to produce rGO with limited solubility and agglomeration in water and organic solvents (J. Kim, 2016). Thermal reduction, on the other hand, avoids the hazards of some chemicals while saving time. The thermal reduction method employs high temperatures to remove H_2O molecules and oxygen functionalities such as carboxyl group –COOH, -OH group, and epoxy group >O. (Huh & Seung Hun, 2011). A study conducted by (Gao et al., 2010) demonstrates the ability of thermal reduction at high temperatures to remove OH and carboxyl groups from GO in comparison to hydrazine, which only results in de-epoxidation. The OH groups at the edges are eliminated as the temperature of the reaction rises above 700 °C. It was suggested that the best deoxygenation efficiency be obtained by combining both chemical and thermal reduction methods. A recent study found that the time of reduction affects the chemistry and interlayer structure of rGO (Fan et al., 2020). H. Huang et al. reported the effect of reaction time. Between 0.5 and 1 h, both GO and rGO exist, combining the hydrophilicity of GO and the lattice spacing of graphite. When the reaction lasts between 2 and 8 h, the material begins to lose its oxygen functional group and gains better electronic properties (H. Huang et al., 2018). Another study obtained different reduction degrees by changing the reaction temperature; as the reaction temperature increased, so did the degree of reduction (Mei et al., 2015). Thermal annealing of GO causes more defect sites or increases the size of the defects. However, substituting alcohol for water, such as ethanol or methanol, can slow the progression of the defects. In

addition, ethanol repairs the flaws by forming new hexagonal carbon (Gong et al., 2012).

Microwaves and photo-assisted procedures can be used to supplement the thermal reduction method and favorable alternative. Microwaves overcome the lengthy process of the thermal reduction method as well as the need for the use of toxic chemicals for reduction (Jakhar et al., 2020). As a result, the microwave and various lasers via photo-irradiation provide rapid and uniform heating (Tarcan et al., 2020). Microwave was used in a study to obtain a very high yield of graphene (W. Chen et al., 2009). As a solvent for rGO, N, N-dimethylacetamide, and water were used to control the temperature of the system up to 165°C. Reduction of GO was obtained in minutes, and the degree of reduction was changed by changing the time of microwave treatment (W. Chen et al., 2009). After treating graphite oxide powder with a microwave at 700 W for 1 minute, another study obtained crumpled, electronically conductive graphitic sheets Microwave irradiation resulted in the expansion of GO powder (Y. Zhu et al., 2010).

The electrochemical reduction method is another option, it is fast, simple, nontoxic and time efficient method (Shahrokhian & Salimian, 2018). When a power source is applied, an electrochemical cell with an aqueous buffer solution is used to drive the reduction process (Tarcan et al., 2020). The electrolysis parameters and electrolyte are in charge of fine-tuning the properties of rGO (Toh et al., 2014).

Among the various methods for synthesizing graphene, reduction of GO is preferable because it is simple and inexpensive to implement, and a wide range of reducing agents and methods can be used (Shao et al., 2010).

1.3.2 Graphene quantum dots

Graphene quantum dots (GQDs), one of graphene's derivatives, are carbon-based nanomaterials made up of a single layer of 2D graphene (Iannazzo et al., 2017). Quantum dots are used to reduce the size of the sheets to less than 100 nm (F. Liu

et al., 2013), showing better properties with more active groups on their surface than normal graphene and GO. Main characteristics of GQDs are their water solubility, non-toxicicty, inexpensiveness, good biocompatibility, large surface area, small size, photostability and better cellular uptake. Additionally, they have fluorescence property due to the optical bandgap open by the sp^2 and sp^3 carbons which helps in bioimaging without the need for external dyes (X. Wang et al., 2014 ; Liang et al., 2020 ; Karimi & Namazi, 2020). Moreover, strong non-covalent interactions with adsorbed biomolecules occur on the 2D surface via π-π interactions, electrostatic forces, or hydrogen bonding (Zheng & Wu, 2017 ; Javanbakht & Namazi, 2018 ; Sawy et al., 2021). Based on their enormus properties, they are being experimented in drug delivery and imaging applications. Top down and bottom up are two strategies to obtain quantum dots. Chemical exfoliation (S. Wei et al., 2016), electrochemical exfoliation (M. He et al., 2018), hydrothermal/solvothermal exfoliation (Nxele & Nyokong, 2022), and microwave/ultrasound assisted exfoliation (Centeno et al., 2021) are all top-down strategies for producing GQDs by cutting down large sheets into small pieces. Carbonization/pyrolysis (Kir et al., 2021), stepwise organic synthesis/cage opening, and chemical vapor deposition (D. Liu et al., 2018), on the other hand, are all bottom-up synthesis methods in which the size of the GQDs are being controlled (Jampilek & Kralova, 2021 ; F. Chen et al., 2017).

1.4 Metal nanoparticles

Metal NPs such as (Al, Au, Fe, Si, Ag, Cu, Ce, Mn, Ni, Ti, and Zn) have become increasingly popular in engineering, cosmetics, medicine, energy, and other fields due to their unique physical, chemical, optical, electrical, and magnetic properties (Barman et al., 2018). Catalytic activity exists on the surface of MNPs with a large surface area to volume ratio (Ahmad Alshammari et al., 2016). Furthermore, gold, silver, and platinum have the property of Localized Surface Plasmon Resonance, which makes them ideal for use in nanomedicine applications (Rai et al., 2002).

1.4.1 Gold nanoparticles

Gold was among the one of the first metals discovered, dating back to the fourth and fifth centuries BC, when colloidal gold was obtained and used for medical purposes. During the Middle Ages, the European Paracelsus reduced gold chloride using vegetable extracts in alcohol or oils, and he used the reduced gold to treat a variety of mental diseases as well as syphilis. Francisco Antonii, a philosopher and doctor of medicine, published the first book on colloidal gold in 1618 (Dykman & Khlebtsov, 2011). Colloidal gold is a water-based suspension of small gold particles (Rahman & Abdullah, 2018). AuNPs are synthesized simply by reducing metal salts with a reducing agent (Chandran & Thomas, 2015) to have sizes between 1 and 100 nm (X. Chen et al., 2014). AuNPs have piqued the interest of many researchers due to their obvious benefits. They can be used in a variety of applications, including electronics, biomedicine, and nanotechnology (Mokammel et al., 2019). Because of their unique properties, AuNPs have a wide range of applications in biomedicine today.

Surface plasmon resonance (SPR) is the maximum oscillation at a specific wavelength of light. When a specific wavelength of light interacts with the conduction electrons of a metal interface, it causes oscillation of the free electrons, which depends on the incident light's electromagnetic field and ionic lattice. Because of their optical properties, AuNPs are ideal for diagnosing with optical imaging, cell imaging, and computed tomography (CT). Furthermore, they can be considered for

photothermal and radiotherapy. However, because of their large surface area, a wide range of molecules, including drugs, targeting ligands, and imaging probes can be conjugated to their surface (Aminabad et al., 2019). Additionally, they can be easily functionalized by all types of biomolecules, including antibodies carrier (Liszbinski et al., 2020), proteins, carbohydrates, and lipids (Pissuwan, 2017) to stabilize AuNPs in biological media (Lee et al., 2021). Furthermore, AuNPs of various shapes, including spherical, rod-like, cage-like, and many others, can be easily synthesized (Kong et al., 2017). For biomedical applications, spherical and rod shapes are widely used due to low toxicity (Pissuwan, 2017). AuNPs are also notable for their small size, biocompatibility, and non-toxicity (Kong et al., 2017). Because of their distinct properties, AuNPs are ideal for targeted drug delivery, bio sensing, bio imaging, and therapeutic applications (Thambiraj et al., 2018).

There are several methods for preparing AuNPs, including top-down and bottom-up approaches. Bottom-up approaches based on chemical, physical, or biological methods are the most common and convenient. Because of the ease of synthesis, controllable size, and stability of AuNPs, chemical methods such as the Turkevich procedure are the most commonly used methods. The chemical method, on the other hand, entails creating an aqueous medium and adding a reducing agent to carry out the chemical reactions. Citrate and sodium borohydride are two commonly used reducing agents (Elahi et al., 2018). After 5 minutes of adding sodium citrate to a boiling chloroauric acid solution, the color changes to deep wine red, indicating the formation of spherical particles 20 nm in diameter, according to the Turkevich method (Turkevich et al., 1951). AuNPs with diameters ranging from 5 to 150 nm can be obtained by varying the reaction conditions. Dong et al. obtained AuNPs with sizes ranging from 15 to 50 nm as the molar ratio of trisodium citrate (NaCt) to gold salt was decreased ($HAuCl_4$) (Dong et al., 2020). Faraday proposed the Brust Schiffrin method for producing AuNPs with sizes ranging from 1-3 nm in a two-phase system. Dodecanethiol is treated with the phase transfer agent tetraoctylammonium bromide (TOAB) and the reducing agent sodium borohydride (Brust et al., 1994). Zhu et al. obtained a complex solution of [TOA] and [AuX_4]

with wine red color (L. Zhu et al., 2013). The seeding growth method allows the growth of small metal particles into larger particles of a predetermined size which allows control of the size of the particles with high monodispersity (nucleation centers). From a seed particle size of 9 nm, monodispersed AuNPs of 80 nm were synthesized. Addition of the reducing agent oleylamine allows the particles to grow (Stanglmair et al., 2014).

Due to the toxicity and high cost of the chemicals required to reduce and stabilize these NPs, metal NPs are only synthesized chemically in a few applications. They would be harmful in biomedical applications as well. The biological method is a low-cost, green, and environmentally friendly procedure that reduces the dangers of toxic chemicals. Microorganisms such as bacteria, fungi, algae, yeast, and viruses, as well as enzymes, plants, and plant extracts, are used to reduce and stabilize the AuNPs. A nontoxic, low-cost, and easily accessible method effectively allows synthesis of NPs of various shapes and sizes for biomedical applications (Herizchi et al., 2016 ; Shah et al., 2014). Xin Lee et al. created environmentally safe AuNPs suitable for biomedical applications by using a Garcinia mangostana (G. mangostana) peel extract as a reducing and stabilizing agent. The synthesized AuNPs had a spherical shape and a size range of 32.96+/- 5.25 nm (Xin Lee et al., 2016). Using Annona muricata leaf extract, Folorunso et al. created a non-hazardous, quick, and cost-effective method for reducing gold chloride which acted as a stabilizer after nanoparticle formation. The average size of the monodispersed spherical NPs was 25.5 nm. When tested against pathogens, AuNPs synthesized proved to be an effective antimicrobial agent, inhibiting fungi by 66% and bacteria by 54% (Folorunso et al., 2019).

Because of its simplicity, eco-friendliness, and low cost, the synthesis of AuNPs using microorganisms such as bacteria, fungi, and microalgae has gained popularity. There are two methods for producing AuNPs: intracellular pathways, in which NPs are produced inside the cell and diffuse to the cell wall, and extracellular pathways, in which NPs are produced outside the cell and diffuse to the cell wall. Gold salt reduction, on the other hand, is the responsibility of enzymes on the cell wall or the

cytoplasmic membrane. Proteins, amino acids, and enzymes are examples of extracellular materials that are involved in the synthesis of NPs (Patil & Kim, 2018). Endophytic fungi are fungi that live inside plants. Fusarium solani was used as a reducing agent to produce AuNPs with a needle, flower-like structure and a size range of 40-45 nm, as well as a characteristic wavelength of 510-560 nm. A dose dependent cytotoxicity of synthesized AuNPs on cervical cancer cells (HeLa) and human breast cancer cells (MCF-7) was reported (Clarance et al., 2020).

Physical methods such as microwave irradiation, ultraviolet (UV) radiation, laser ablation, photochemical or thermolytic processes are also used to synthesize AuNPs. Irradiation is the most effective method for producing controllable AuNPs with sizes ranging from 5 to 40 nm (A. K. Khan et al., 2014). Microwave irradiation was used with the aid of cellulose nanocrystal as a reducing and stabilizing agent for gold salt. The irradiation time is between 5 and 25 seconds, and the power is 500 watts. The size of the AuNPs synthesized ranged from 6 to 8 nm (Alle et al., 2020).

1.5 Nanocomposites

Nanocomposites are made up of two or more components that are combined to form a multiphase single compound with combined properties from the parent and unknown properties that are different and new from the parent constituent properties. Reinforcement and matrix phases combine to form nanocomposites. The materials that can be used to make reinforcing material include fiber, sheet, and particles. The reinforcement phase has a high surface-to-volume ratio, which distinguishes nanocomposites from conventional composite materials (Chikwendu Okpala, 2006). Nanocomposites have become very appealing for increasing therapeutic efficacy, specifically targeting sites of interest, and improving overall system stability or performance. There are numerous types of bionanocomposites, including polymeric nanocomposite hydrogels, bioinspired metallic NPs, bioactive silicate-based nanocomposites, hydroxyapatite nanocomposites, rosette nanotube composites, graphene enhanced polymeric nanocomposites, and polymeric nanocomposites loaded with metallic NPs (Mishra et al., 2019). However, there are three types of

nanocomposites: First, nanoscale alternating layer dimensions are known as nano layered composites. Second, nano filamentary composites are matrices that contain nanoscale diameter filaments. Third, nano particulate composites are made up of nanoscale particles that have been embedded in matrices (Sohani et al., 2015). Controlling the size, surface chemistry, and shape of nanocomposites changes their physical and chemical properties; as a result, they will play an important role in many biomedical applications such as drug delivery, biosensing, and imaging (Mishra et al., 2019). The degree of mixing of the phases affects the property of the nanocomposites (Ishida et al., 2000). Nanocomposites have significant advantages over conventional composites, such as adding a small amount of the reinforcement material as nanofiller to improve the properties of the matrix material, whereas conventional composites require a high concentration of microparticles. Nanomaterials improve thermal, chemical, mechanical, optical, magnetic, and electrical properties to a greater extent than conventional materials. Furthermore, they are more dispersible in aqueous medium and significantly lighter in weight (Kaurav et al., 2018).

1.6 GO, rGO, AuNPs and AuNPs-rGO as drug delivery systems

Nanoscience and nanotechnology have expanded rapidly, particularly in medicine. Nanotechnology is being used in diagnosing and treatment of diseases. Because these NPs have unique and important properties. The primary goals of using these NPs are to deliver drugs to specific targets in a biocompatible, non-toxic or less toxic manner while maintaining therapeutic effects, and to develop these NPs quickly. Efficient drug delivery systems should be present in the circulation for a long time, which is accomplished by surface modification with polyethylene glycol (PEG), which can also be used to prevent nanoparticle agglomeration. Another critical parameter is nanoparticle size, which influences nanoparticle distribution (De Jong & Borm, 2008). Nanosized devices or systems can be made from a wide range of materials, including polymers, lipids, viruses, and even organometallic compounds with submicron dimensions (3-200 nm). Polymeric NPs are polymers that occur naturally, such as chitosan, albumin, and heparin. These polymers are employed in the delivery

of DNA, protein, oligonucleotides, and drugs. Synthetic polymers, on the other hand, such as polyethylene glycol (PEG), biodegradable polymer poly-L-glutamic acid (PGA), and N-(2-hydroxypropyl)-methacrylamide copolymer, are used for the synthesis of the conjugate (HPMA) (George et al., 2019). Liposomes are spherical drug carriers composed of an outer lipid bilayer surrounding a central aqueous space. Many anticancer drugs are being clinically used in this lipid-based system. To combat various viruses, viral NPs have been developed for tissue targeting and drug delivery. Cowpea mosaic virus, cowpea chlorotic mottle virus, canine parvovirus, and bacteriophages have capsid surfaces that can display peptides and targeting molecules such as transferrin, FA, and single-chain antibodies, and conjugation to viruses results in specific tumor targeting in vivo. The final type of drug carrier is carbon nanotubes, which are made up of an insoluble benzene ring and a carbon cylinder. Because of their complete insolubility, these nanotubes are toxic; however, chemical modifications can make them water soluble and functional (Cho et al., 2008).

NPs as drug carriers face two limitations, making it difficult to select and design suitable NPs. The drug loading is poor, either because the weight percent of the drug in relation to the carrier is low, resulting in insufficient pharmacological active concentration in the body, or because of side effects caused by a large amount of the carrier material. On the other hand, burst release, which is rapid drug release after administration, results in significant release before reaching the target in the body, resulting in lower activity and more side effects. As a result, many studies are being conducted to develop safe (bio) materials for drug targeting with controlled drug loading and releasing. Simultaneously, the construction of NPs with multifunctional properties, dubbed "Nanotheragnostics," has become difficult (Couvreur, 2013).

One disadvantage of conventional drug delivery is the random distribution of the drug throughout the body; however, using nanosystems will overcome this problem by prolonging, localizing, and targeting, and thus using nanocomposites shows great advantages in targeting.

GO has a high loading efficiency and good dispersion due to the presence of oxygen groups and a large surface area. Qi et al.created a hybrid nanoparticle made of PEGylated GO and capped with core shell nanorods and mesoporous silica NPs. The hybrid is a pH/near infrared NIR-responsive drug release system. The nanocomposite demonstrated excellent high loading of the drug DOX and photothermal conversion efficiency. Because of the presence of GO-PEG, the hybrid was photothermally stable in physiological or acidic media (Qi et al., 2019). Hyaluronic acid (HA) functionalized GO showed low cytotoxicity on Hela cells Even at high exposure level up to 10 mg/kg on mice, the composition GO-HA had no toxicity. *In vivo* studies showed that DOX loaded GO-HA had the capability to reach tumors which resulted inhibition of tumor growth(Wu et al., 2014). In a study by Weaver et al. the drug release was electrically controlled. The release of the anti-inflammatory drug dexamethasone (DEX) was fully controlled by a stimulation of a GO film placed inside a conducting polymer poly(pyrrole) scaffold synthesized by Weaver et al. It was discovered that ultrasonication can be used to tune the properties of a drug delivery system by changing the size and thickness of GO sheets. The system emits nontoxic byproducts (Weaver et al., 2014). In a recent study, dual-function of GO (fluorescence for imaging and carrier for drug) was investigated. Protein loaded GO were efficient, both in terms of cellular imaging agent and delivery system when applied on CT26 cancer cells. Mild thermal annealing was used to induce blue fluorescence in a GO suspension. The material was shown to be non-toxic (Cheng et al., 2018).

rGO, on the other hand, has ultrahigh drug loading efficiency, the ability to absorb near-infrared energy, and bioactive properties (Ma et al., 2015 ; Al-Ani et al., 2019). Moreover, rGO enables the π-π interaction with the aromatic part of the drug, because of the abundant π-electron on its surface (Hazhir et al., 2019). They also provide mechanical stability, cellular interaction, effective functionalization, and drug loading. H. Kim et al. synthesized functionalized rGO capable of loading a large amount of DOX which released their contents in the cytosol via near infrared (NIR) photothermal triggering. Furthermore, the nanocomposite of PEG-BPEI-rGO

demonstrated excellent water stability. Because of its aromatic structure prior to reduction, rGO outperformed GO in terms of efficiency (H. Kim et al., 2013). GO has biocompatibility issue due to reactivity of oxygen functionalities which result in sever toxicity even at low concentrations (Al-Ani et al., 2019). Hashemi et al. grafted rGO with R9 peptides to serve as a carrier for the hydrophobic chemotherapeutic anticancer drug Paclitaxel. They caused a 90% reduction in viability against Hela and MCF-7 cancer cell lines after 72 h (Hashemi et al., 2016). Miao et al. (2013) synthesized rGO coated with cholersteryl hyaluronic acid (CHA-rGO) to increase colloidal stability under physiological conditions, *in vivo* safety, and a significant increase in the loading capacity of DOX compared to rGO. When compared to rGO, these coated nanosheets resulted in increased drug uptake by CD44 cells (Miao et al., 2013). G. Wei et al. functionalized rGO with p-aminobenzoic for excellent solubility and with polyethyleneimine (PEI) and covalently attached FA molecules (Wei et al., 2012). Elsinochrome (EA) and DOX were also loaded to the functionalized rGO sheets. EA and DOX loading ratios were 45.56% and 28.62%, respectively. The release profile of the drug was affected by pH and salt. It was shown that the combination of rGO-PEI-FA and DOX increased cancer cell apoptosis and made the cancer cell more susceptible to damage from drugs or radiation because it enters the G2 phase of the cell cycle (G. Wei et al., 2012). A DOX drug-loaded at rGO was anchored with the protein tyrosine kinase 7 receptor (PTK7). Furthermore, the addition of the OligoT Bridge domain aided increasing the anchoring onto rGO sheets to achieve DOX- PNTrGO. The effects of these nanosheets were studied under *in vivo* conditions. The results showed a 12% reduction in tumor weight, indicating that PNTrGO was effective in terms of targeting and treatment (M. G. Kim et al., 2015).

When compared to carbon, boron chemistry is a relatively new field of study. Boron is also found in trace amounts in human body. Boron, on the other hand, can be used in pharmaceutical drug design and as a catalyst for new biological activities (Ali et al., 2020). Boron and carbon are neighbors on the periodic table, with boron exhibiting high chemical stability, superconductivity, thermoelectricity, and partial

ionic bonding. Boron nanosheets were studied for their potential applications in anticancer drug delivery and imaging. Furthermore, these nanosheets excelled in photothermal therapy due to their superior photothermal conversion efficiency (Ji et al., 2018).

The chemistry of graphene can be altered by doping, which involves replacing one carbon atom with another element. As a result, modified graphene is commonly used in a wide range of technologies. Because their atomic radii are similar to carbon's, doping graphenes with boron and nitrogen has gained popularity (Agnoli & Favaro, 2016). However, due to the oxygen functionalities, the electrical properties, thermomechanical stability, and carrier mobility of carbon-based materials are all declining; thus, the incorporation of non-metallic elements into the layers of GO, such as boron, nitrogen, and phosphorous, will aid in minimizing the problem and improving the electrochemical properties (Mannan et al., 2018). Boron doped graphene quantum dots have been used successfully in a variety of biomedical applications, including DNA/RNA detection and other bioimaging capabilities. Boron doped graphene can also be used for cell culture, controlled drug release, and chemical sensors for biomolecules (Banerjee, 2018). A 2020 study demonstrated the effect of different boron concentrations doped in rGO, and as the boron percentage increases, there is a significant change in the physicochemical, optical, electrochemical, and great conductivity properties, and the boron doping caused the nanocomposite to have strong absorption in the ultraviolet region (Ngidi et al., 2020)

Because of their large surface area, biocompatibility, low toxicity, and other distinguishing characteristics, AuNPs are effective in drug and gene delivery. They are excellent for increasing drug concentration in the targeted cells, thereby reducing therapeutic dosage and mitigating drug dose dependent damage to healthy tissues. Many studies have shown that AuNPs are rapidly cleared before they can successfully deliver the drug. Furthermore, in order to reach the targeted tissue and blood circulation time, they must hide from the immune system and reticuloendothelial system (RES) (Aminabad et al., 2019). However, conjugation of polyethylene glycol (PEG) to the surface of AuNPs will avoid the RES clearance,

increase the blood circulation time and thus sufficient drug transfer (Aminabad et al., 2019; Elahi et al., 2018).

Aside from having a large specific surface area, using a graphene-based drug delivery system prevents the drug from discharging outside the target cells. Furthermore, due to the strong interaction between the drug and the carboxyl group of the graphene-based structure, forming a nanocomposite based on graphene will allow more drug loading and promote sustainable release behavior (Kaurav et al., 2018). Hydrophobicity and self-aggregation, as well as restacking, between graphene nanosheets, on the other hand, are caused by strong van der waals interactions and stronger stacking, both of which are known for graphene. They are, however, solvable through functionalization and the formation of a hybrid composite. (Kadiyala et al., 2018). In fact, many studies illustrate and prove how graphene based composites are very suitable and have great advantages in cancer nano-therapy (Al-Ani et al., 2019). AuNPs are well-known for their stability, biocompatibility, and other characteristics, which lead to their widespread use with various nanomaterials, resulting in the synthesis of AuNPs-graphene hybrid composite materials and their application in cancer nano-therapy (Al-Ani et al., 2019). A group produced nanocomposites containing iron oxide NPs, AuNPs, and GO. Each component has unique properties. Superparamagnetic iron oxide NPs increased relaxivity. Furthermore, the surface plasmon peak of AuNPs was observed in this hybrid structure. Furthermore, nanocomposite as a nanocarrier demonstrated extremely high drug loading capacity DOX. However, because of the hybrid's anticancer drug loading capacity and contrast agent composition, it can be used as a theranostic nanocomposite (Balcioglu et al., 2013). In 2018, a nanodelivery system based on GO was synthesized as a therapeutic by loading naturally occurring anticancer agent protocatechuic acid (PA) and gadolinium III nitrate hexahydrate (Gd) as starting material for a contrast agent in imaging, and AuNPs were loaded as a second diagnostic agent. The nanocomposite was tested with Tesla 3.0 MRI equipment, and the results revealed an increase in contrast, which aided in the enhancement of imaging modalities. Furthermore, the release of the anticancer agent

PA was investigated, and it was discovered that in acidic environment like tumor microenvironment, the release rate reached to 60%, whereas in alkaline media, the release rate was less than 40%. A cytotoxicity test confirmed the results of drug release study, and 100 g/mL of the nanocomposite dose caused cancer cell death (Usman et al., 2018). Samadian et al. created a biocompatible nanocomposite based on AuNPs and decorated with poly ethylene glycol (PEG) and FA, all of which were conjugated into GO. This nanosystem was tested against human breast cancer (MCF-7) and demonstrated a high loading capacity for DOX drug. The pH of the release media affects drug release. This nanocarrier demonstrated excellent cancer chemotherapy capabilities. Furthermore, it was also concluded that GO-PEG-FA/AuNP nanocomposites had theranostics properties and can be used in chemo-photothermal therapy (Samadian et al., 2020).

Fabrication of Au-rGO nanocomposites has grabbed more attention nowadays due to their superior performance in various areas such as biosensors (Seifati et al., 2018), surface-enhanced Raman scattering (Ying Hu et al., 2012; G. Lu et al., 2011), catalysis (Zoladek et al., 2018), antimicrobial activity (Aljaafari et al., 2020) and cytotoxicity. Malekmohammadi et al. developed a nanocomposite of AuNPs onto which FA was immobilized for targeted delivery. These rGO nanosheets coated with dendritic mesoporus silica were designed to act as nanocarriers for the anticancer compound curcumin. This system demonstrated biocompatibility, biodegradability, and an appropriate surface area, resulting in high drug loading capacity and pH-responsive release. The nanocarrier was tested against two cancer cell lines, MCF-7 and A549, and demonstrated specific targeted ability as well as photothermal potency toward MCF-7 (Malekmohammadi et al., 2018). According to Otari et al., rGO decorated with AuNPs was synthesized using a thermostable antimicrobial nisin peptide as an environmentally friendly method. Nanocomposites were used for their photothermal effects and they were tested against MCF-7 breast cancer cells. Cell growth was inhibited by more than 80% after 5 minutes of exposure to near infrared radiation (Otari et al., 2017). rGO has limitation such as poor dispensability, high

cytotoxicity and irreversible aggregation. Consequently, functionalizing rGO is a way to overcome these limitations (Yanfang Hu et al., 2016).

1.7 Aim of the study

-To develop drug loaded nano carriers using graphene derivatives for cancer therapy.

-To functionalize the nanocarriers to enhance their properties.

-To investigate:

-physicochemical properties

-drug loading and release profiles.

-the effect on MCF-7 cancer cells (viability, cellular uptake) of the nanocomposites

CHAPTER 2

MATERIALS & METHODS

2.1 Materials

-Materials used for synthesis of GO; Graphite powder (Ave.size: 3 mm, Ege Nanotek, Turkey), potassium permanganate ($KMnO_4$) (ISOlab, Germany), sulphuric acid (H_2SO_4), phosphoric acid (H_3PO_4) (ISOlab, Germany), hydrogen peroxide (H_2O_2) (ISOlab, Germany), hydrochloric acid (HCl) (Merk, Germany).

-Materials used for synthesis of AuNPs; Chloroauric acid ($HAuCl_4 \cdot 3H_2O$), gum Arabic (Sigma-Aldrich, USA), black seed from local market (Turkey).

-Materials used for doping of boron; boric acid (H_3BO_3) (Merck, Germany), ethanol (C_2H_5OH)

-Materials used for functionalization; Chitosan oligosaccharide (Sigma-Aldrich, USA), N-(3-dimethylaminopropyl)-N′-ethylcarbodiimide hydrochloride (EDC) (Sigma-Aldrich, USA), N-hydroxysuccinimide (NHS) (Sigma-Aldrich, USA), Hydroxyethyl cellulose (HEC) (Sigma-Aldrich, USA), polyethylene glycol 6000 (PEG 6000) (Merck, Germany), 2-(N-Morpholino) ethanesulfonic acid (MES).
- Reducing agent; L- ascorbic acid (LAA) (Sigma-Aldrich, USA).
-Drug used; Adrimisin 10 mg doxorubicin hydrochloride (DOX.HCl) ($C_{27}H_{30}ClNO_{11}$) (Saba, Turkey).

-Buffer preparation; Sodium chloride (NaCl) (Merk, Germany), potassium chloride (KCl) (Riedel-de-haen, Germany), disodium hydrogen phosphate (Na_2HPO_4) (Merk, Germany), potassoum dihydrogen phosphate (KH_2PO_4) (Merk, Germany), sodium citrate dihydrate ($C_6H_9Na_3O_9$), citric acid ($C_6H_8O_7$) (Sigma-Aldrich, USA).

-Reagents for cell culture study; fetal bovine serum (FBS), Penicillin/Streptomycin, Sodium pyruvate, Dulbecco's Modified Eagle Medium (DMEM) high glucose, 3-(4,5-dimethylthiazol-2-yl)-2,5-diphenyltetrazolium bromide (MTT), Dimethyl sulfoxide (DMSO), penicillin/streptomycin and trypsin/ethylenediamineteraacetic acid (Trypsin/EDTA) were the products of Biological Industries (Israel), paraformaldeyde powder (Sigma, USA)

2.2 Methods

2.2.1 Synthesis of graphene oxide

Graphene oxide (GO) was synthesized by Tour method (Dalgic et al., 2018). Firstly, 3 g of graphite powder was mixed with 18 g of potassium permanganate ($KMnO_4$) in glass beaker. Secondly, sulphuric acid (H_2SO_4) 360 ml and phosphoric acid (H_3PO_4) 40 ml (75%) solution was prepared in a a volume ratio (9:1). Then, the solution was added into powder mixture while stirring, and an increase in temperature up to 45°C was observed. The solution was continued to be stirred at 50°C for 12 h. After 12 h of stirring, heating was stopped and the solution color changed from greenish to purple brown. Then, 400 ml of dH_2O ice cubes were added to the solutiıon to stop the reaction. Afterwards, 3ml Hydrogen peroxide (H_2O_2) solution was added to the mixture after ice melted, and the color changed to light yellow, which is an indication of GO formation. After that tap water was added. The mixture was left for 3 days until all the GO settle down and then the solution was taken out and the precipitate was washed 3 times with dH_2O, one time with HCl (30%) and again 3 times with dH_2O. Afterwards, the precipitate was collected by centrifugation (5000 g for 8 min) (Hettich EBA 20, UK) and the homogenized at 12000 r/min as shown in (Figure 2.1).

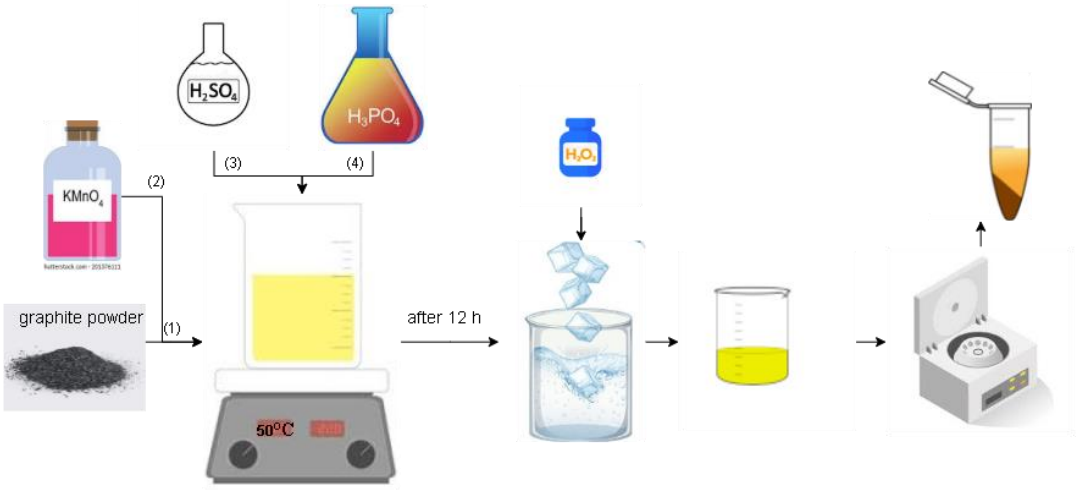

Figure 2.1 GO synthesis flowchart.

2.2.2 Synthesis of boron doped reduced graphene oxide

240 mg of GO was dispersed in 100 ml of dH_2O by ultrasonication (Branson SFX, USA) until a clear solution was obtained. 28.6 mg of boric acid at 60°C was dispersed in 10 ml of ethanol. The two solutions were then mixed and stirred for 8 h at 80°C. The sample was ultrasonicated (Branson SFX, USA) and then washed with dH_2O. After that, it was dried in a fanned convection laboratory oven (Carbolite Eurotherm,England) at 180°C for 24 h (Shuaib et al., 2020) as seen in Figure 2.2.

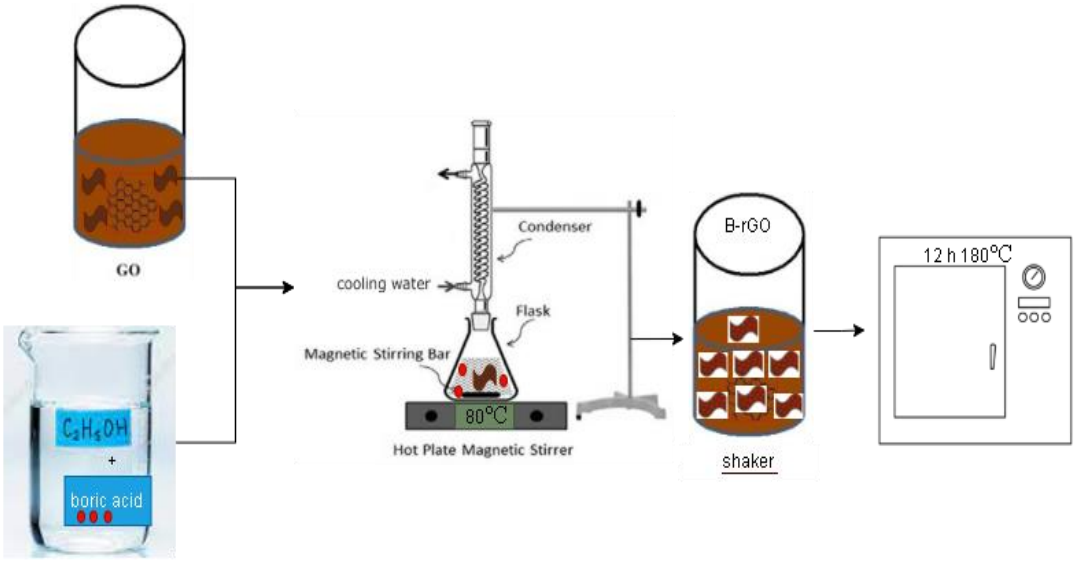

Figure 2.2 B-rGO synthesis flowchart.

2.2.3 Synthesis of B-rGO decorated with AuNPs

After stirring B-rGO at 80°C for 8 h, 50 ml of the mixture was taken and 1 ml of gold salt solution was added and kept under shaking for 4 h, after which 15 ml of black seed extract, 8.6 ml of dH_2O, and 103.4 mg of gum Arabic were added and stirred before being placed in a microwave at 700 W for 1 minute. The sample was ultrasonicated (Branson SFX, USA) and then washed three times with dH_2O. Then it was dried in a fanned convection laboratory oven (Carbolite Eurotherm, England) at 180°C in for 24 h as seen in Figure 2.3.

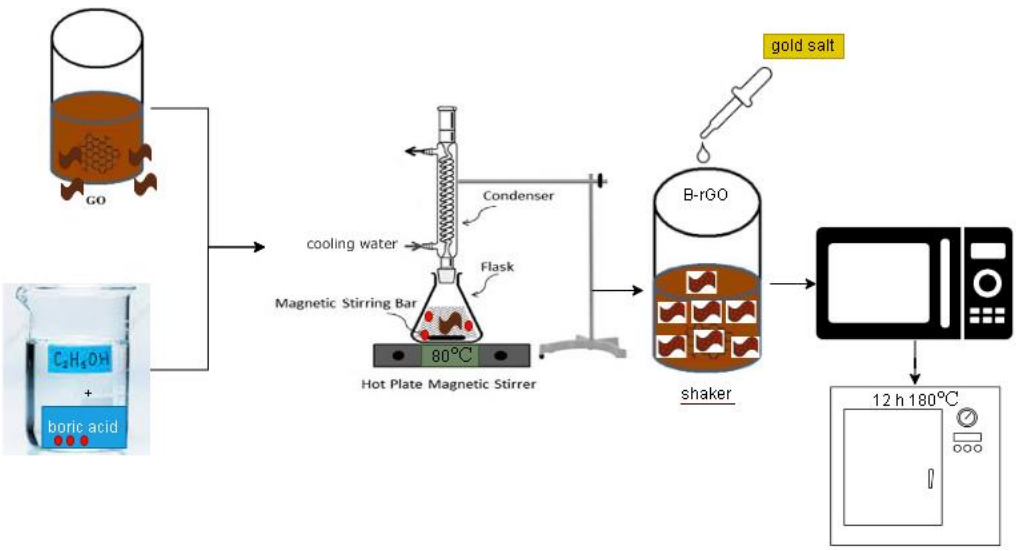

Figure 2.3 Au-B-rGO synthesis flowchart.

2.2.4 Synthesis of boron doped graphene oxide

Boric acid saturated solution was made and 30 mg of GO was dispersed in 10 mL of boric acid solution. 90 minutes of ultrasonication was performed using a sonicator (Branson SFX, USA) and the solution was lyophilized for two days using a freezedryer (Labconco, USA). The dried B-GO was annealed in an oven set at 700°C at a rate of 5° min^{-1} under argon gas. The sample was kept at this temperature for 1 h before being gradually cooled to room temperature using argon gas, as seen in Figure 2.4 (M. Zhang et al., 2019).

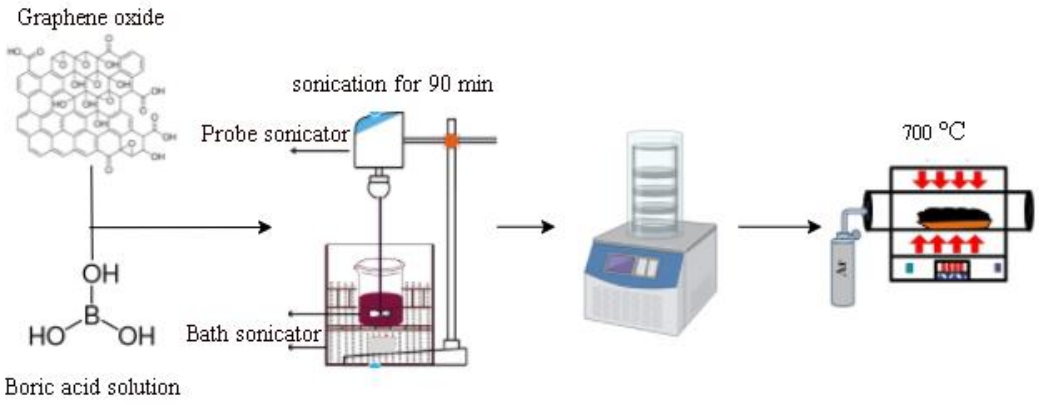

Figure 2.4 B-GO synthesis flow diagram.

2.2.5 Surface modification of graphene oxide and derivatives

The synthesized materials were functionalized with chitosan oligosaccharide (COS) to prevent agglomeration. The synthesized materials are COS-GO, COS-rGO, COS-B-rGO, COS-B-GO and COS-Au-B-rGO.

2.2.5.1 COS-GO

GO was modified with COS to see its effect on loading, release of the drug and cells. 0.250 g of COS and 50 mg of GO were dispersed in 25 ml of MES buffer (0.1 M, pH 5). For 1 h, the mixture was ultrasonicated using a probe sonicator (Branson SFX, USA). Chitosan was conjugated with GO via amidation in the presence of EDC and NHS. Both 0.326 g EDC and 0.391 g NHS were dissolved in 1 ml dH_2O and gradually added to the COS-GO mixture. The entire mixture was bath sonicated for 6 h at room temperature before being mixed for 16 h. The suspension was then dialyzed for 3~4 days against dH_2O by using (MWCO= 21 kDa). After that, the chitosan-grafted GO was lyophilized for two days (COS-GO) (D. Huang & Wang, 2013).

2.2.5.2 COS-rGO

rGO was modified with COS to enhance dispersibility of the semi hydrophobic material. Moreover, prevent agglomeration. 50 mg of COS-GO was dispersed in 100 ml of dH_2O and the pH was adjusted to 4 with acetic acid. L-ascorbic acid (50 mg) was added to the suspension for reduction GO and incubated at 90°C for 6 h. After the reaction was completed, the solution was dialyzed overnight to remove the excess L-ascorbic acid. Finally, COS-rGO was lyophilized for two days.

2.2.5.3 COS-B-rGO, COS-Au-B-rGO and COS-B-GO

50 mg of B-rGO/ Au-B-rGO/ B-GO was dispersed in 25 ml of MES buffer (0.1 M, pH 5) and the mixture was sonicated for 1 h to get a clear solution. Then, 0.250 g of COS was added. For 1 h, the mixture was ultrasonicated. COS was conjugated with B-rGO/ Au-B-rGO/ B-GO via amidation in the presence of EDC and NHS. Both 0.326 g EDC and 0.391 g NHS were dissolved in 1 ml dH_2O and gradually added to the COS-B-rGO/ COS-Au-B-rGO/ COS- B-GO mixture. The entire mixture was bath sonicated (Branson SFX, USA) for 6 h at room temperature before stirred for 16 h. The suspension was then dialyzed for 3~4 days against dH_2O by using (MWCO= 21 kDa). After that, COS-B-rGO/ COS-Au-B-rGO/ B-GO was lyophilized for two days (D. Huang & Wang, 2013).

2.2.5.4 Decoration of AuNPs onto COS-B-GO

COS-B-GO was decorated with AuNPs to enhance the drug loading of the nanocomposite. AuNPs were decorated after lyophilization of COS-B-GO. 100 mg of COS-B-GO was dispersed in 100 ml of dH_2O and sonicated until a clear solution was obtained. 1 ml of gold salt solution was added and shaken for 4 h before adding 15 ml of black seed extract, 8.6 mL of dH2O, and 103.4 mg of gum Arabic were added and mixed before placing in a microwave at 700W for 1 minute (Fragoon et al., 2012). The decoration was done after surface modification due to agglomeration problem. Modifying the surface with COS was not enough, it was observed to be pH dependent even with amide bond conjugation and the problem has not been solved. Another modification by Hydroxyethyl cellulose (HEC) was done.

To synthesize HEC-COS-rGO, 16.2 mg of GO was dispersed in 3 ml of dH_2O, 60 ml of acetic acid with (0.1 M) was added and sonicated to ensure good dispersion. After adding 48.6 mg of COS powder to the suspension and sonicated for 15 minutes, 48.6 mg of HEC was added to the suspension and sonicated for 30 minutes. The overall ratio of nanocarrier:COS:HEC was 1:3:3. 75 mg of L-AA was added and the mixture was stirred for 1 h at 70 °C (Mianehrow et al., 2016).

To synthesize HEC-COS-Au-rGO, 16.2 mg of GO was dispersed in 3 ml of dH_2O, 60 ml of acetic acid with 0.1 M was added and sonicated to ensure good dispersion. 1.6 ml of gold salt of 5 mg/ml was added and the suspension was shaken for 30 min. Afterwards, 40 mg of L-AA were added, the color changed to redish purple. Then, 48.6 mg of COS powder was added to the suspension and sonicated for 15 minutes. Afterwards, 48.6 mg of HEC was added to the suspension and sonicated for 30 minutes. 40 mg of L-AA was added and the mixture was stirred at 70°C for 1 h (Mianehrow et al., 2016).

2.2.6 Synthesis of graphene oxide quantum dots (GOQDs)

To syntheize GOQDs, 24 mg of GO was dispersed in 3 ml, at 80 °C, and 40 ml of H_2O_2 (30%) was added. Afterwards, 7 ml of ammonia (25-28%) was gradually added to the mixture and the entire mixture was left for 24 h with vigorous stirring to obtain a light yellow transparent solution. To remove large particles, a 0.22 µm membrane was used (Ghanbari et al., 2021). The quantum dots were lyophilized for 3 days before being dispersed in 24 ml of MES buffer of pH 6 at a concentration of 1 mg/ml.

2.2.6.1 Conjugation of gluocose amine (GlcN) on GOQDs

20 ml of GOQDs (1 mg/ml) was added to 10 ml of MES buffer (0.1 M, pH 6) containing 13.3 mg of glucosamine. 320 mg of EDC and 106.6 mg of NHS were each dissolved in 5 ml of MES buffer separately, then slowly added to the GOQDs-GlcN solution. The reaction was completed after 20 h, filtered using an Amicon

ultra-centrifugal filter (3 kDa). After that thesolution was lyophilized for two days (Ghanbari et al., 2021).

2.2.6.2 Synthesis of GOQD-GlcN with boric acid (BA)

Sodium bicarbonate and sodium carbonate were used to prepare the bicarbonate buffer. In 5 ml dH_2O, 315 mg of sodium bicarbonate (0.747 M) and 44 mg of sodium carbonate (0.083 M) were dissolved and the pH was adjusted up to pH 9. 3.4 ml of GOQD-GlcN was mixed with 0.6 ml of bicarbonate buffer. An excess of BA 500 mg in 1 ml of water and then added to the mixture. Then, 5 ml of the mixture was kept under stirring for 24 h. The nanocomposite was dialyzed for 24 h against (1 M) NaCl to remove BA bind with ionic interaction, and then against dH_2O to remove BA and NaCl. Dialysis was performed using an Amicon ultra-centrifugal filter (cut off: 3 kDa) (Islam et al., 2021).

2.3 Characterization of the nanomaterials and quantum dots

The nanomaterials were characterized with Fourier transform infrared spectroscopy (FTIR), X-ray diffraction (XRD), X-ray photoelectron spectroscopy (XPS) and energy dispersive X-ray spectroscopy (EDS), Scanning electron microscopy (SEM), and Transmission electron microscopy (TEM).

The quantum dots were characterized with FTIR, Inductively Coupled Plasma-Mass Spectrometry (ICP-MS), and TEM.

The FTIR spectra were used to identify the bonds formed on all synthesized material. For FTIR analysis, the compound system consisting of a spectrometer and a microscope (Bruker IFS 66/S and Hyperion 1000, Germany) was used. The samples were examined in the mid-infrared (MIR) range (between 4000-400 cm^{-1}).

The XRD analysis was used to determine the crystals defraction of GO, B- rGO, and Au-B-rGO. The analysis was performed with a diffractometer (Rigaku Ultima-IV,

Japan) with Cu-Kα radiation at 40 kV and 30 mA. The scan range was between 5 and 80˚ in 2θ. The ratio of duration time/scan was 1 deg/min and the ratio of step/sampling step was 0.02 deg. The phases present in the coatings were determined by using the pdf database of International Centre for Diffraction Data® (ICDD).

XPS was performed to identify the functional groups at GO and Au-B-rGO, COS-GO, COS-rGO, COS-B-rGO, and COS-Au-B-rGO. XPS was performed by using a PHI 5000 VersaProbe. XPS is a technique for analyzing the surface chemistry of a material. XPS can measure the elemental composition, empirical formula, chemical state and electronic state of the elements within a material.

The surface morphology of GO and B-Au-rGO nanocomposite was observed with a SEM. The microscopic images were taken by a field emission scanning electron microscope (FE-SEM, FEI Quanta 400F, USA). The images were taken without Au/Pd coating. In addition, elemental composition of the coatings was analyzed by using the energy dispersive X-ray spectroscopy (EDS) set-up.

Zeta potential of the nanocomposites was determined by Laser Doppler Electrophoresis using zeta sizer NanoZS (METU Biomatten) to assess the surface charge of COS-GO, COS-rGO, COS-B-rGO, and COS-Au-B-rGO.

ICP-MS was used to determine the elements in the sample. ICP-MS was performed by (ICP-MS, Perkin Elmer Plasma 400). For qunatum dots, it was used to determine the presence of boron element.

TEM was used to determine the morphology and size of the quantum dots (TEM) (FEI Tecnai G2 Spirit BioTwin CTEM, Middle East Technical University Central Laboratory). Before analysis the samples were dispered in water dH_2O. The samples were prepared by using 300-mesh carbon film coated copper grids. The size of the nanoassemblies were measured by Image J program. The area of the particles were obtained from TEM images and then the diameters of 50 particles from each nanoassembly were calculated.

2.4 Drug loading and release studies

2.4.1 Preparation of buffers at different pH

PBS buffer (pH 7.4, 1M) was prepared by dissolving 8 g of NaCl, 0.2 g of KCl, 1.44 g of Na_2HPO_4 and 0.24 g of KH_2PO_4 in 800 ml of dH_2O. The pH was adjusted to 7.4 with NaOH. Finally, adjust the volume to 1 L with additional dH_2O.

Citrate buffer (pH 5.5, 1M) was prepared using sodium citrate dihydrate and citric acid. To make 0.5 L of buffer, 10.342 g of sodium citrate dihydrate was dissolved in 400 ml of dH_2O, then 2.85 g of citric acid was added to the solution. The pH was adjusted to the final pH by adding NaOH. dH_2O was added until the volume reached 0.5 L

Citrate buffer (pH 4, 1M) was prepared using sodium citrate dihydrate and citric acid. To make 0.5 L of buffer, 4.964 g of sodium citrate dihydrate was dissolved 400 ml of dH_2O, then 3.363 g of citric acid was added to the solution. The pH was adjusted to the final pH by adding NaOH or HCL. dH_2O was added until the volume reached 0.5 L.

2.4.2 Doxorubicin loading of the synthesized nanomaterials

2.4.2.1 DOX loading in GO, COS-rGO, COS-B-rGO, COS-Au-B-rGO, PEG-B-GO

0.4 ml of 1 mg/ml DOX in DMSO was combined with 1.2 ml of nanomaterial suspension (1 mg/ml of in PBS). The drug to carrier ratio was one-to-three (w/w). 2.4 mL of PBS was then added. The loading media contained 10% DMSO. The mixture was then stirred at room temperature for 24 h. After 24 h, unbound DOX was removed by centrifugation (11500 g, 15 min) (Hettich EBA 20, UK). The fluorescence of the supernatant was measured by spectrofluorometer to detect the fluorescence intensity, with excitation wavelength 490 nm and emission 600 nm. The amount of unbound in the supernatant was determined using a calibration

constructed with different comcentrations of DOX in PBS (0- 60 µg/ml) (Figure A 1 & Figure A 2) and the loading efficiency and drug loading capacity of the nanomaterials were calculated using Eq.1 and 2.

$$\% \text{ Loading efficiency} = \frac{\text{Weight of loaded drug} - \text{Weight of unbound drug}}{Weight\ of\ loaded\ drug} \times 100 \quad (1)$$

$$\text{Drug loading capacity} = \frac{Weight\ of\ the\ loaded\ drug}{\text{Total weight of the nanocomposite}} \times 100 \quad (2)$$

2.4.2.2 DOX loading into GOQD-GlcN and GOQD-GlcN-BA

0.45 ml of 1.2 mg of the nanocomposite suspension was dispersed in 0.85 ml dH_2O. Afterwards, 0.2 ml of 2 mg/ml DOX was then added and stirred at room temperature for 24 h. The drug to carrier ratio was one-to-three (w/w). After 24 h, unbound DOX was removed by dialysis using dialysis bags with a cutoff 3.5 kDa. After 8 and 24 h, the medium was refreshed with 5 ml PBS. The fluorescence intensity of the dialysates was measured using excitation wavelength 490 nm and emission 600 nm via microplate spectrophotometer (µOuantTM, Biotek Instruments Inc., USA) and the total amount of unbound DOX was determined using the calibration curve constructed with different concentrations of DOX in PBS. The loading efficiency and drug loading capacity OF GOQD-GlcN and GOQD-GlcN-BA were determined using Eq.1 and 2.

2.4.2.3 In vitro release studies

The drug release from the GO was studied at 37.5°C at two different recipient media: pH 4 (citric buffer saline) and pH 7.4 (phosphate buffer saline) (n=3). 0.2 mg/ml of the sample was placed in the receptor media in Eppendorf tubes. The media contained 10% DMSO. At various time intervals (1, 2, 6, 8, 24, 48, and 72 h) the released drug was detected, and replaced with same amount of fresh medium.

Centrifugation was used to obtain a pellet and detect the amount of the released drug in the supernatant and and the fluorescence of the supernatant was measured. The amount of DOX released was determined using the calibration curves (Figure A 1 & Figure A 2). To compute the percentage of drug release Eq.3 was used.

The drug release from the nanocomposites GOQD-GlcN and GOQD-GlcN-BA was studied at 37.5°C in two different recipient media: pH 5.5 (citric buffer saline) and pH 7.4 (phosphate buffer saline). 0.6 mg of the sample was placed in dialysis bag with 3 ml media. At various time intervals (1, 2, 6, 8, 24, 48, 72 and 96 h), aliquots (0.1 ml) from the release media was withdrawn and replaced with same amount of fresh medium. The fluorescence of the supernatant was measured. The amount of DOX released was determined using the calibration curves (Figure A 3 & Figure A 4). To compute the percentage of drug release Eq.3 was used.

$$\% \text{ Drug release} = \frac{Weight\ of\ free\ DOX}{Weight\ of\ loaded\ DOX} \times 100 \quad (3)$$

2.4.3 Cell culture studies

MCF-7 cells were cultured in media composed of 10% FBS, 1% penicillin/streptomycin, 1% sodium pyruvate, and 88% DMEM.

Cytotoxicity study was performed to see the effect of different concentrations of the synthesized quantum dots on MCF-7 breast cancer cells. MCF-7 cells were seeded in 96 well plates (4×10^3 cells/well) and cultured in a DMEM cell culture medium for 5 h under humidified atmosphere of 5% CO_2 – 95% air in incubator (SHEL LAB, USA). The cells were then treated for 24 h in a DMEM medium with various concentrations of nanomaterials (0, 1.25, 2.5, 5, 10, and 20 µg/ml) of GO, (0, 6.25, 12.5, 25 and 50 µg/ml) of GOQD-GlcN and GOQD-GlcN-BA, and (0, 2, 4, 8,16, 32 µg/ml) of GOQD-GlcN-DOX, GOQD-GlcN-BA-DOX and only DOX (Ghanbari et al., 2021). After 24 h, the cells were washed with PBS, fixed with 100 µl paraformaldahyde for 15 min, and then washed again with PBS after washing, the well plate was stored at 4°C with 100 µl PBS and they were used to take imagies of the cells. Phase contrast images were taken for each concentration by phase contrast

microscope (Nikon Eclipse TS 100). After that, the medium was discarded and the cells were washed with 150 µl PBS, to remove the physically adsorbed nanomaterials before adding MTT solution. 100 µl of fresh DMEM and 10 µl of MTT solution were added (5 mg/ml, 10 µl) to each well and cells were incubated for a 4-h. Finally, the medium was discarded and 50 µl of DMSO was added to dissolve the formed formazan violet crystals after the medium was removed. At 570 nm, a microplate reader was used to measure the absorbance of formazan in DMSO solution.

The % viability of the cells was calculated by the optical density (ODs) Eq. (4)

$$\% \text{ Cell viability} = \frac{ODs\ of\ the\ cells\ treated\ with\ the\ samples}{ODs\ of\ the\ control} \times 100 \qquad (4)$$

2.4.3.1 Confocal laser microscopy assay

MCF-7 cells were used to verify the drug delivery of DOX, GOQD-GlcN-DOX and GOQD-GlcN-BA-DOX. The cells (17 x 10^3 cells/well) were seeded onto 24 well plate and cultured for 24 h. After 24 h, the cells were washed with PBS and then incubated with DOX (33.7 µg/ml), GOQD-GlcN-DOX and GOQD-GlcN-BA-DOX at 37°C for 1, 8 and 24 h. After incubation, the cells were washed with PBS and then fixed for 20 min with 200 µl paraformaldehyde, after washing with PBS, the well plate was stored at 4°C with 200 µl PBS after cell fixation. The quantum dots were excited with 488 nm laser and the emission was collected from 500 nm to 530 nm. The DOX drug was excited with 488 nm laser and the emission signal was collected from 552 nm to 617 nm (X. Wang et al., 2014).

2.4.4 Statistical analysis

To compare groups for single parameter, one-way Analysis of Variance (ANOVA) test was applied. Tukey's Multiple Comparison Test for the post-hoc pairwise comparisons (SPSS-22 Software Programme, SPPS Inc., USA) was used; $p < 0.05$ was considered as statistically significant results.

CHAPTER 3

RESULTS & DISCUSSION

3.1 Characterization results

3.1.1 FTIR

The FTIR spectra of GO, B-rGO, Au-rGO, and B-Au-rGO nanocomposites are shown in Figure 3.1. The oxidation of graphite produces GO, which contains a large number of oxygen-containing functional groups. These groups are depicted in Figure 3.1 (a), At 3196 cm^{-1}, a broad band corresponding to the hydroxyl group O-H and the presence of oxygen functional groups in GO is assigned. C-H stretch is at 2917 cm^{-1}. The stretching vibrations of C=O carboxylic acid groups at 1729 cm^{-1} (Emadi et al., 2017) and C=C are represented by peaks at 1616 cm^{-1}. Furthermore, epoxy stretching C-O occurs at 1220 cm^{-1}, O-H deformation occurs at 1373 cm^{-1}, and alkoxy stretching occurs at 1040 cm^{-1} (Xu et al., 2015) and C-O-C groups at 1159 cm^{-1} (Mianehrow et al., 2016). In FTIR spectra shown in parts (b) and (c) it is observed that when GO is reduced and the oxygen-functional groups are reduced and some of the peaks are completely removed, such as the O-H group, carbonyl and epoxy groups, indicating the removal of oxygen to a certain level. Furthermore, the decrease in GO shifted the C=C peak from 1616 cm^{-1} to 1558 cm-1. Doping rGO with boron results in the formation of some peaks due to boron atom bonding. At point (b). The peak at 1104 cm^{-1} corresponds to the B-C stretching vibration, which was observed between 1050 and 1200 cm^{-1} (Shuaib et al., 2020). In addition, the peak at 776 cm^{-1} is the bending vibration of bridge oxygen B-O-B (C. C. Zhang et al., 2020). (c) shows the spectrum of Au-B-rGO nanocomposite, and the decoration had no effect on the FTIR spectrum. Finally, the spectrum of the nanocomposite combining B, Au, and rGO results in the appearance of boron peaks at 1167 cm^{-1}

corresponding to the stretching vibration B-C (Shuaib et al., 2020) and BO_3 at 757 cm^{-1} (C. C. Zhang et al., 2020).

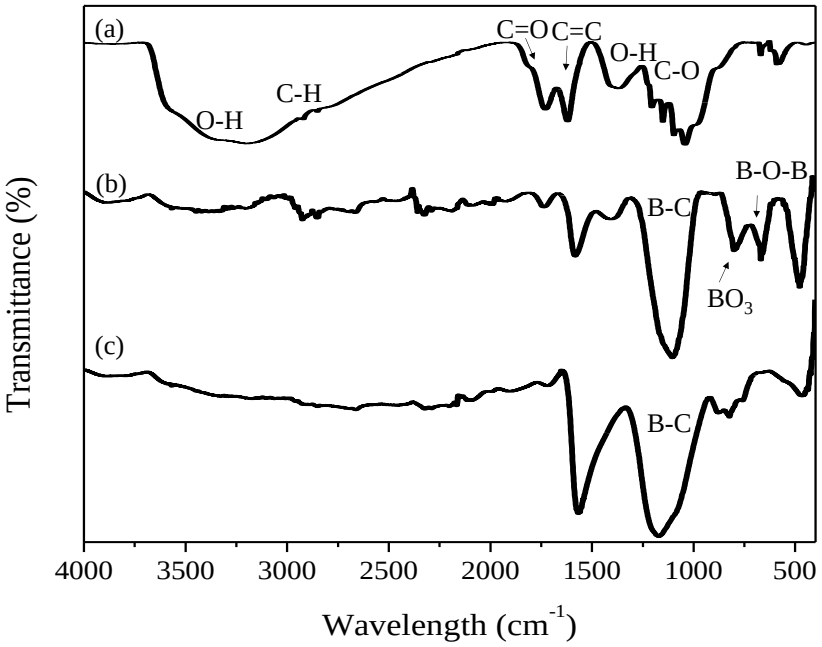

Figure 3.1 FTIR results of (a) GO, (b) B-rGO, and (c) Au-B-rGO.

The FTIR spectra of GO, COS-GO, COS-rGO, COS-B-rGO and COS-Au-B-rGO nanocomposites are shown in Figure 3.2. The oxidation of graphite results in the formation of GO, which contains a large number of oxygen-containing functional groups. These groups are depicted in Figure 3.2 (a). The spectra of COS can be found at Figure 3.2 (b). 3241 cm^{-1} corresponds to the –OH and N-H stretching. The C-H symmetric and asymmetric stretching occurred at approximately 2932 and 2875 cm^{-1}. The peak at 1243 cm^{-1} represents the free primary amino group (-NH_2). 1311 cm^{-1} corresponds to the stretching of amide III. The N-H bending of amide II occurred at 1511 cm^{-1}. Furthermore, the peak at 1375 cm^{-1} confirmed the CH_3 symmetrical deformations. Asymmetric stretching of the C-O-C bridge occurred in the absorption band at 1159 cm^{-1}. Finally, the two bands 1057 and 1029 cm^{-1} correspond to C-O stretching (Queiroz et al., 2015). COS conjugation with GO, rGO, B-rGO, and Au-

B-rGO are represented by (c), (d), (e), and (f) respectively. The reaction of the carboxylic group of GO with the NH_2 group of chitosan resulted in a peak at 1634 cm^{-1} corresponding to the amide linkage NHCO, resulting in the disappearance of the carboxylic acid peak when compared to GO at both COS-GO and COS-rGO. Furthermore, when the OH group of GO interacts with COS, the primary alcohol C-O peak becomes more intense (Emadi et al., 2017). At 1559 cm^{-1}, a newly formed amide bond caused N-H bending of secondary amide (D. Huang & Wang, 2013). The peak at 898 cm^{-1} corresponds to the CH bending (Queiroz et al., 2015).

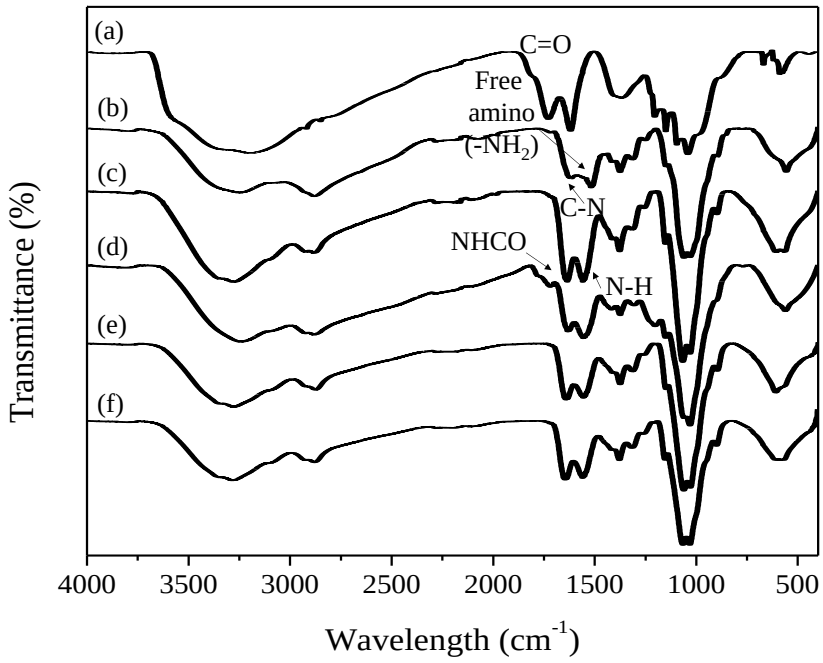

Figure 3.2 FTIR patterns of (a) GO, (b) COS, (c) COS-GO, (d) COS-rGO, (e) COS-B-rGO, and (f) COS-Au-B-rGO.

The FTIR spectra of GOQD, GOQD-GlcN, GlcN, GOQD-GlcN-BA, BA are illustrated in Figure 3.3. The surface functional groups of GOQD characterized with large number of oxygen functional groups are shown in Figure 3.3 (a). 3423 cm^{-1} corresponds to the –OH. The stretching vibrations of C=O carboxylic acid groups at 1748 cm^{-1}, and C=C are represented by peaks at 1616 cm^{-1}. The peak at 1381 cm^{-1}

represents streching vibration of C-O of the carboxyl group. Asymmetric stretching of the C-O-C bridge occurred in the absorption band at1123 cm^{-1}. At (b) is the nanocomposite with GOQD-GlcN, conjugated with EDC/NHS reaction, and at (c) is the spectrum of glucosamine. The conjugation of GlcN to GOQD confirmed with NH-CO and N-H groups at 1635 cm^{-1} and 1554 cm^{-1}, respectivly (Ghanbari et al., 2021). Thus resulting in the disappearance of the carboxylic acid peak. BA spectrum is shown at (e), and the addition of BA to GOQD-GlcN is shown at (d), the peak at 1388 cm^{-1} representing the B-O (W. Zhang et al., 2016).

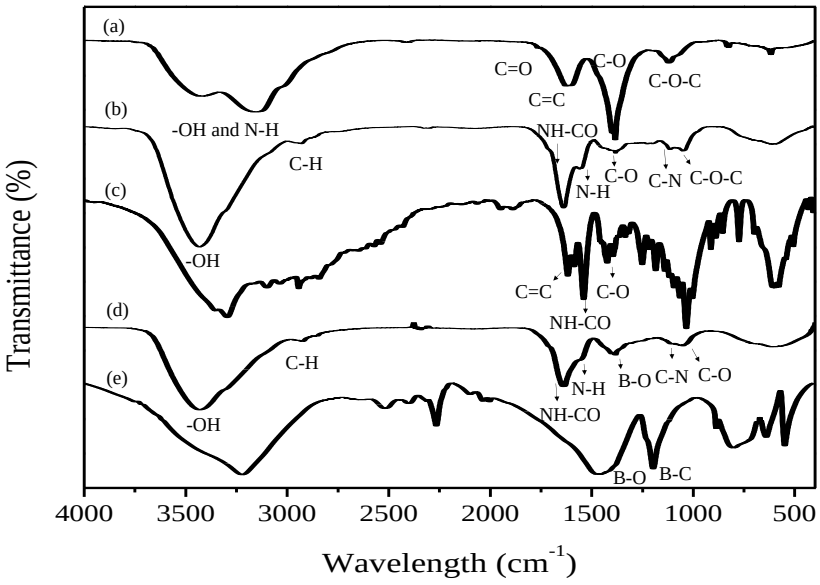

Figure 3.3 FTIR patterns of (a) GOQD, (b) GOQD-GlcN, (c) GlcN, (d) GOQD-GlcN-BA, (e) BA.

3.1.2 XRD

The crystal structure of GO, B- rGO, and Au-B-rGO were analyzed and determined by XRD and the patterns are represented in Figure 3.4 (a), (b), and (c) respectively. Figure 3.4 (a) demonstrated GO, and since there is no JCPDS standard for GO the results agreed with literature. However, strong peak at $2\Theta=10.62°$ with (001) plane

occurred with an interlayer spacing of 8.3 Å corresponding to the presence of oxidized graphite layers. Nanocomposite structure of boron doped rGO is shown in Figure 3.4 (b). However, a broad diffraction peak at 2Θ=26.2° with d-spacing 3.86 Å, corresponding the successful reduction of GO. Figure 3.4 (c) shows the nanocomposite structure of Au-B-rGO. The diffraction peak at 26° with (002) plane corresponds the great reduction of GO. At the same time AuNPs crystal structure occurred at 2Θ=38.3°, 44.6°, 64.6° and 77.9° diffraction peaks and they reflect (111), (200), (220), (311) and (222) planes, respectively, the face centered cubic (FCC) structure of metallic gold. In addition, the sharp peak at (111) suggests the crystalline nature of AuNPs. However, the results confirm the formation of the nanocomposite (Otari et al., 2017). Moreover, all the results agree with the JCPDS standard for rGO (JCPDS file #75-1621) and for AuNPs (JCPDS file # 04-0784). Doping rGO with boron illustrate great effect on preventing stacking of the sheets.

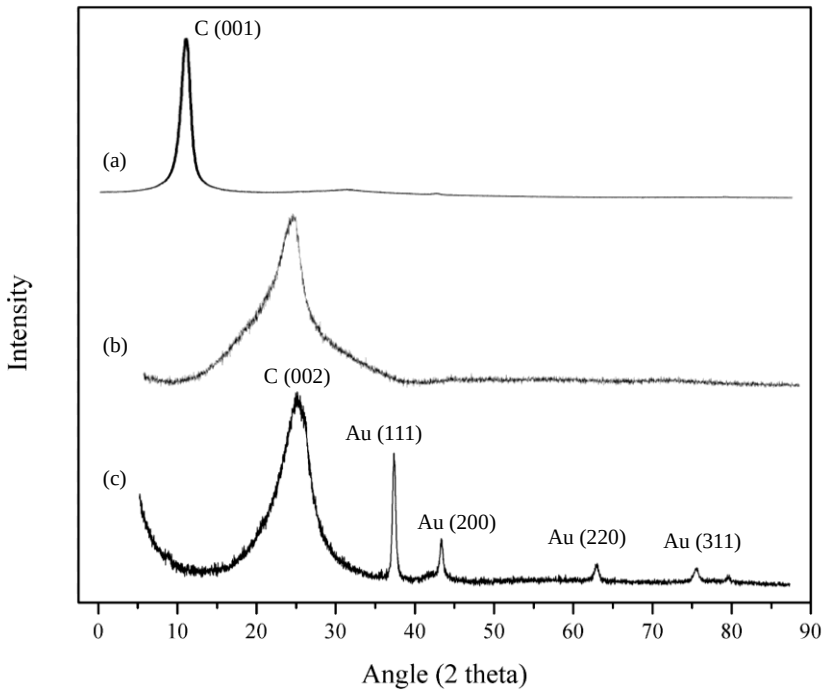

Figure 3.4 XRD pattern of (a) GO, (b) B- rGO, and (c) Au-B-rGO.

3.1.3 XPS

Figure 3.5 shows the XPS analysis of GO and Au-B-rGO, COS-GO, COS-rGO, COS-B-rGO, and COS-Au-B-rGO to determine their chemical composition. The XPS spectrum depicts the C1s and Au characteristic bands. The C1 spectrum of GO and Au-B-rGO nanocomposite is shown in (a) and (b), with three main peaks arising at binding energies of 283.6 eV corresponding to C-H bonding and 285.9 eV corresponding to C-O single bond network of epoxide and hydroxyl oxygen functional groups. Furthermore, small and broad shoulders at 287.9 eV correspond to carbonyl groups C=O, whereas Au-B-rGO shows nearly identical groups with one of the oxygen functional groups removed, indicating the removal of the oxygen functional group. The double peaks of the elemental states Au4f that result from spin-orbit coupling ($4f_{7/2}$ and $4f_{5/2}$) clearly show the Au element in (c). With binding

energies of 83.9 and 87.6 eV, respectively, $Au4f_{7/2}$ and $Au4f_{5/2}$ are attributing to metallic Au^0. (Kadiyala et al., 2018). However, that is confirming the formation and decoration of AuNPs on Au-B-rGO. The C1 spectrum of the chitosan functionalized materials, COS-GO, COS-rGO, COS-B-rGO, and COS-Au-B-rGO, is shown in (d), (e), (f), and (g). The peak at 284.9-285 eV corresponds to the C-N bond between the COS and GO/rGO in all of the spectrums, indicating successful conjugation. Moreover, two additional peaks occurs at 283 eV and 286 eV corresponding to C-C and C-O bond, respectively (D. Huang & Wang, 2013).

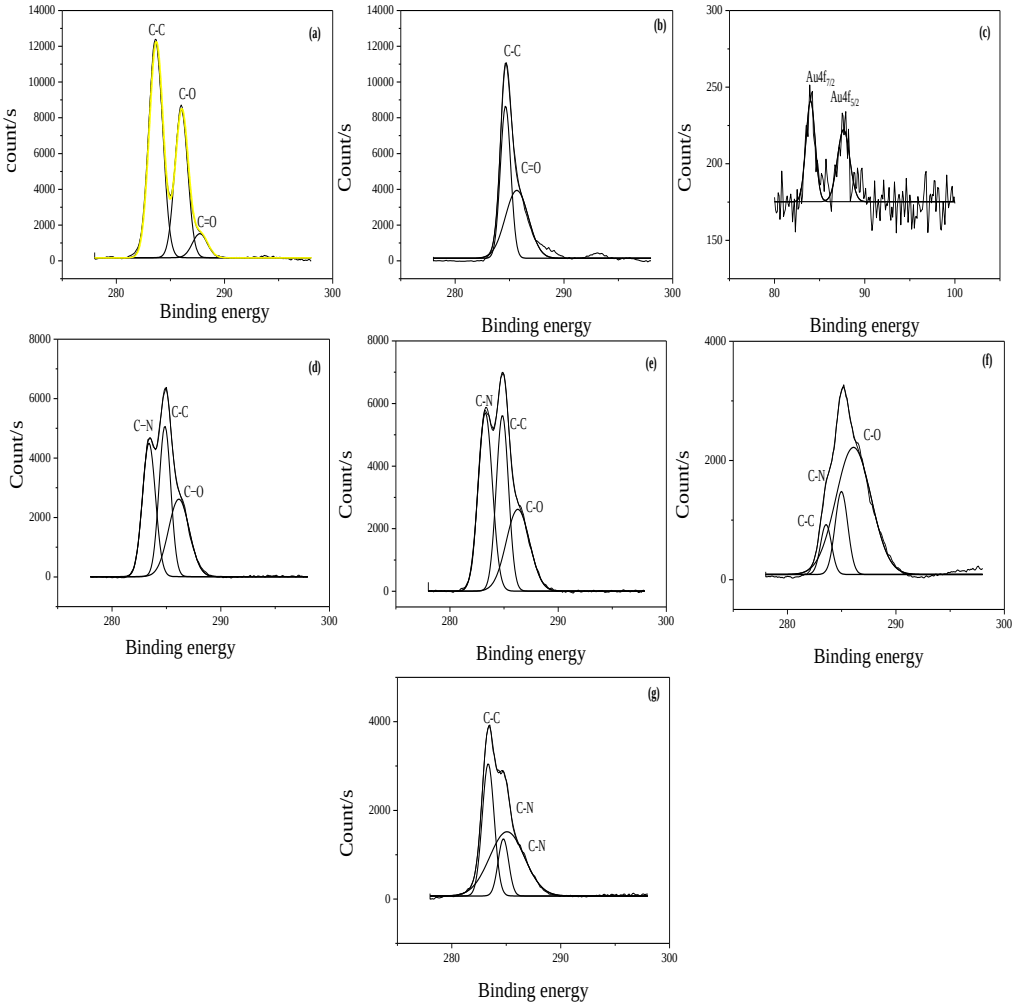

Figure 3.5 XPS results of C1s (a) GO, (b) Au-B-rGO, At (c) is the Au of Au-B-rGO nanocomposite, (d) COS-GO, (e) COS-rGO, (f) COS-B-rGO, (g) COS-Au-B-rGO nanocomposites.

3.1.4 SEM and EDS of GO, B-rGO, and Au-B-rGO

SEM image was taken to see the the surface morphology of GO. The surface morphology was similar (Figure 3.6), with the literature (T. Lu et al., 2020). The image shows the bulk size of GO after drying, with sheets stacking on top of one another to form a thick sheet. The surface structure changed after boron doping and

GO reduction, with bumps and rough surface due to the loss of many oxygen functional groups and the presence of boron (Y. Huang et al., 2017), as shown in Figure 3.7 (a) and the EDS showed a significant reduction in high carbon content when compared to the oxygen shown in Figure 3.7 (b). Boron peak did not appear due to the low doping percentage.

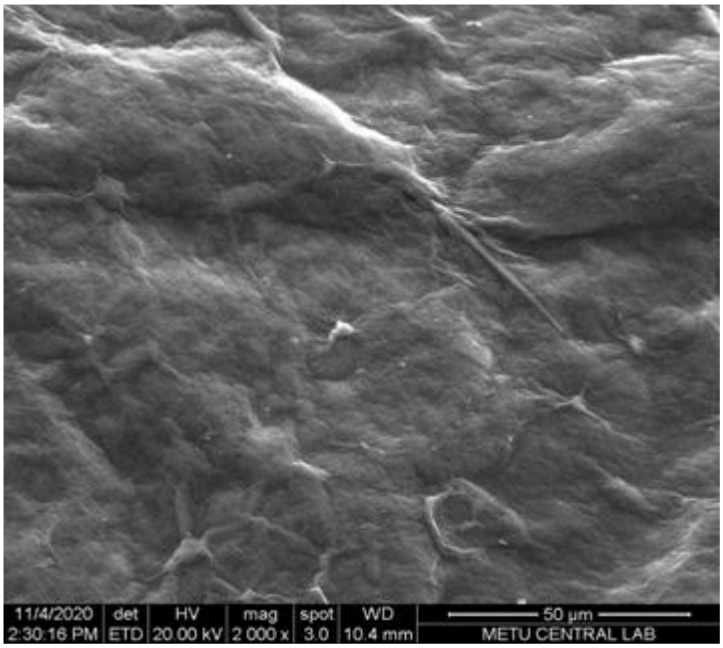

Figure 3.6 SEM image of the GO surface after drying at 50 °C, for 24 h in a fanned convection laboratory oven.

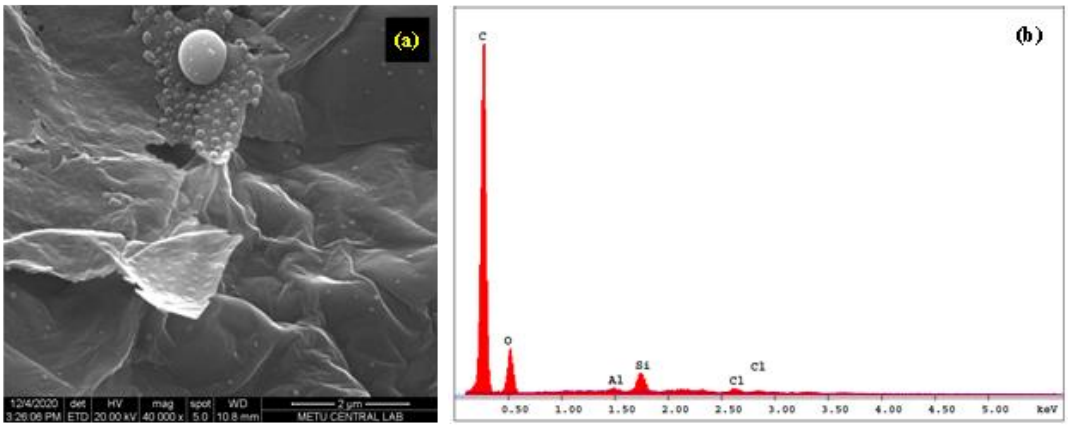

Figure 3.7 SEM image of B-rGO nanocomposite (a) the surface of B-rGO (b) the EDS of B-rGO.

Presence of AuNPs at the top of the rGO sheet is clearly shown in Figure 3.8 (a). Furthermore, EDS demonstrated the presence of Au element with good GO reduction In Figure 3.8 (b) high carbon percentages in comparison to oxygen percentages, indicated the removal of oxygen functional groups (Sadhukhan et al., 2016).

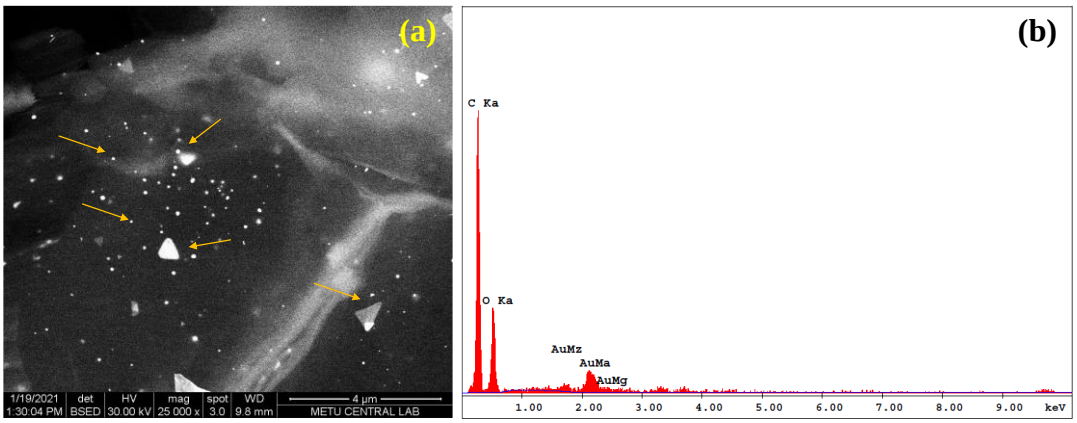

Figure 3.8 SEM image of the surface of Au-B-rGO nanocomposite (a) (b) EDS result of Au-B-rGO.

3.1.5 TEM

The morphology and size of the QDs (GOQD, GOQD-GlcN and GOQD-GlcN-BA) were characterized by TEM (Figure 3.9). The unmodified GOQDs showed spherical shape with average diameter was about 15.9 nm (Biswas et al., 2021)as seen in Figure 3.9 (a). The modification of the QDs with GlcN occurred as thin layer as in Figure 3.9 (b) the. However, the size of the spherical GOQD-GlcN did not change much and the average diameter was found as 26.6 nm (Karimi & Namazi, 2020). Figure 3.9 (c) shows the morphology of GOQD-GlcN-BA. Some of the QD showed some change in the shape whereas, some were still spherical. The average diameter of GOQD-GlcN-BA is 51 nm and it is suitable as drug carrier. Similarly, sizes reported in the literature for quantum dots nanocomposite drug carriers were at nanoscale (i.e., 129 nm (Javadian et al., 2021) and 25 nm at (Su et al., 2017)).

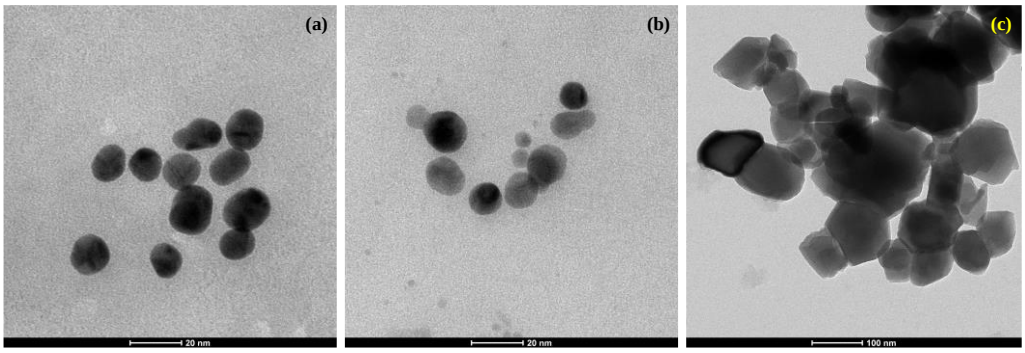

Figure 3.9 TEM images of (a) GOQD, (b) GOQD-GlcN, (c) GOQD-GlcN-BA.

3.1.6 ICP

ICP was done to GOQD-GlcN-BA material to determine the amount of boron element. The weight percent of boron in the nanocomposite was 4%, comparing to only 9% obtained by (Islam et al., 2021).

3.1.7 Surface charge analysis

The surface charge of the materials after functionalization was determined using zeta potential as shown in Figure 3.10. GO and rGO are typically characterized by negative charge due to the COO- functional groups, and the greater the number of these groups, the more –ve and stable the surface charge, as it reflects the degree of repulsion between similar charged surfaces (Navaee & Salimi, 2015). However, the functionalization of GO, B-rGO, and Au-B-rGO resulted in a positive surface charge, which reflects the surface charge of chitosan and successful conjugation (Yan et al., 2017). Functionalized rGO, on the other hand, had a negative surface charge. Although the surface charge is not high, it indicates that only a few of the oxygen functional groups in the system have not been functionalized. The amount of chitosan, on the other hand, was lower, resulting in partial precipitation after one day, indicating low stability due to π-π stacking in the deoxygenated surfaces (Shu et al., 2021).

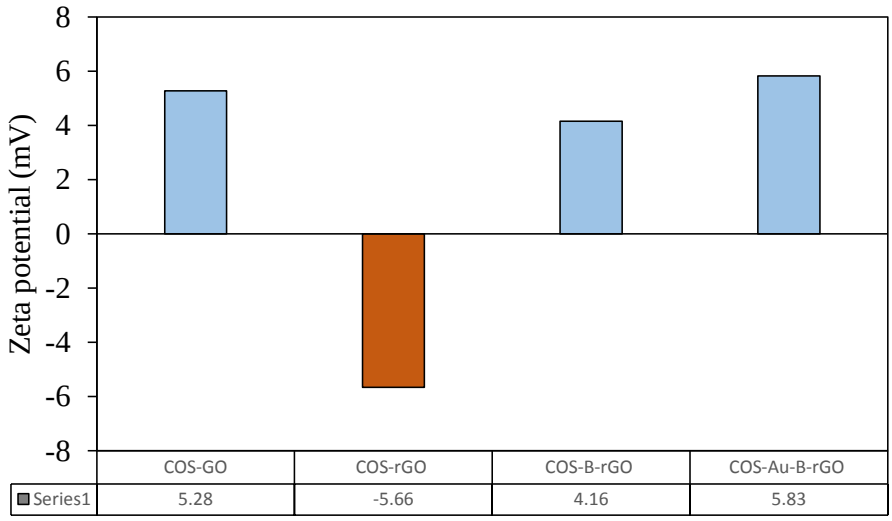

Figure 3.10 Zeta potential after functionalization with chitosan.

3.2 Drug loading and drug release results

3.2.1 GO and (b) rGO (c) B-rGO and (d) Au-B-rGO.

DOX has strong fluorescence (Shah et al., 2017), thus the DOX amount was measured by fluorescence readings. Insensitivity of DOX to 2-8 pH range was reported (Yamada, 2020), and accurate fluorescence intensity obtained for pure DOX. Doxorubicin hydrochloride drug has limited solubility and precipitate at PBS buffer due to dimerization (Yamada, 2020). Therefore, DMSO was used to ensure complete solubility of DOX drug before dispersing it in PBS. On the other hand, DOX is readily soluble in water (Agrawal, 2007).

Many functional groups are either eliminated or reduced in number as GO is reduced. As a result, rGO is hydrophobic. The precipitation and agglomeration of sheets caused by attraction force is a problem that must be addressed. The first solution was to use ultrasonication to shrink the size of the rGO. However, due to the partial precipitation obtained, it did not work, and the agglomeration did not end.

The nanosheets were then functionalized with COS as the second solution. The electrostatic interaction between the nanosheets and COS was the first method used.

However, because COS is a pH sensitive polymer, at pH 7.4 it has become deprotonated, losing its +ve charge resulting precipitation of the nanosheets. The second method was to conjugate COS to the nanosheets with NHS and EDC through amide bond (D. Huang & Wang, 2013). Despite the fact that successful conjugation was established, precipitation occurred in neutral environment due to the deprotonation of COS amino groups. However, this precipitation is not seen at acidic pH due to the protonation of amino groups on COS chains (D. Huang & Wang, 2013), as seen in Figure 3.10 (c) COS-B-rGO and (d) COS-Au-B-rGO groups showed no precipitations because either the amount of material was very small due to the color of the solutions, or the presence of boron prevented the crumbling of the COS, which causes agglomeration in the the absence of boron as shown in Figure 3.11 (a) COS-GO and (b) COS-rGO.

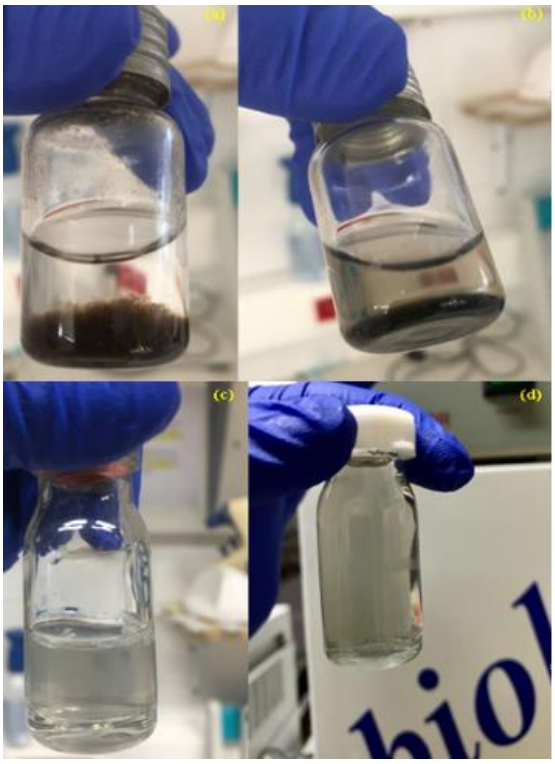

Figure 3.11 The precipitation obtained after COS conjugation with (a) GO and (b) rGO (c) B-rGO and (d) Au-B-rGO.

Another method which involved the use of COS and HEC was also tried (Mianehrow et al., 2016). Both polymers are electrostatically attached on the synthesized

nanomaterials forming polyelectrolytic complex. The presence of HEC acts as a barrier to prevent COS from crumbling in a neutral environment when it loses its deprotonated state. The successful functionalization of HEC-COS-rGO and HEC-COS-Au-rGO is shown in Figure 3.12. The loading of DOX with the same ratio obtained by GO resulted in a drug loading of only 5% for HEC-COS-rGO composition. This could be due to the carrier's high functionalization. In neutral environment the loading of DOX in GO occurs by hydrogen bonding, ($-COOH_{GO}$ and $-OH_{DOX}$), ($-COOH_{GO}$ and $-NH_{2DOX}$), ($-OH_{GO}$ and $-OH_{DOX}$) and ($-OH_{GO}$ and $-NH_{2DOX}$) (Yang et al., 2008). Since already many groups have been removed after reduction and the rest was linked with COS and HEC and few groups left for DOX drug. However, Mianehrow et al have used folic acid (FA), highly water soluble.Vitamin B instead of DOX and they obtained high loading. This could be related with the readiness of FA in the COS/HEC coat layer (Mianehrow et al., 2016).

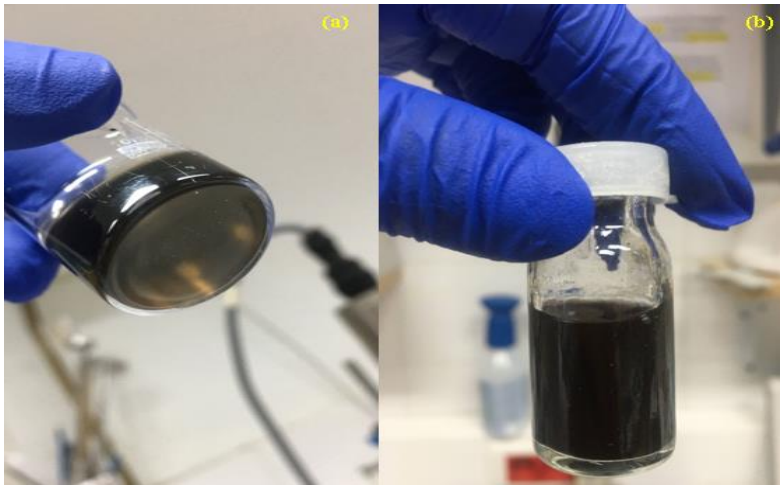

Figure 3.12 Functionalization of (a) rGO and (b) Au-rGO with HEC and COS.

The chemotherapeutic drug DOX and GO have two interactions that result in good drug loading: hydrophobic interaction and π-π stacking (Yang et al., 2008; Q. Zhang et al., 2013). The loading was applied to all groups by simply mixing for 24 h. The drug was noncovalently loaded onto water-dispersible GO. Because of the large

number of OH and carboxylic groups, GO had a high loading efficiency of 91.7% and a loading capacity of 30.58% in a 3:1 ratio of GO:DOX when compared to other groups of synthesized nanocarriers, as shown in (Figure 3.13), comparing to literature, this percentage is higher to some studies (Rao et al., 2018; B. Zhang et al., 2017; Yang et al., 2008) due to the ratio between GO and DOX drug, furthermore, some studies are conducting functionalization, which affects the percentage of bonding. GO nanosheets had an exceptional high loading capacity and efficiency. COS-rGO has a loading efficiency of 79% and a loading capacity of 26.35%. The remaining two compositions have extremely low loading, as illustrated in Figure 3.13. Figure 3.13 (a) and (b), demonstrate that all of the compositions were significantly ($p<0.05$) different from one another.

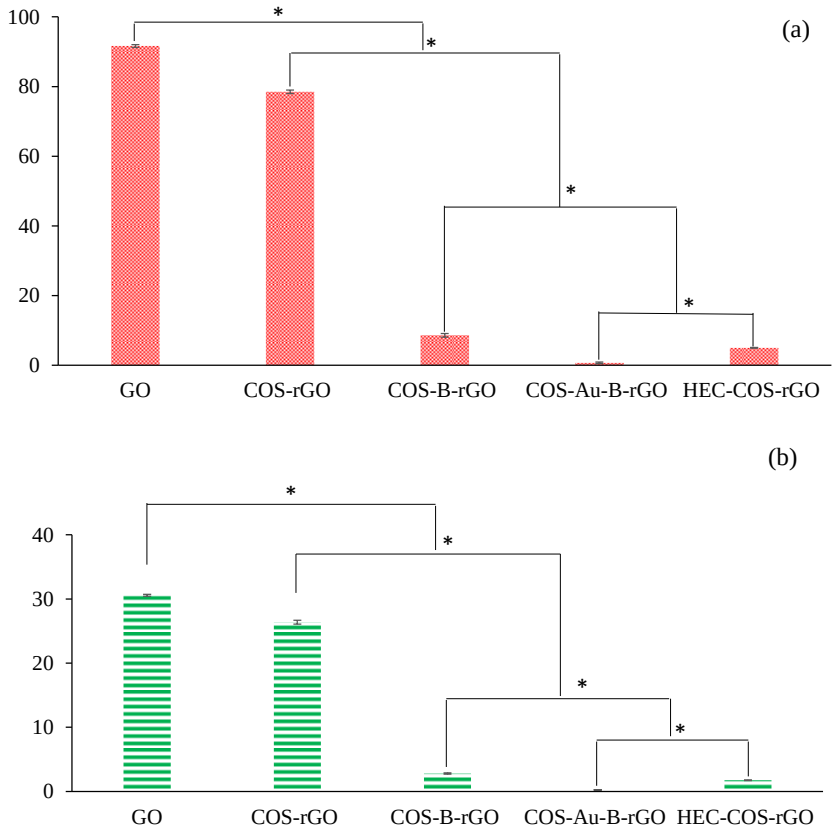

Figure 3.13 (a) Loading efficiency and (b) loading capacity of GO, COS-rGO, COS-B-rGO, COS-Au-B-rGO and HEC-COS-rGO for DOX. "*" indicates statistical significant difference between different compositions of the loading efficiency and loading capacity (n=3, $p<0.05$).

Low loading result could be due to the concentration of grafted COS as observed in literature. High molecular weight COS and high concentration were found to be better for drug loading by Baktash et al., whereas low molecular weight resulted in low drug loading. High concentration produced a dense layer of COS, which disrupted the π-π stacking interaction but enhanced hydrogen bonding with the drug (Baktash et al., 2021). So another method applied, COS was replaced with PEG. It also did not reflect any higher loading.

The release study was conducted for 72 h using the compositions, GO which had high loading according to the literature, GO and its derivatives are pH sensitive. After 1 h, higher release was obtained in an acidic environment for GO, (Figure 3.14), with approximately 8% drug released compared to those observed in neutral

media (4.6%). After three days, GO at pH 4 released approximately 23% of the drug, whereas at pH 7.4 only 12.4% was released. This releasing result agreed with literature (C. Wang et al., 2018).

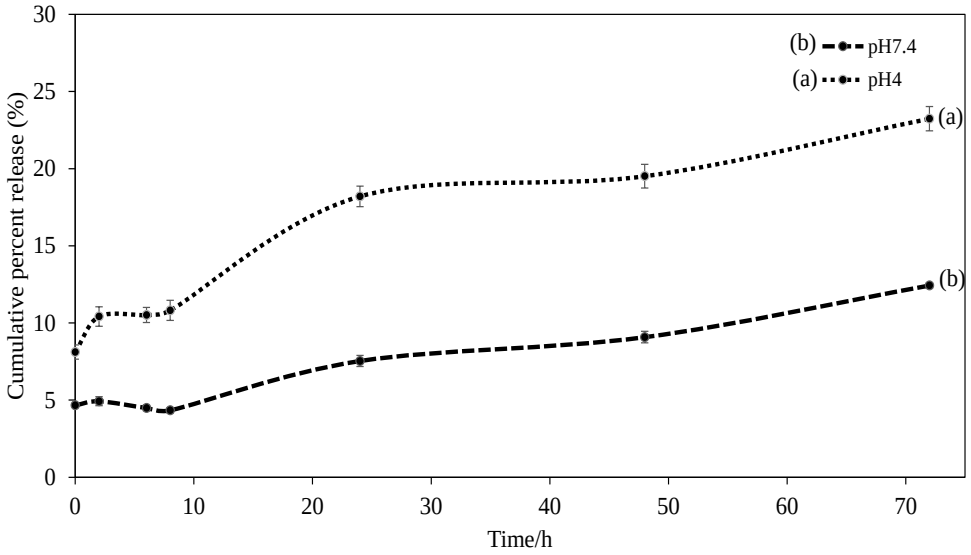

Figure 3.14 Cumulative release of DOX from GO in PBS at at pH values (a) 4, (b) 7.4. at 37°C for 72 h. The values given are the mean ± SD and (n = 3).

3.2.2 GOQD-GlcN and GOQD-GlcN-BA.

QDs, in general, are characterized with many properties such as tunable size, high surface area, stability, optical property and much more (Badıllı et al., 2020). GOQDs have the same property as GO and similary they can be functionalized. Furthermore, the abundance of oxygen functional groups contributes to its solubility and stability. This property, however, causes GOQDs to form hydrophobic interactions and π-π stack with aromatic drugs. (Ghanbari et al., 2021).

DOX was loaded into GOQDs-GlcN at a 1:3 ratio and 57% drug loading efficiency and 19 wt% loading capacity were obtained. According to the literature, no one has ever combined GOQDs-GlcN and BA. The nanocomposite loaded with DOX in the same 1:3 ratio had higher loading efficiency (around 90%) and a loading capacity (30 wt %) compared to just GOQD-GlcN (loading efficiency 57% and 19 wt%

loading capacity). This is a clear demonstration of the effect of boric acid on increasing drug-nanocomposite interaction. Because of the nanocomposite's negative charge, the interaction could be enhanced. Because boron has a -ve charge and GOQD as well, more negative charge attracts the drug molecule.

The release study was conducted with GOQD-GlcN and GOQD-GlcN-BA for 96 h at neutral pH 7.4 and acidic pH 5.5. The nanocomposite GOQDs-GlcN proved its pH sensivity though higher release was observed at pH 5.5. The cumulative drug percent release after 96 h at netural pH was around 5.7 %, whereas in acidic medium the release went up to 8.6 %, (Figure 3.15). Similarly, higher release rate was observed with boron incorporation GOQD-GlcN-BA at pH 5.5 (20 %) compared to pH 7.4 (around 10%) as illustrated in Figure 3.16.

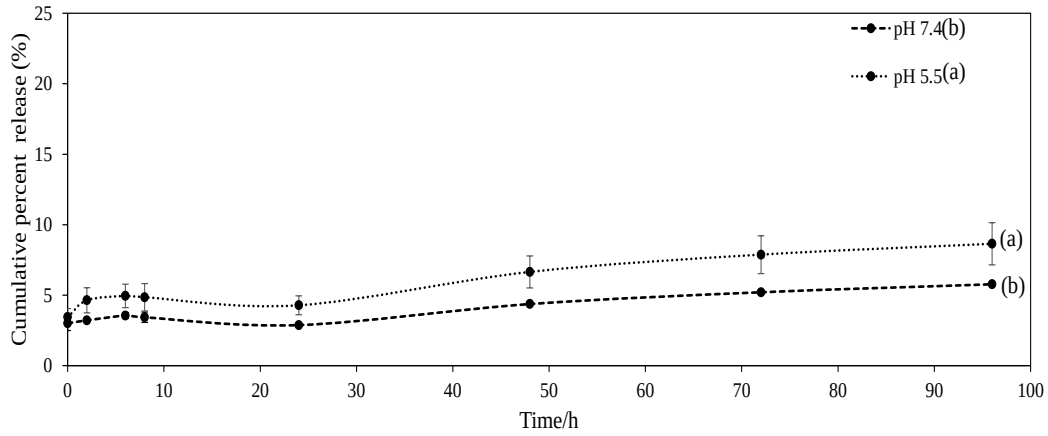

Figure 3.15 Cumulative release profile of DOX from GOQD-GlcN nanocomposites in PBS at pH values (a) 5.5, (b) 7.4. At 37°C for 96 h. The values given are the mean ± SD (n = 3).

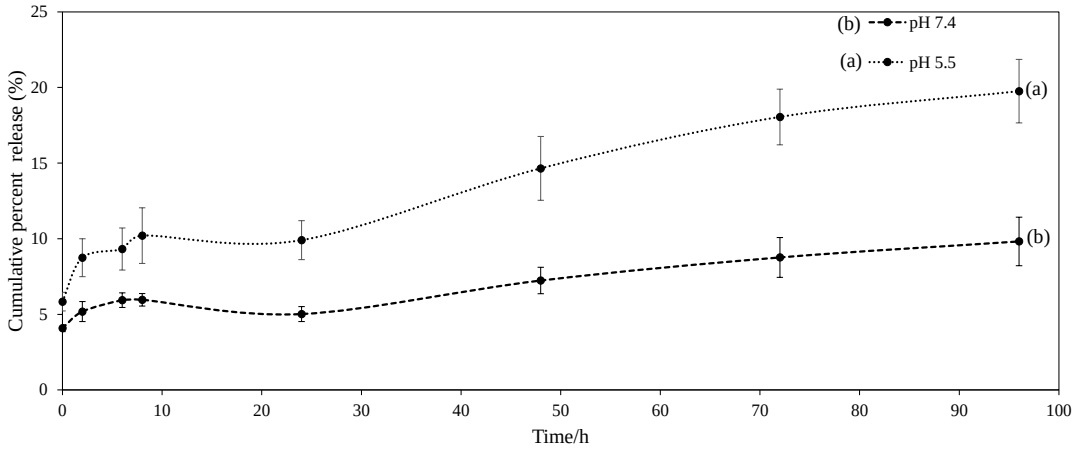

Figure 3.16 Cumulative release profile of DOX from GOQD-GlcN-BA nanocomposite in PBS at pH (a) 5.5, (b) 7.4. At 37°C for 96 h. The values given are the mean ± SD (n=3).

3.3 Cell culture studies

3.3.1 *In vitro* cytotoxicity of GO

Dose dependent cytotoxicity of GO was tested using MTT test (Figure 3.17). All concentrations tested did not show cytotoxicity which was similar to the findings of Kenry et al.. The group did not observe any cytotoxicity at MCF-7 cancer cells and hypothesized that it was due to the material's higher cellular protein adsorption capability (Kenry et al., 2016). No statistical significant difference was obtained between different concentrations of the same composition (Figure 3.17). In this thesis, the pH of the GO solution was 2.5, indicating that it was highly acidic. Because cancerous cells thrive in an acidic environment, incubating them in that environment encourages them to proliferate (Estrella et al., 2013). Figure 3.18 shows the morphology of the cells after treatment with various concentrations, with no change in morphology as the concentration of GO was increased.

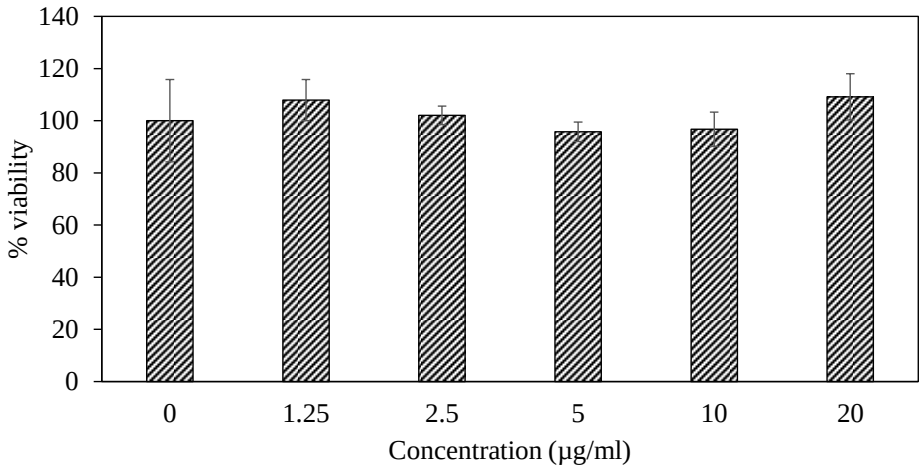

Figure 3.17 Effect of GO with different concentrations on viability of MCF-7 cells after 24 h of incubation. No statistical significant difference was obtained between the groups (n=4).

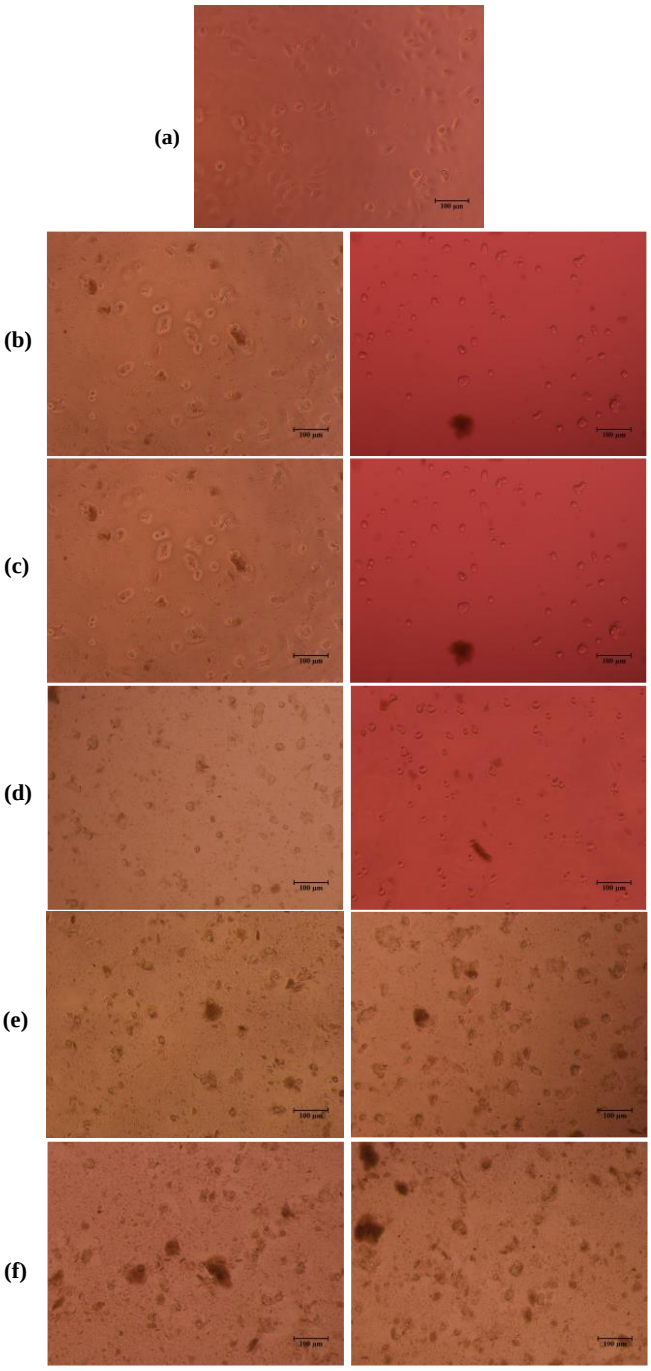

Figure 3.18 Morphology of MCF-7 cells treated with GO with different concentrations (a) 0 µg/ml GO (b) 1.25 µg/ml GO, (c) 2.5 µg/ml GO, (d) 5 µg/ml GO, (e) 10 µg/ml GO, and (f) 20 µg/ml GO.

3.3.2 Cytotoxicity of GOQD-GlcN & GOQD-GlcN-BA

The relative viability of MCF-7 cells treated with different concentrations of GOQD-GlcN & GOQD-GlcN-BA was determined with respect to the control (cells cultured in medium only) after 24 h of incubation (Figure 3.19). No dose dependent cytotoxicity was observed. Cells incubated in media containing GOQD-GlcN and GOQD-GlcN-BA resulted in a relative cell viability slightly above 100% due to the presence of glucosamine (Ghanbari et al., 2021; Thasneem et al., 2013). The induction of GLUT1 and SGL1 by the tumor cells enhances glucose uptake, thus increase glycolysis as glucose uptake increased (Ganapathy et al., 2009). At the same time, GOQD-GlcN-BA showed lower cell viability comparing to GOQD-GlcN due to the presence of BA. Therefore, both groups with drug free are safe and biocompatible for drug delivery system uses. This result is in complete agreement with the obtained in literature (Ghanbari et al., 2021). The nanoassemblies GOQD-GlcN and GOQD-GlcN-BA showed no significant difference (Figure 3.19).

The morphology of the cells is shown in (Figure 3.20). Comparing un-treated cells (only cells) wih the treated cells, no change in the morphology of cells was observed and cells looked healthy.

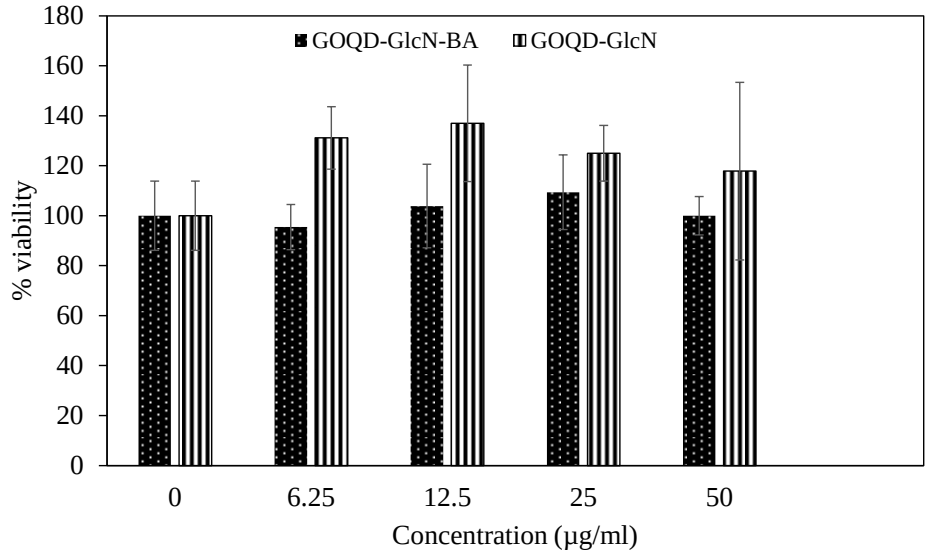

Figure 3.19 Dose dependent cytotoxicity of GOQD-GlcN and GOQD-GlcN-BA on MCF-7 cell line. MTT was conducted after 24 h of incubation. Cells cultured in medium only were used as the control. There is no significant difference among the groups (n=5).

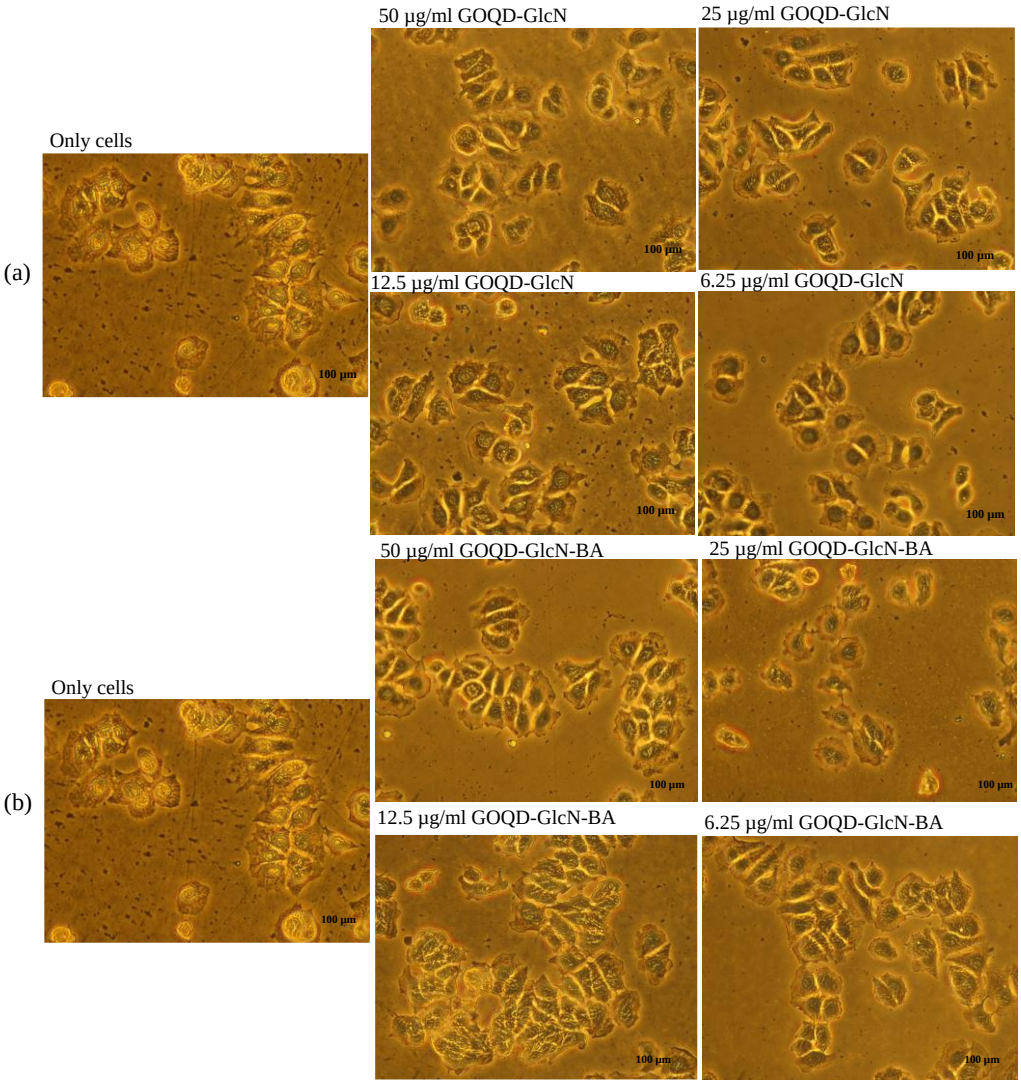

Figure 3.20 Morphology of MCF-7 cells treated with (a) GOQD-GlcN and (b) GOQD-GlcN-BA. Different concentrations (50, 25, 12.5 and 6.25 µg/ml) were given to the cells and incubated for 24 h at 37 °C.

3.3.3 Cytotoxicity of GOQD-GlcN-DOX & GOQD-GlcN-BA-DOX

To evaluate the anticancer potential of the nanocomposites, the relative viability of MCF-7 cells were treated with different concentrations (2, 4, 8, 16 and 32 µg/ml) of GOQD-GlcN-DOX & GOQD-GlcN-BA-DOX, and they were determined with respect to the control (cells cultured in medium only) and only DOX (cells treated with DOX drug only) after 24 h of incubation (Figure 3.21). The viability of the cells

treated with GOQD-GlcN-DOX and GOQD-GlcN-BA-DOX decreased as the concentration of DOX was increased. The nanocomposite containing BA showed lower cell viability compared to the nanocomposite without BA as the concentration was increased. This could be due to the sialic acids which are highly expressed by the MCF-7 cancer cells which resulted in reaction between BA and diols groups leads to actively crossing the cell membrane (Zhan & Liang, 2016). For the highest concentration 32 µg/ml, free DOX showed the highest cell death compared to the nanocomposites.

All the groups with the same concentration showed statistically significant difference ($p<0.05$) with free DOX with the same concentration. For the concentration (32 µg/ml), only GOQD-GlcN-DOX showed the statistically significant difference ($p<0.05$) with free DOX (32 µg/ml) (Figure 3.21).

(Figure 3.22) shows the morphology of the cells treated with nanocomposite loaded with the drug. It was clearly showing that, as the concentration of the drug loaded was high as the viability of the cells reduced. Moreover, the morphology of the cells was also changed and more dead cells obtained with higher concentrations.

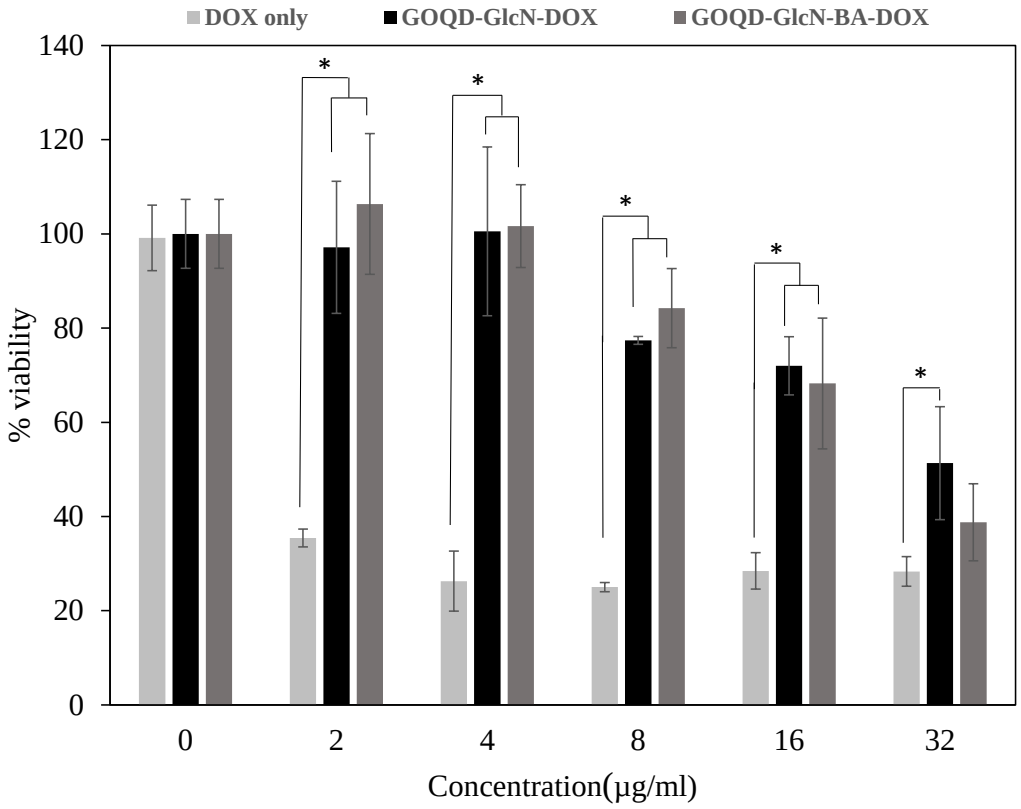

Figure 3.21 Dose dependent cytotoxicity of only DOX, GOQD-GlcN-DOX and GOQD-GlcN-BA-DOX on MCF-7 cell line. MTT was conducted after 24 h of incubation at 37°C. Cells cultured in medium only and treated with drug only, were used as the control. "*" indicates statistically significant difference between the groups with the same concentrations (n=3, $p<0.05$).

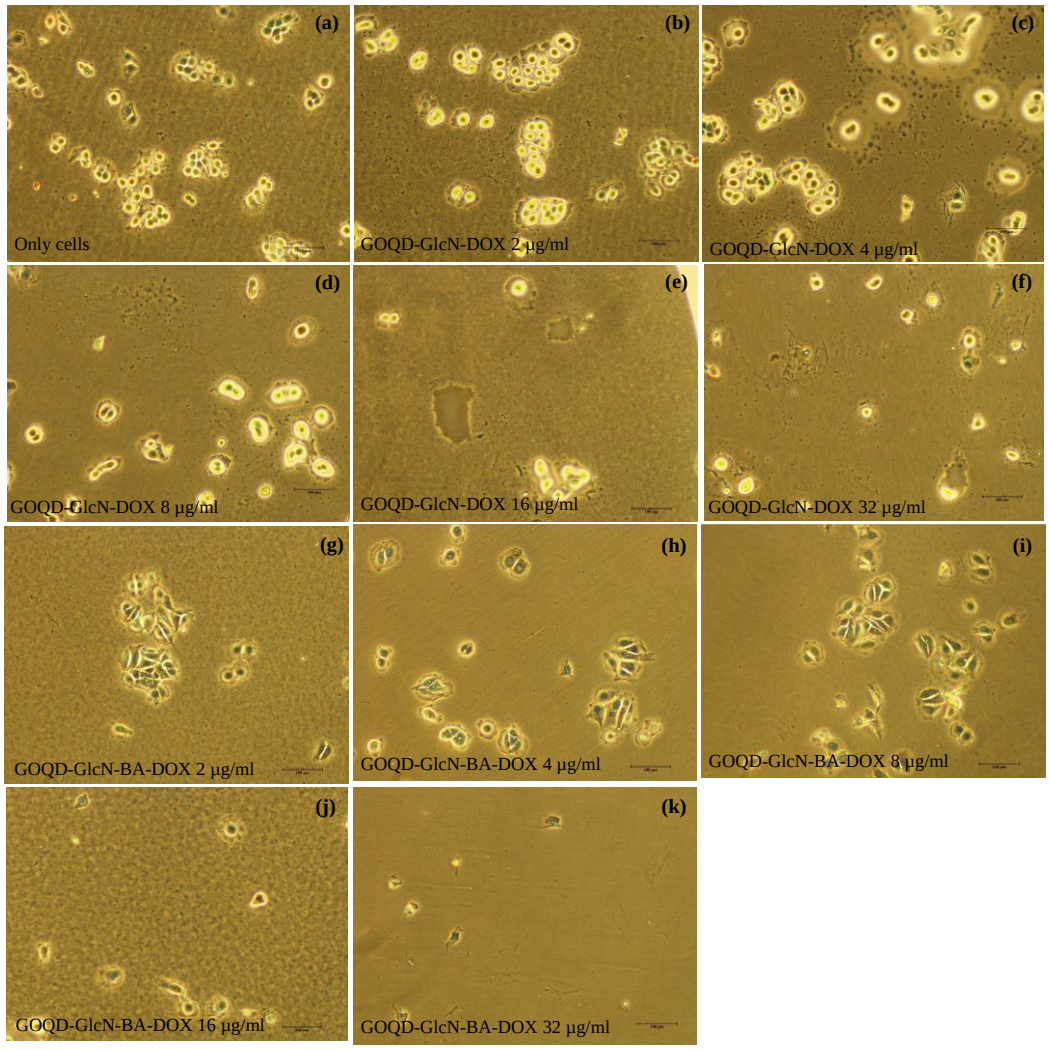

Figure 3.22 Morphology of MCF-7 cells treated with different concentrations of drug loaded nanocomposites GOQD-GlcN-DOX and GOQD-GlcN-BA-DOX, (a) normal cells, (b-f) GOQD-GlcN-DOX, (g-k) GOQD-GlcN-BA-DOX, after 24 h incubation at 37°C.

3.3.4 Confocal laser microscopy assay

In vitro cytotoxicity test of the nanocomposites on MCF-7 cells (Figure 3.21) showed that GOQD-GlcN-BA-DOX was more cytotoxic compared to GOQD-GlcN-DOX. Confocal microscopy analysis revealed higher cell internalization of GOQD-GlcN-BA-DOX compared to, GOQD-GlcN-DOX. This could be explained by the selecitivity of BA to sialic acid expressed by MCF-7 cancer cells which resulted in

good cellular permeability (Zhan & Liang, 2016), thus GOQD-GlcN-BA-DOX exhibited much better cellular uptake as in (Figure 3.23) even after 8 h of incubation.

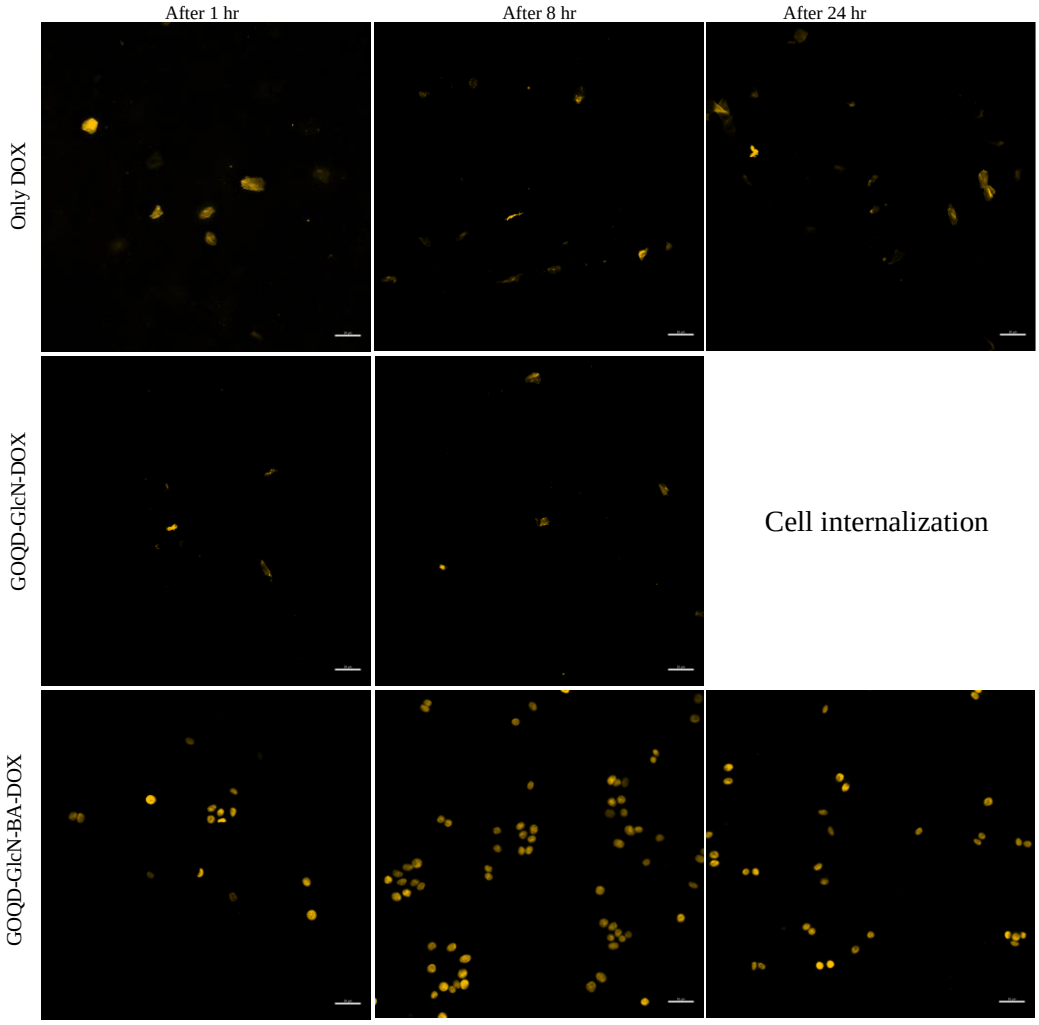

Figure 3.23 Confocal laser scanning microscopy of MCF-7, incubated with (only DOX, GOQD-GlcN-DOX and GOQD-GlcN-BA-DOX) at 37 °C for 1, 8 and 24 h.

CHAPTER 4

CONCLUSION

Different nanocomposites were synthesized in this study to. To improve dispersibility in neutral environments, GO, rGO, B-rGO, and Au-B-rGO were synthesized and functionalized. Because of their hydrophobicity, rGO, B-rGO, and Au-B-rGO were functionalized with COS. COS, on the other hand, exhibits sensitivity to neutral pH that becomes deprotonated. The precipitation was then successfully overcome in the presence of COS and HEC. When compared to the other compositions, GO alone has a high loading efficiency. However, this high loading may be due to the high number of functional groups available for the drug to attach to, whereas in the other compositions there were few groups left for the drug to attach to due to the presence of AuNPs, COS, and HEC.

GOQDs with excellent drug delivery properties were functionalized with gluocoseamine and boric acid. GOQDs-GlcN had a low drug loading efficiency of 57 %, which is comparable to what has been reported in the literature. Furthermore, the drug is released slowly, with only 8% released in 96 h. The addition of boric acid, however, altered the loading and releasing results. High loading efficiency of up to 90% and high releasing percentage in acidic environments of up to 20%. The morphology and nanosize of the nanoassembly (GOQD, GOQD-GlcN and GOQD-GlcN-BA) were conformed by TEM. The MTT assay of the bare nanocomposites resulted in cell viability more than 100% at 50 µg/ml concentration, while GOQD-GlcN-BA-DOX exhibited more cytotoxicity against MCF-7 cells compared to GOQD-GlcN-DOX. Moreover, GOQD-GlcN-BA-DOX has stronge fluorescence through fluorescence microscopy owing to higher MCF-7 cellular internalization via sialic acid and BA interaction. This thesis shows the addition of BA enhanced the loading and releasing of anticancer drug, nontoxicity of the system with higher cellular internalization thus superior potential for anticancer drug delivery.

REFERENCES

Abraham, J., & Staffurth, J. (2016). Hormonal therapy for cancer. *Medicine (United Kingdom)*, *44*(1), 30–33. https://doi.org/10.1016/j.mpmed.2015.10.014

Agnoli, S., & Favaro, M. (2016). Doping graphene with boron : a review of synthesis methods, physicochemical characterization, and emerging applications. *Journal of Materials Chemistry A*, *4*, 5002–5025. https://doi.org/10.1039/C5TA10599D

Agrawal, K. (2007). Doxorubicin. In S. J. Enna & D. B. Bylund (Eds.), *xPharm: The Comprehensive Pharmacology Reference* (pp. 1–5). Elsevier. https://doi.org/https://doi.org/10.1016/B978-008055232-3.61650-2

Ahammad, A. J. S., Islam, T., & Hasan, M. M. (2019). Graphene-based electrochemical sensors for biomedical applications. In *Biomedical Applications of Graphene and 2D Nanomaterials* (pp. 249–282). Elsevier. https://doi.org/10.1016/B978-0-12-815889-0.00012-X

Ahmad Alshammari, Kalevaru, V. N., & Martin, A. (2016). Metal Nanoparticles as Emerging Green Catalysts. In *Intechopen* (Vol. 32, Issue tourism, pp. 137–144). https://www.intechopen.com/books/advanced-biometric-technologies/liveness-detection-in-biometrics

Akbari jonous, Z., Shayeh, J. S., Yazdian, F., Yadegari, A., Hashemi, M., & Omidi, M. (2019). An electrochemical biosensor for prostate cancer biomarker detection using graphene oxide–gold nanostructures. *Engineering in Life Sciences*, *19*(3), 206–216. https://doi.org/10.1002/elsc.201800093

Al-Ani, L. A., AlSaadi, M. A., Kadir, F. A., Hashim, N. M., Julkapli, N. M., & Yehye, W. A. (2017). Graphene– gold based nanocomposites applications in cancer diseases; Efficient detection and therapeutic tools. *European Journal of Medicinal Chemistry*, *139*, 349–366. https://doi.org/10.1016/j.ejmech.2017.07.036

Al-Ani, L. A., Yehye, W. A., Kadir, F. A., Hashim, N. M., AlSaadi, M. A., Julkapli, N. M., & Hsiao, V. K. S. (2019). Hybrid nanocomposite curcumin-capped gold nanoparticle-reduced graphene oxide: Antioxidant potency and selective cancer cytotoxicity. *PLoS ONE*, *14*(5), 1–24. https://doi.org/10.1371/journal.pone.0216725

Ali, F., S Hosmane, N., & Zhu, Y. (2020). Boron Chemistry for Medical Applications. *Molecules (Basel, Switzerland)*, *25*(4). https://doi.org/10.3390/molecules25040828

Aljaafari, A., Ahmed, F., & Husain, F. M. (2020). Bio-inspired facile synthesis of graphene-based nanocomposites: Elucidation of antimicrobial and biofilm inhibitory potential against foodborne pathogenic bacteria. *Coatings*, *10*(12), 1–15. https://doi.org/10.3390/coatings10121171

Alle, M., Lee, S. H., & Kim, J. C. (2020). Ultrafast synthesis of gold nanoparticles on cellulose nanocrystals via microwave irradiation and their dyes-degradation catalytic activity. *Journal of Materials Science and Technology*, *41*, 168–177. https://doi.org/10.1016/j.jmst.2019.11.003

Aminabad, N. S., Farshbaf, M., & Akbarzadeh, A. (2019). Recent advances of gold nanoparticles in biomedical applications: State of the art. *Cell Biochemistry and Biophysics*, *77*(2), 123–137. https://doi.org/10.1007/s12013-018-0863-4

Badıllı, U., Mollarasouli, F., Bakirhan, N. K., Ozkan, Y., & Ozkan, S. A. (2020). Role of quantum dots in pharmaceutical and biomedical analysis, and its application in drug delivery. *TrAC - Trends in Analytical Chemistry*, *131*. https://doi.org/10.1016/j.trac.2020.116013

Baek, S. H., Roh, J., Park, C. Y., Kim, M. W., Shi, R., Kailasa, S. K., & Park, T. J. (2020). Cu-nanoflower decorated gold nanoparticles-graphene oxide nanofiber as electrochemical biosensor for glucose detection. *Materials Science and Engineering C*, *107*, 110273. https://doi.org/10.1016/j.msec.2019.110273

Baktash, M. S., Zarrabi, A., Avazverdi, E., & Reis, N. M. (2021). Development and

optimization of a new hybrid chitosan-grafted graphene oxide/magnetic nanoparticle system for theranostic applications. *Journal of Molecular Liquids*, *322*, 114515. https://doi.org/10.1016/j.molliq.2020.114515

Balcioglu, M., Rana, M., & Yigit, M. V. (2013). Doxorubicin loading on graphene oxide, iron oxide and gold nanoparticle hybrid. *Journal of Materials Chemistry B*, *1*(45), 6187–6193. https://doi.org/10.1039/c3tb20992j

Banerjee, A. N. (2018). Graphene and its derivatives as biomedical materials: Future prospects and challenges. *Interface Focus*, *8*(3), 20170056. https://doi.org/10.1098/rsfs.2017.0056

Barkalina, N., Charalambous, C., Jones, C., & Coward, K. (2014). Nanotechnology in reproductive medicine: Emerging applications of nanomaterials. *Nanomedicine: Nanotechnology, Biology, and Medicine*, *10*(5), e921–e938. https://doi.org/10.1016/j.nano.2014.01.001

Barman, S. R., Nain, A., Jain, S., Punjabi, N., Mukherji, S., & Satija, J. (2018). Dendrimer as a multifunctional capping agent for metal nanoparticles for use in bioimaging, drug delivery and sensor applications. *Journal of Materials Chemistry B*, *6*(16), 2368–2384. https://doi.org/10.1039/c7tb03344c

Beik, J., Alamzadeh, Z., Mirrahimi, M., Sarikhani, A., Ardakani, T. S., Asadi, M., Irajirad, R., Mirrahimi, M., Mahabadi, V. P., Eslahi, N., Bulte, J. W. M., Ghaznavi, H., & Shakeri-Zadeh, A. (2021). Multifunctional theranostic graphene oxide nanoflakes as mr ımaging agents with enhanced photothermal and radiosensitizing properties. *ACS Applied Bio Materials*, *4*(5), 4280–4291. https://doi.org/10.1021/acsabm.1c00104

Biswas, M. C., Islam, M. T., Nandy, P. K., & Hossain, M. M. (2021). Graphene quantum dots (gqds) for bioimaging and drug delivery applications: a review. *ACS Materials Letters*, *3*(6), 889–911. https://doi.org/10.1021/acsmaterialslett.0c00550

Brust, M., Walker, M., Bethell, D., Schiffrin, D. J., & Whyman, R. (1994). Synthesis

of thiol-derivatised gold nanoparticles in a two-phase liquid-liquid system. *Journal of the Chemical Society, Chemical Communications*. *7*, 801–802.

Centeno, L., Romero-García, J., Alvarado-Canché, C., Gallardo-Vega, C., Télles-Padilla, G., Díaz Barriga-Castro, E., Cabrera-Álvarez, E. N., Ledezma-Pérez, A., & de León, A. (2021). Green synthesis of graphene quantum dots from Opuntia sp. extract and their application in phytic acid detection. *Sensing and Bio-Sensing Research*, *32*, 100412. https://doi.org/10.1016/j.sbsr.2021.

Chandran, P. R., & Thomas, R. T. (2015). Gold nanoparticles in cancer drug delivery. In *Nanotechnology Applications for Tissue Engineering*. Elsevier Inc. https://doi.org/10.1016/B978-0-323-32889-0.00014-5

Chang, G., Wang, Y., Gong, B., Xiao, Y., Chen, Y., Wang, S., Li, S., Huang, F., Shen, Y., & Xie, A. (2015). Reduced graphene oxide/amaranth extract/AuNPs composite hydrogel on tumor cells as integrated platform for localized and multiple synergistic therapy. *ACS Applied Materials and Interfaces*, *7*(21), 11246–11256. https://doi.org/10.1021/acsami.5b03907

Chen, F., Gao, W., Qiu, X., Zhang, H., Liu, L., Liao, P., Fu, W., & Luo, Y. (2017). Graphene quantum dots in biomedical applications: Recent advances and future challenges. *Frontiers in Laboratory Medicine*, *1*(4), 192–199. https://doi.org/10.1016/j.flm.2017.12.006

Chen, S., Yang, K., Leng, X., Chen, M., Novoselov, K. S., & Andreeva, D. V. (2020). Perspectives in the design and application of composites based on graphene derivatives and bio-based polymers. *Polymer International*, *69*(12), 1173–1186. https://doi.org/10.1002/pi.6080

Chen, W., Yan, L., & Bangal, P. R. (2009). Preparation of graphene by the rapid and mild thermal reduction of graphene oxide induced by microwaves. *Carbon*, *48*(4), 1146–1152. https://doi.org/10.1016/j.carbon.2009.11.037

Chen, X., Li, Q. W., & Wang, X. M. (2014). Gold nanostructures for bioimaging, drug delivery and therapeutics. *Precious Metals for Biomedical Applications*,

163–176. https://doi.org/10.1533/9780857099051.2.163

Cheng, S. J., Chiu, H. Y., Kumar, P. V., Hsieh, K. Y., Yang, J. W., Lin, Y. R., Shen, Y. C., & Chen, G. Y. (2018). Simultaneous drug delivery and cellular imaging using graphene oxide. *Biomaterials Science*, *6*(4), 813–819. https://doi.org/10.1039/c7bm01192j

Chikwendu Okpala, C. (2006). The benefits and applications of nanocomposites. *International Journal of Advanced Engineering Technology E- Int J Adv Engg Tech*, 12–18.

Cho, K., Wang, X., Nie, S., Chen, Z. G., & Shin, D. M. (2008). Therapeutic nanoparticles for drug delivery in cancer. *Clinical Cancer Research*, *14*(5), 1310–1317. https://doi.org/10.1158/1078-0432.CCR-07-1441

Chun, S., Chua, K., & Pumera, M. (2016). The reduction of graphene oxide with hydrazine : elucidating its reductive capability based on a reaction-model approach. *Chemical Communications*, *52*, 72–75. https://doi.org/10.1039/c5cc08170j

Clarance, P., Luvankar, B., Sales, J., Khusro, A., Agastian, P., Tack, J. C., Al Khulaifi, M. M., AL-Shwaiman, H. A., Elgorban, A. M., Syed, A., & Kim, H. J. (2020). Green synthesis and characterization of gold nanoparticles using endophytic fungi Fusarium solani and its in-vitro anticancer and biomedical applications. *Saudi Journal of Biological Sciences*, *27*(2), 706–712. https://doi.org/10.1016/j.sjbs.2019.12.026

Couvreur, P. (2013). Nanoparticles in drug delivery: Past, present and future. *Advanced Drug Delivery Reviews*, *65*(1), 21–23. https://doi.org/10.1016/j.addr.2012.04.010

Cui, F., Ji, J., Sun, J., Wang, J., Wang, H., Zhang, Y., Ding, H., Lu, Y., Xu, D., & Sun, X. (2019). A novel magnetic fluorescent biosensor based on graphene quantum dots for rapid, efficient, and sensitive separation and detection of circulating tumor cells. *Analytical and Bioanalytical Chemistry*, *411*(5), 985–

995. https://doi.org/10.1007/s00216-018-1501-0

Dalgic, A. D., Alshemary, A. Z., Tezcaner, A., Keskin, D., & Evis, Z. (2018). Silicate-doped nano-hydroxyapatite/graphene oxide composite reinforced fibrous scaffolds for bone tissue engineering. *Journal of Biomaterials Applications*, *32*(10), 1392–1405. https://doi.org/10.1177/0885328218763665

Damyanov, C. A., Maslev, I. K., & Pavlov, V. S. (2018). Conventional treatment of cancer realities and problems. *Annals of Complementary and Alternative Medicine*, *1*(1), 1–9.

Darabdhara, G., Das, M. R., Singh, S. P., Rengan, A. K., Szunerits, S., & Boukherroub, R. (2019). Ag and Au nanoparticles/reduced graphene oxide composite materials: Synthesis and application in diagnostics and therapeutics. *Advances in Colloid and Interface Science*, *271*, 101991. https://doi.org/10.1016/j.cis.2019.101991

De Jong, W. H., & Borm, P. J. A. (2008). Drug delivery and nanoparticles: Applications and hazards. *International Journal of Nanomedicine*, *3*(2), 133–149. https://doi.org/10.2147/ijn.s596

De Silva, K. K.H., Huang, H. H., Joshi, R. K., & Yoshimura, M. (2017). Chemical reduction of graphene oxide using green reductants. *Carbon*, *119*, 190–199. https://doi.org/10.1016/j.carbon.2017.04.025

De Silva, K. Kanishka H., Huang, H. H., & Yoshimura, M. (2018). Progress of reduction of graphene oxide by ascorbic acid. *Applied Surface Science*, *447*, 338–346. https://doi.org/10.1016/j.apsusc.2018.03.243

Dong, J., Carpinone, P. L., Pyrgiotakis, G., Demokritou, P., & Moudgil, B. M. (2020). Synthesis of precision gold nanoparticles using Turkevich method. *KONA Powder and Particle Journal*, *37*(37), 224–232. https://doi.org/10.14356/kona.2020011

DS, A., MJ, S., P, F., & A, H. (2016). Nanotechnology: the risks and benefits for

medical diagnosis and treatment. *Journal of Nanomedicine & Nanotechnology*, *7*(4), 1–2. https://doi.org/10.4172/2157-7439.1000e143

Dykman, L. A., & Khlebtsov, N. G. (2011). Gold nanoparticles in biology and medicine: recent advances and propsects. *Acta Naturae*, *51*(3), 3(2), 34–55.

Ealias, A. M., & M P, S. (2017). A review on the classifiacation , characterisation , synthesis of nanoparticles and their application. *IOP Conference Series: Materials Science and Engineering*, *263*(3), 032019. https://doi.org/10.1088/1757-899X/263/3/032019

Elahi, N., Kamali, M., & Baghersad, M. H. (2018). Recent biomedical applications of gold nanoparticles: A review. *Talanta*, *184*, 537–556. https://doi.org/10.1016/j.talanta.2018.02.088

Emadi, F., Amini, A., Gholami, A., & Ghasemi, Y. (2017). Functionalized graphene oxide with chitosan for protein nanocarriers to protect against enzymatic cleavage and retain collagenase activity. *Scientific Reports*, *7*, 1–13. https://doi.org/10.1038/srep42258

Eskiizmir, G., Baskin, Y., & Yapici, K. (2018). Graphene-based nanomaterials in cancer treatment and diagnosis. In *Fullerenes, Graphenes and Nanotubes: A Pharmaceutical Approach* (pp. 331–374). https://doi.org/10.1016/B978-0-12-813691-1.00009-9

Estrella, V., Chen, T., Lloyd, M., Wojtkowiak, J., Cornnell, H. H., Ibrahim-Hashim, A., Bailey, K., Balagurunathan, Y., Rothberg, J. M., Sloane, B. F., Johnson, J., Gatenby, R. A., & Gillies, R. J. (2013). Acidity generated by the tumor microenvironment drives local invasion. *Cancer Research*, *73*(5), 1524–1535. https://doi.org/10.1158/0008-5472.CAN-12-2796

Fan, X., Cai, C., Gao, J., Han, X., & Li, J. (2020). Hydrothermal reduced graphene oxide membranes for dyes removing. *Separation and Purification Technology*, *241*, 116730. https://doi.org/10.1016/j.seppur.2020.116730

Farkona, S., Diamandis, E. P., & Blasutig, I. M. (2016). Cancer immunotherapy: The beginning of the end of cancer? *BMC Medicine*, *14*(1), 1–18. https://doi.org/10.1186/s12916-016-0623-5

Fasakin, I. O. F. O., Adekunle, B. O. A. S., & Eleruja, T. V. O. M. A. (2019). The comparative analyses of reduced graphene oxide (RGO) prepared via green , mild and chemical approaches. *SN Applied Sciences*, *1*(10), 1–7. https://doi.org/10.1007/s42452-019-1188-7

Feynman, R. P. (1960). *There's Plenty of Room at the Bottom*. *XXIII*(5).

Folorunso, A., Akintelu, S., Oyebamiji, A. K., Ajayi, S., Abiola, B., Abdusalam, I., & Morakinyo, A. (2019). Biosynthesis, characterization and antimicrobial activity of gold nanoparticles from leaf extracts of Annona muricata. *Journal of Nanostructure in Chemistry*, *9*(2), 111–117. https://doi.org/10.1007/s40097-019-0301-1

Fragoon, A., Li, J., Zhu, J., & Zhao, J. (2012). Biosynthesis of controllable size and shape gold nanoparticles by black seed (Nigella Sativa) extract. *Journal of Nanoscience and Nanotechnology*, *12*(3), 2337–2345. https://doi.org/10.1166/jnn.2012.5739

Francia, V., Montizaan, D., & Salvati, A. (2020). Interactions at the cell membrane and pathways of internalization of nano-sized materials for nanomedicine. *Beilstein Journal of Nanotechnology*, *11*, 338–353. https://doi.org/10.3762/bjnano.11.25

Friedersdorf, L. E., & Spadola, Q. A. (2020). *Introduction to Nanotechnology*. Women in Nanotechnology, 1-14. http://link.springer.com/10.1007/978-3-030-19951-7

Ganapathy, V., Thangaraju, M., & Prasad, P. D. (2009). Nutrient transporters in cancer: Relevance to Warburg hypothesis and beyond. *Pharmacology and Therapeutics*, *121*(1), 29–40. https://doi.org/10.1016/j.pharmthera.2008.09.005

Gao, X., Jang, J., & Nagase, S. (2010). Hydrazine and thermal reduction of graphene oxide : reaction mechanisms , product structures , and reaction design. *The Journal of Physical Chemistry C*, *114*, 832–842.

Geim, A. K., & Novoselov, K. S. (2009). The rise of graphene. In *Nanoscience and Technology: A Collection of Reviews from Nature Journals* (pp. 11–19). World Scientific Publishing Co. https://doi.org/10.1142/9789814287005_0002

George, A., Shah, P. A., & Shrivastav, P. S. (2019). Natural biodegradable polymers based nano-formulations for drug delivery: A review. *International Journal of Pharmaceutics*, *561*, 244–264. https://doi.org/10.1016/j.ijpharm.2019.03.011

Ghanbari, N., Salehi, Z., Khodadadi, A. A., Shokrgozar, M. A., & Saboury, A. A. (2021). Glucosamine-conjugated graphene quantum dots as versatile and pH-sensitive nanocarriers for enhanced delivery of curcumin targeting to breast cancer. *Materials Science and Engineering C*, *121*, 111809. https://doi.org/10.1016/j.msec.2020.111809

Ghawanmeh, A. A., Ali, G. A. M., Algarni, H., Sarkar, S. M., & Chong, K. F. (2019). Graphene oxide-based hydrogels as a nanocarrier for anticancer drug delivery. *Nano Research*, *12*(5), 973–990. https://doi.org/10.1007/s12274-019-2300-4

Goas, M. Le, Testard, F., Tache, O., Debou, N., Carrot, G., & Renault, J. (2020). How do surface properties of nanoparticles influence their diffusion in the extracellular matrix? A model study in matrigel using polymer-grafted nanoparticles′. *Langmuir*, *36*, 10460–10470. https://doi.org/10.1021/acs.langmuir.0c01624

Gong, C., Acik, M., Abolfath, R. M., Chabal, Y., & Cho, K. (2012). Graphitization of graphene oxide with ethanol during thermal reduction. *The Journal of Physical Chemistry C*, *116*(18), 9969–9979.

Gupta, J., Prakash, A., Jaiswal, M. K., Agarrwal, A., & Bahadur, D. (2018). Superparamagnetic iron oxide-reduced graphene oxide nanohybrid-a vehicle for targeted drug delivery and hyperthermia treatment of cancer. *Journal of*

Magnetism and Magnetic Materials, *448*, 332–338. https://doi.org/10.1016/j.jmmm.2017.05.084

Gurunathan, S., & Kim, J. (2016). Synthesis, toxicity, biocompatibility, and biomedical applications of graphene and graphene-related materials. *International Journal of Nanomedicine*, 11, 1927–1945.

Hashemi, M., Yadegari, A., Yazdanpanah, G., Jabbehdari, S., Omidi, M., & Tayebi, L. (2016). Functionalized R9-reduced graphene oxide as an efficient nano-carrier for hydrophobic drug delivery. *RSC Advances*, *6*(78), 74072–74084. https://doi.org/10.1039/c6ra13822e

Hazhir, N., Chekin, F., Raoof, J. B., & Fathi, S. (2019). A porous reduced graphene oxide/chitosan-based nanocarrier as a delivery system of doxorubicin. *RSC Advances*, *9*(53), 30729–30735. https://doi.org/10.1039/c9ra04977k

He, M., Guo, X., Huang, J., Shen, H., Zeng, Q., & Wang, L. (2018). Mass production of tunable multicolor graphene quantum dots from an energy resource of coke by a one-step electrochemical exfoliation. *Carbon*, *140*, 508–520. https://doi.org/10.1016/j.carbon.2018.08.067

He, T., Li, F., Huang, Y., Sun, T., Lin, J., & Huang, P. (2018). Graphene as 2D nano-theranostic materials for cancer. In *Handbook of Nanomaterials for Cancer Theranostics*. Elsevier Inc. https://doi.org/10.1016/B978-0-12-813339-2.00004-9

Herizchi, R., Abbasi, E., Milani, M., & Akbarzadeh, A. (2016). Current methods for synthesis of gold nanoparticles. *Artificial Cells, Nanomedicine and Biotechnology*, *44*(2), 596–602. https://doi.org/10.3109/21691401.2014.971807

Hu, Yanfang, Sun, D., Ding, J., Chen, L., & Chen, X. (2016). Decorated reduced graphene oxide for photo-chemotherapy. *Journal of Materials Chemistry B*, *4*(5), 929–937. https://doi.org/10.1039/c5tb02359a

Hu, Ying, Lu, L., Liu, J., & Chen, W. (2012). Direct growth of size-controlled gold nanoparticles on reduced graphene oxide film from bulk gold by tuning electric field: Effective methodology and substrate for surface enhanced Raman scattering study. *Journal of Materials Chemistry*, *22*(24), 11994–12000. https://doi.org/10.1039/c2jm31483e

Huang, C. Y., Ju, D. T., Chang, C. F., Muralidhar Reddy, P., & Velmurugan, B. K. (2017). A review on the effects of current chemotherapy drugs and natural agents in treating non-small cell lung cancer. *BioMedicine (France)*, *7*(4), 12–23. https://doi.org/10.1051/bmdcn/2017070423

Huang, D., & Wang, A. (2013). Non-covalently functionalized multiwalled carbon nanotubes by chitosan and their synergistic reinforcing effects in PVA films. *RSC Advances*, *3*(4), 1210–1216. https://doi.org/10.1039/c2ra22016d

Huang, H., Silva, K. K. H. De, Kumara, G. R. A., & Yoshimura, M. (2018). Structural evolution of hydrothermally derived reduced graphene oxide. *Scientific Reports*, *8*(1), 1–9. https://doi.org/10.1038/s41598-018-25194-1

Huang, Y., Zhu, C., Pan, H., Xu, D., Lu, T., Mao, L., Meng, X., Chen, Z., Zhang, D., & Zhu, S. (2017). Fabrication of AgBr / boron-doped reduced graphene oxide aerogels for photocatalytic removal of Cr (VI) in water. *RSC Advances*, *7*, 36000–36006.

Huh, & Seung Hun. (2011). Thermal reduction of graphene oxide. In *Physics and Applications of Graphene-Experiments* (pp. 73–90). https://books.google.com.tr/books?hl=en&lr=&id=Z8ePDwAAQBAJ&oi=fnd&pg=PA73&dq=Thermal+reduction+of+graphene+oxide&ots=H29B9a_4eF&sig=uGDJuLBnEIqGAJLkMYfi2IrzaAk&redir_esc=y#v=onepage&q=Thermal reduction of graphene oxide&f=false

Hwang, M. T., Heiranian, M., Kim, Y., You, S., Leem, J., Taqieddin, A., Faramarzi, V., Jing, Y., Park, I., van der Zande, A. M., Nam, S., Aluru, N. R., & Bashir, R. (2020). Ultrasensitive detection of nucleic acids using deformed graphene

channel field effect biosensors. *Nature Communications*, *11*. 1543. https://doi.org/10.1038/s41467-020-15330-9

Iannazzo, D., Pistone, A., Salamò, M., Galvagno, S., Romeo, R., Giofré, S. V., Branca, C., Visalli, G., & Di Pietro, A. (2017). Graphene quantum dots for cancer targeted drug delivery. *International Journal of Pharmaceutics*, *518*(1–2), 185–192. https://doi.org/10.1016/j.ijpharm.2016.12.060

Ishida, H., Campbell, S., & Blackwell, J. (2000). General approach to nanocomposite preparation. *Chemistry of Materials*, *12*(5), 1260–1267. https://doi.org/10.1021/cm990479y

Islam, W., Matsumoto, Y., Fang, J., Harada, A., Niidome, T., Ono, K., Tsutsuki, H., Sawa, T., Imamura, T., Sakurai, K., Fukumitsu, N., Yamamoto, H., & Maeda, H. (2021). Polymer-conjugated glucosamine complexed with boric acid shows tumor-selective accumulation and simultaneous inhibition of glycolysis. *Biomaterials*, *269*, 120631. https://doi.org/10.1016/j.biomaterials.2020.120631

Jakhar, R., Yap, J. E., & Joshi, R. (2020). Microwave reduction of graphene oxide. *Carbon*, *170*, 277–293. https://doi.org/10.1016/j.carbon.2020.08.034

Jampilek, J., & Kralova, K. (2021). Advances in drug delivery nanosystems using graphene- based materials and carbon nanotubes. *Materials*, *14*(5), 1–39. https://doi.org/10.3390/ma14051059

Javadian, S., Najafi, K., Sadrpoor, S. M., Ektefa, F., Dalir, N., & Nikkhah, M. (2021). Graphene quantum dots based magnetic nanoparticles as a promising delivery system for controlled doxorubicin release. *Journal of Molecular Liquids*, *331*, 115746. https://doi.org/10.1016/j.molliq.2021.

Javanbakht, S., & Namazi, H. (2018). Doxorubicin loaded carboxymethyl cellulose/graphene quantum dot nanocomposite hydrogel films as a potential anticancer drug delivery system. *Materials Science and Engineering C*, *87*, 50–59. https://doi.org/10.1016/j.msec.2018.02.010

Ji, X., Kong, N., Wang, J., Li, W., Xiao, Y., Gan, S. T., Tao, W., Zhang, H., Mei, L., & Shi, J. (2018). A novel top-down synthesis of ultrathin 2D boron nanosheets for multimodal imaging-guided cancer therapy. *Advanced Materials*, *1803031*, 1–11. https://doi.org/10.1002/adma.201803031

Kadiyala, N. K., Mandal, B. K., Ranjan, S., & Dasgupta, N. (2018). Bioinspired gold nanoparticles decorated reduced graphene oxide nanocomposite using Syzygium cumini seed extract: Evaluation of its biological applications. *Materials Science and Engineering C*, *93*, 191–205. https://doi.org/10.1016/j.msec.2018.07.075

Kandru, A. (2020). Nanotechnology: Application in biology and medicine. In *Model Organisms to Study Biological Activities and Toxicity of Nanoparticles*. Springer. https://doi.org/10.1007/978-981-15-1702-0

Kargozar, S., & Mozafari, M. (2018). Nanotechnology and Nanomedicine: Start small, think big. *Materials Today: Proceedings*, *5*(7), 15492–15500. https://doi.org/10.1016/j.matpr.2018.04.155

Karimi, S., & Namazi, H. (2020). Simple preparation of maltose-functionalized dendrimer/graphene quantum dots as a pH-sensitive biocompatible carrier for targeted delivery of doxorubicin. *International Journal of Biological Macromolecules*, *156*, 648–659. https://doi.org/10.1016/j.ijbiomac.2020.04.037

Kaurav, H., Manchanda, S., Dua, K., & Kapoor, D. N. (2018). Nanocomposites in controlled & targeted drug delivery systems. *Nano Hybrids and Composites*, *20*, 27–45. https://doi.org/10.4028/www.scientific.net/nhc.20.27

Kenry, Chaudhuri, P. K., Loh, K. P., & Lim, C. T. (2016). Selective accelerated proliferation of malignant breast cancer cells on planar graphene oxide films. *ACS Nano*, *10*(3), 3424–3434. https://doi.org/10.1021/acsnano.5b07409

Khan, A. K., Rashid, R., Murtaza, G., & Zahra, A. (2014). Gold nanoparticles: Synthesis and applications in drug delivery. *Tropical Journal of*

Pharmaceutical Research, *13*(7), 1169–1177. https://doi.org/10.4314/tjpr.v13i7.23

Khan, I., Saeed, K., & Khan, I. (2019). Nanoparticles : Properties , applications and toxicities. *Arabian Journal of Chemistry*, *12*(7), 908–931. https://doi.org/10.1016/j.arabjc.2017.05.011

Kim, H., Lee, D., Kim, J., Kim, T. Il, & Kim, W. J. (2013). Photothermally triggered cytosolic drug delivery via endosome disruption using a functionalized reduced graphene oxide. *ACS Nano*, *7*(8), 6735–6746. https://doi.org/10.1021/nn403096s

Kim, M. G., Park, J. Y., Miao, W., Lee, J., & Oh, Y. K. (2015). Polyaptamer DNA nanothread-anchored, reduced graphene oxide nanosheets for targeted delivery. *Biomaterials*, *48*, 129–136. https://doi.org/10.1016/j.biomaterials.2015.01.009

Kir, Ş., Dehri, İ., Önal, Y., & Esen, R. (2021). Graphene quantum dots prepared from dried lemon leaves and microcrystalline mosaic structure. *Luminescence*, *36*(6), 1365–1376. https://doi.org/10.1002/bio.4060

Kong, F. Y., Zhang, J. W., Li, R. F., Wang, Z. X., Wang, W. J., & Wang, W. (2017). Unique roles of gold nanoparticles in drug delivery, targeting and imaging applications. *Molecules*, *22*(9), 1445. https://doi.org/10.3390/molecules22091445

Lamb, J., Fischer, E., Rosillo-Lopez, M., Salzmann, C. G., & Holland, J. P. (2019). Multi-functionalised graphene nanoflakes as tumour-targeting theranostic drug-delivery vehicles. *Chemical Science*, *10*(38), 8880–8888. https://doi.org/10.1039/c9sc03736e

Lee, J. W., Choi, S. R., & Heo, J. H. (2021). Simultaneous stabilization and functionalization of gold nanoparticles via biomolecule conjugation: progress and perspectives. *ACS Applied Materials and Interfaces*. 42311-42328. https://doi.org/10.1021/acsami.1c10436

Levy J.G. (1994). *Photosensitizers in photodynamic therapy,* Semin Oncol. 6, 4-10. https://pubmed.ncbi.nlm.nih.gov/7992105/

Li, L., Xi, W., Su, Q., Li, Y., Yan, G., Liu, Y., & Wang, H. (2019). Unexpected size effect : The interplay between different- sized nanoparticles in their cellular uptake. *Small*, *1901687*, 1–8. https://doi.org/10.1002/smll.201901687

Liang, J., Liu, J., Jin, X., Yao, S., Chen, B., Huang, Q., Hu, J., Wan, J., Hu, Z., & Wang, B. (2020). Versatile nanoplatform loaded with doxorubicin and graphene quantum dots/methylene blue for drug delivery and chemophotothermal/photodynamic synergetic cancer therapy. *ACS Applied Bio Materials*, *3*(10), 7122–7132. https://doi.org/10.1021/acsabm.0c00942

Liszbinski, R. B., Romagnoli, G. G., Gorgulho, C. M., Basso, C. R., Pedrosa, V. A., & Kaneno, R. (2020). Anti-EGFR-coated gold nanoparticles in vitro carry 5-fluorouracil to colorectal cancer cells. *Materials*, *13*(2). 375 https://doi.org/10.3390/ma13020375

Liu, D., Chen, X., Hu, Y., Sun, T., Song, Z., Zheng, Y., Cao, Y., Cai, Z., Cao, M., Peng, L., Huang, Y., Du, L., Yang, W., Chen, G., Wei, D., Wee, A. T. S., & Wei, D. (2018). Raman enhancement on ultra-clean graphene quantum dots produced by quasi-equilibrium plasma-enhanced chemical vapor deposition. *Nature Communications*, *9*(1), 1–10. https://doi.org/10.1038/s41467-017-02627-5

Liu, F., Jang, M. H., Ha, H. D., Kim, J. H., Cho, Y. H., & Seo, T. S. (2013). Facile synthetic method for pristine graphene quantum dots and graphene oxide quantum dots: Origin of blue and green luminescence. *Advanced Materials*, *25*(27), 3657–3662. https://doi.org/10.1002/adma.201300233

Liu, P., Wu, Q., Li, Y., Li, P., Yuan, J., & Meng, X. (2019). DOX-Conjugated keratin nanoparticles for pH-Sensitive drug delivery. *Colloids and Surfaces B: Biointerfaces*, *181*, 1012–1018. https://doi.org/10.1016/j.colsurfb.2019.06.057

Liu, W., Zhang, X., Zhou, L., Shang, L., & Su, Z. (2019). Reduced graphene oxide

(rGO) hybridized hydrogel as a near-infrared (NIR)/pH dual-responsive platform for combined chemo-photothermal therapy. *Journal of Colloid and Interface Science*, *536*, 160–170. https://doi.org/10.1016/j.jcis.2018.10.050

Lopez-chaves, C., Soto-alvaredo, J., Montes-bayon, M., Bettmer, J., Llopis, J., & Sanchez-gonzalez, C. (2018). Gold nanoparticles : Distribution , bioaccumulation and toxicity . In vitro and in vivo studies. *Nanomedicine: Nanotechnology, Biology, and Medicine*, *14*(1), 1–12. https://doi.org/10.1016/j.nano.2017.08.011

López Marzo, A. M., Mayorga-Martinez, C. C., & Pumera, M. (2020). 3D-printed graphene direct electron transfer enzyme biosensors. *Biosensors and Bioelectronics*, *151*. *111980* . https://doi.org/10.1016/j.bios.2019.111980

Lu, G., Li, H., Liusman, C., Yin, Z., Wu, S., & Zhang, H. (2011). Surface enhanced Raman scattering of Ag or Au nanoparticle-decorated reduced graphene oxide for detection of aromatic molecules. *Chemical Science*, *2*(9), 1817–1821. https://doi.org/10.1039/c1sc00254f

Lu, T., Nong, Z., Wei, L., Wei, M., Li, G., Wu, N., Liu, C., Tang, B., Qin, Q., Li, X., & Meng, F. (2020). Preparation and anti-cancer activity of transferrin/folic acid double-targeted graphene oxide drug delivery system. *Journal of Biomaterials Applications*, *35*(1), 15–27. https://doi.org/10.1177/0885328220913976

Ma, N., Zhang, B., Liu, J., Zhang, P., Li, Z., & Luan, Y. (2015). Green fabricated reduced graphene oxide: Evaluation of its application as nano-carrier for pH-sensitive drug delivery. *International Journal of Pharmaceutics*, *496*(2), 984–992. https://doi.org/10.1016/j.ijpharm.2015.10.081

Magaela, N. B., Matshitse, R., & Nyokong, T. (2022). The effect of charge on Zn tetra morpholine porphyrin conjugated to folic acid-nitrogen doped graphene quantum dots for photodynamic therapy studies. *Photodiagnosis and Photodynamic Therapy*, 39, 102898. https://doi.org/10.1016/j.pdpdt.2022.102898

Maleki, A. A., & Fotouhi, A. (2019). Nanoparticles and cancer therapy : Perspectives for application of nanoparticles in the treatment of cancers. *Cellular Physiology*, *235*, 1962–1972. https://doi.org/10.1002/jcp.29126

Malekmohammadi, S., Hadadzadeh, H., Farrokhpour, H., & Amirghofran, Z. (2018). Immobilization of gold nanoparticles on folate-conjugated dendritic mesoporous silica-coated reduced graphene oxide nanosheets: A new nanoplatform for curcumin pH-controlled and targeted delivery. *Soft Matter*, *14*(12), 2400–2410. https://doi.org/10.1039/c7sm02248d

Mannan, M. A., Hirano, Y., Quitain, A. T., M, K., & Kida, T. (2018). Boron doped graphene oxide: synthesis and application to glucose responsive reactivity. *Journal of Material Science & Engineering*, *07*(05), 1–6. https://doi.org/10.4172/2169-0022.1000492

Mei, X., Meng, X., & Wu, F. (2015). Hydrothermal method for the production of reduced graphene oxide GO colloidal solution GO lamellar solid sample for conductivity test. *Physica E: Low-Dimensional Systems and Nanostructures*, *68*, 81–86. https://doi.org/10.1016/j.physe.2014.12.011

Mianehrow, H., Afshari, R., Mazinani, S., Sharif, F., & Abdouss, M. (2016). Introducing a highly dispersed reduced graphene oxide nano-biohybrid employing chitosan/hydroxyethyl cellulose for controlled drug delivery. *International Journal of Pharmaceutics*, *509*(1–2), 400–407. https://doi.org/10.1016/j.ijpharm.2016.06.015

Miao, W., Shim, G., Kang, C. M., Lee, S., Choe, Y. S., Choi, H. G., & Oh, Y. K. (2013). Cholesteryl hyaluronic acid-coated, reduced graphene oxide nanosheets for anti-cancer drug delivery. *Biomaterials*, *34*(37), 9638–9647. https://doi.org/10.1016/j.biomaterials.2013.08.058

Mishra, S., Sharma, S., Javed, M. N., Pottoo, F. H., Barkat, M. A., Harshita, Alam, M. S., Amir, M., & Sarafroz, M. (2019). Bioinspired nanocomposites: applications in disease diagnosis and treatment. *Pharmaceutical*

Nanotechnology, *7*(3), 206–219. https://doi.org/10.2174/2211738507666190425121509

Mokammel, M. A., Islam, M. J., Hasanuzzaman, M., & Hashmi, S. (2019). Nanoscale materials for self-cleaning and antibacterial applications. In *Reference Module in Materials Science and Materials Engineering* (pp. 1–10). https://doi.org/10.1016/b978-0-12-803581-8.11585-1

Mostafavi, F. S., & Imani, R. (2021). *Synthesis and characterization of functionalized reduced graphene oxide for drug delivery application*. *Pathobiology Research, 23*(5), 75–85.

Nasrollahzadeh, M., Sajadi, S. M., Sajjadi, M., & Issaabadi, Z. (2019). An Introduction to Nanotechnology. In *Interface Science and Technology* (1st ed., Vol. 28). Elsevier Ltd. https://doi.org/10.1016/B978-0-12-813586-0.00001-8

Navaee, A., & Salimi, A. (2015). Efficient amine functionalization of graphene oxide through the Bucherer reaction: An extraordinary metal-free electrocatalyst for the oxygen reduction reaction. *RSC Advances*, *5*(74), 59874–59880. https://doi.org/10.1039/c5ra07892j

Ngidi, N. P. D., Ollengo, M. A., & Nyamori, V. O. (2020). Tuning the properties of boron-doped reduced graphene oxide by altering the boron content. *New Journal of Chemistry*, *44*(39), 16864–16876. https://doi.org/10.1039/d0nj03909h

Nxele, S. R., & Nyokong, T. (2022). Time-dependent characterization of graphene quantum dots and graphitic carbon nitride quantum dots synthesized by hydrothermal methods. *Diamond and Related Materials*, *121*, 108751. https://doi.org/10.1016/j.diamond.2021.108751

Otari, S. V., Kumar, M., Anwar, M. Z., Thorat, N. D., Patel, S. K. S., Lee, D., Lee, J. H., Lee, J. K., Kang, Y. C., & Zhang, L. (2017). Rapid synthesis and decoration of reduced graphene oxide with gold nanoparticles by thermostable peptides for memory device and photothermal applications. *Scientific Reports*,

7(1), 1–14. https://doi.org/10.1038/s41598-017-10777-1

Park, S., Hu, Y., Hwang, J. O., Lee, E., Casabianca, L. B., Cai, W., Potts, J. R., Ha, H., Chen, S., Oh, J., Kim, S. O., Kim, Y., Ishii, Y., & Ruoff, R. S. (2012). Chemical structures of hydrazine-treated graphene oxide and generation of aromatic nitrogen doping. *Nature Communications*. 3, 638. https://doi.org/10.1038/ncomms1643

Patil, M. P., & Kim, G. Do. (2018). Marine microorganisms for synthesis of metallic nanoparticles and their biomedical applications. *Colloids and Surfaces B: Biointerfaces*, *172*, 487–495. https://doi.org/10.1016/j.colsurfb.2018.09.007

Pissuwan, D. (2017). Monitoring and tracking metallic nanobiomaterials in vivo. In *Monitoring and Evaluation of Biomaterials and their Performance In Vivo* (pp. 135–149). Elsevier. https://doi.org/10.1016/B978-0-08-100603-0.00007-9

Pooresmaeil, M., & Namazi, H. (2021). Fabrication of a smart and biocompatible brush copolymer decorated on magnetic graphene oxide hybrid nanostructure for drug delivery application. *European Polymer Journal*, *142*, 110126. https://doi.org/10.1016/j.eurpolymj.2020.110126

Qi, Z., Shi, J., Zhang, Z., Cao, Y., Li, J., & Cao, S. (2019). PEGylated graphene oxide-capped gold nanorods/silica nanoparticles as multifunctional drug delivery platform with enhanced near-infrared responsiveness. *Materials Science and Engineering C*, *104*, 109889. https://doi.org/10.1016/j.msec.2019.109889

Queiroz, M. F., Melo, K. R. T., Sabry, D. A., Sassaki, G. L., & Rocha, H. A. O. (2015). Does the use of chitosan contribute to oxalate kidney stone formation? *Marine Drugs*, *13*(1), 141–158. https://doi.org/10.3390/md13010141

Rahman, M. M., & Abdullah, M. A. (2018). Introductory Chapter: Basic concept of gold nanoparticles. *Intechopen*, *32*, 137–144. https://www.intechopen.com/books/advanced-biometric-technologies/liveness-detection-in-biometrics

Rai, M., Nagaonkar, D., & Ingle, A. P. (2018). Metal nanoparticles as therapeutic agents: A paradigm shift in medicine. Metal Nanoparticles: Synthesis and Publications in Pharmaceutical Sciences. (Vol. 2002, Issue 8). https://doi.org/10.1016/s1351-4180(02)00858-9

Rao, Z., Ge, H., Liu, L., Zhu, C., Min, L., Liu, M., Fan, L., & Li, D. (2018). Carboxymethyl cellulose modified graphene oxide as pH-sensitive drug delivery system. *International Journal of Biological Macromolecules*, *107*(PartA), 1184–1192. https://doi.org/10.1016/j.ijbiomac.2017.09.096

Rizvi, S. A. A., & Saleh, A. M. (2018). Applications of nanoparticle systems in drug delivery technology. *Saudi Pharmaceutical Journal*, *26*(1), 64–70. https://doi.org/10.1016/j.jsps.2017.10.012

Robertson, C. A., Evans, D. H., & Abrahamse, H. (2009). Photodynamic therapy (PDT): A short review on cellular mechanisms and cancer research applications for PDT. *Journal of Photochemistry and Photobiology B: Biology*, *96*(1), 1–8. https://doi.org/10.1016/j.jphotobiol.2009.04.001

Sadhukhan, S., Ghosh, T. K., Rana, D., Roy, I., Bhattacharyya, A., Sarkar, G., Chakraborty, M., & Chattopadhyay, D. (2016). Studies on synthesis of reduced graphene oxide (RGO) via green route and its electrical property. *Materials Research Bulletin*, *79*, 41–51. https://doi.org/10.1016/j.materresbull.2016.02.039

Saini, R., Saini, S., & Sharma, S. (2010). Nanotechnology: The future medicine. *Journal of Cutaneous and Aesthetic Surgery*, *3*(1), 32. https://doi.org/10.4103/0974-2077.63301

Sali, S., Mackey, H. R., & Abdala, A. A. (2019). Effect of graphene oxide synthesis method on properties and performance of polysulfone-graphene oxide mixed matrix membranes. *Nanomaterials*, *9*(5), p.769. https://doi.org/10.3390/nano9050769

Samadian, H., Mohammad-Rezaei, R., Jahanban-Esfahlan, R., Massoumi, B.,

Abbasian, M., Jafarizad, A., & Jaymand, M. (2020). A de novo theranostic nanomedicine composed of PEGylated graphene oxide and gold nanoparticles for cancer therapy. *Journal of Materials Research*, *35*(4), 430–441. https://doi.org/10.1557/jmr.2020.3

Sawy, A. M., Barhoum, A., Abdel Gaber, S. A., El-Hallouty, S. M., Shousha, W. G., Maarouf, A. A., & Khalil, A. S. G. (2021). Insights of doxorubicin loaded graphene quantum dots: Synthesis, DFT drug interactions, and cytotoxicity. *Materials Science and Engineering C*, *122*, 111921. https://doi.org/10.1016/j.msec.2021.111921

Seifati, S. M., Nasirizadeh, N., & Azimzadeh, M. (2018). Nano-biosensor based on reduced graphene oxide and gold nanoparticles, for detection of phenylketonuria-associated DNA mutation. *IET Nanobiotechnology*, *12*(4), 417–422. https://doi.org/10.1049/iet-nbt.2017.0128

Sengupta, I., Chakraborty, S., & Talukdar, M. (2018). Thermal reduction of graphene oxide : How temperature influences purity. *Journal of Materials Research*, *33*(23), 4113–4122. https://doi.org/10.1557/jmr.2018.338

Shah, S., Chandra, A., Kaur, A., Sabnis, N., Lacko, A., Gryczynski, Z., Fudala, R., & Gryczynski, I. (2017). Fluorescence properties of doxorubicin in PBS buffer and PVA films. *Journal of Photochemistry and Photobiology. B, Biology*, *170*, 65–69. https://doi.org/10.1016/j.jphotobiol.2017.03.024

Shahrokhian, S., & Salimian, R. (2018). Ultrasensitive detection of cancer biomarkers using conducting polymer/electrochemically reduced graphene oxide-based biosensor: Application toward BRCA1 sensing. *Sensors and Actuators, B: Chemical*, *266*, 160–169. https://doi.org/10.1016/j.snb.2018.03.120

Shao, Y., Wang, J., Engelhard, M., Wang, C., & Lin, Y. (2010). Facile and controllable electrochemical reduction of graphene oxide and its applications. *Journal of Materials Chemistry*, *20*(4), 743–748.

https://doi.org/10.1039/b917975e

Sheng, Y., Dai, W., Gao, J., Li, H., Tan, W., Wang, J., Deng, L., & Kong, Y. (2020). pH-sensitive drug delivery based on chitosan wrapped graphene quantum dots with enhanced fluorescent stability. *Materials Science and Engineering C*, *112*, 110888. https://doi.org/10.1016/j.msec.2020.110888

Shewach, D. S. (2014). Introduction to Cancer Chemotherapeutics. *NIH Public Access*, *23*(1), 1–7. https://doi.org/10.1021/cr900208x.Introduction

Shu, M., Gao, F., Zeng, M., Yu, C., Wang, X., Huang, R., Yang, J., Su, Y., Hu, N., Zhou, Z., Liu, K., Yang, Z., Tan, H., & Xu, L. (2021). Microwave-assisted chitosan-functionalized graphene oxide as controlled ıntracellular drug delivery nanosystem for synergistic antitumour activity. *Nanoscale Research Letters*, *16*(1), 1–12. https://doi.org/10.1186/s11671-021-03525-y

Shuaib, M., Saheed, M., Kumar, P., Ullah, Z., & Yar, A. (2020). Boron-doped reduced graphene oxide with tunable bandgap and enhanced surface plasmon resonance. *Molecules*, *25*(16), 3646.

Silva, K Kanishka H De, Huang, H., & Yoshimura, M. (2018). Applied Surface Science Progress of reduction of graphene oxide by ascorbic acid. *Applied Surface Science*, *447*, 338–346. https://doi.org/10.1016/j.apsusc.2018.03.243

Singh, R. K., Kumar, R., & Singh, D. P. (2016). Graphene oxide: Strategies for synthesis, reduction and frontier applications. *RSC Advances*, *6*(69), 64993–65011. https://doi.org/10.1039/c6ra07626b

Sohani, O. R., Phatak, A. A., & Chaudhari, P. D. (2015). Use of nanocomposites in drug delivery systems. *Pharma Times*, *47*(4), 33–35.

Stanglmair, C., Scheeler, S. P., & Pacholski, C. (2014). Seeding growth approach to gold nanoparticles with diameters ranging from 10 to 80 nanometers in organic solvent. *European Journal of Inorganic Chemistry*, *23*, 3633–3637. https://doi.org/10.1002/ejic.201402467

Su, X., Chan, C., Shi, J., Tsang, M. K., Pan, Y., Cheng, C., Gerile, O., & Yang, M. (2017). A graphene quantum dot@Fe3O4@SiO2 based nanoprobe for drug delivery sensing and dual-modal fluorescence and MRI imaging in cancer cells. *Biosensors and Bioelectronics*, *92*, 489–495. https://doi.org/10.1016/j.bios.2016.10.076

Sun, J., & Du, S. (2019). Application of graphene derivatives and their nanocomposites in tribology and lubrication: A review. *RSC Advances*, *9*(69), 40642–40661. https://doi.org/10.1039/c9ra05679c

Tang, X., Li, X., Cao, Z., & Yu, Z. (2013). Synthesis of graphene decorated with silver nanoparticles by simultaneous reduction of graphene oxide and silver ions with glucose. *Carbon*, *59*, 93–99. https://doi.org/10.1016/j.carbon.2013.02.058

Tarcan, R., Todor-Boer, O., Petrovai, I., Leordean, C., Astilean, S., & Botiz, I. (2020). Reduced graphene oxide today. *Journal of Materials Chemistry C*, *8*(4), 1198–1224. https://doi.org/10.1039/c9tc04916a

Thambiraj, S., Hema, S., & Ravi Shankaran, D. (2018). Functionalized gold nanoparticles for drug delivery applications. *Materials Today: Proceedings*, *5*(8), 16763–16773. https://doi.org/10.1016/j.matpr.2018.06.030

Thasneem, Y. M., Sajeesh, S., & Sharma, C. P. (2013). Glucosylated polymeric nanoparticles: A sweetened approach against blood compatibility paradox. *Colloids and Surfaces B: Biointerfaces*, *108*, 337–344. https://doi.org/10.1016/j.colsurfb.2013.03.001

Toh, S. Y., Loh, K. S., Kamarudin, S. K., & Daud, W. R. W. (2014). Graphene production via electrochemical reduction of graphene oxide: Synthesis and characterisation. *Chemical Engineering Journal*, *251*, 422–434. https://doi.org/10.1016/j.cej.2014.04.004

Turan, N. B., Erkan, H. S., Engin, G. O., & Bilgili, M. S. (2019). Nanoparticles in the aquatic environment: Usage, properties, transformation and toxicity—A

review. *Process Safety and Environmental Protection*, *130*, 238–249. https://doi.org/10.1016/j.psep.2019.08.014

Turkevich, J., Stevenson, P. C., & Hillier, J. (1951). A study of the nucleation and growth processes in the synthesis of colloidal gold. *Discussions of the Faraday Society*, *11*(c), 55–75. https://doi.org/10.1039/DF9511100055

Understanding Cancer. (2007). *National Institutes of Health Study, Biological Sciences Curriculum*. https://www.ncbi.nlm.nih.gov/books/NBK20362/

Ur Rehman, S. R., Augustine, R., Zahid, A. A., Ahmed, R., Tariq, M., & Hasan, A. (2019). Reduced graphene oxide incorporated gelma hydrogel promotes angiogenesis for wound healing applications. *International Journal of Nanomedicine*, *14*, 9603–9617. https://doi.org/10.2147/IJN.S218120

Usman, M. S., Hussein, M. Z., Kura, A. U., Fakurazi, S., Masarudin, M. J., & Saad, F. F. A. (2018). Graphene oxide as a nanocarrier for a theranostics delivery system of protocatechuic acid and gadolinium/gold nanoparticles. *Molecules*, *23*(2), 1–16. https://doi.org/10.3390/molecules23020500

Wang, C., Zhang, Z., Chen, B., Gu, L., Li, Y., & Yu, S. (2018). Design and evaluation of galactosylated chitosan/graphene oxide nanoparticles as a drug delivery system. *Journal of Colloid and Interface Science*, *516*, 332–341. https://doi.org/10.1016/j.jcis.2018.01.073

Wang, Q., Tu, Y., Ichii, T., Utsunomiya, T., Sugimura, H., Hao, L., Wang, R., & He, X. (2017). Decoration of reduced graphene oxide by gold nanoparticles: An enhanced negative photoconductivity. *Nanoscale*, *9*(38), 14703–14709. https://doi.org/10.1039/c7nr05143c

Wang, X., Sun, X., Lao, J., He, H., Cheng, T., Wang, M., Wang, S., & Huang, F. (2014). Multifunctional graphene quantum dots for simultaneous targeted cellular imaging and drug delivery. *Colloids and Surfaces B: Biointerfaces*, *122*, 638–644. https://doi.org/10.1016/j.colsurfb.2014.07.043

Weaver, C. L., Larosa, J. M., Luo, X., & Cui, X. T. (2014). Electrically controlled drug delivery from graphene oxide nanocomposite films. *ACS Nano*, *8*(2), 1834–1843. https://doi.org/10.1021/nn406223e

Wei, G., Yan, M., Dong, R., Wang, D., Zhou, X., Chen, J., & Hao, J. (2012). Covalent modification of reduced graphene oxide by means of diazonium chemistry and use as a drug-delivery system. *Chemistry - A European Journal*, *18*(46), 14708–14716. https://doi.org/10.1002/chem.201200843

Wei, S., Zhang, R., Liu, Y., Ding, H., & Zhang, Y. L. (2016). Graphene quantum dots prepared from chemical exfoliation of multiwall carbon nanotubes: An efficient photocatalyst promoter. *Catalysis Communications*, *74*, 104–109. https://doi.org/10.1016/j.catcom.2015.11.010

Wu, H., Shi, H., Wang, Y., Jia, X., Tang, C., Zhang, J., & Yang, S. (2014). Hyaluronic acid conjugated graphene oxide for targeted drug delivery. *Carbon*, *69*, 379–389. https://doi.org/10.1016/j.carbon.2013.12.039

Xin Lee, K., Shameli, K., Miyake, M., Kuwano, N., Bt Ahmad Khairudin, N. B., Bt Mohamad, S. E., & Yew, Y. P. (2016). Green synthesis of gold nanoparticles using aqueous extract of garcinia mangostana fruit peels. *Journal of Nanomaterials*, *2016, , 8489094* . https://doi.org/10.1155/2016/8489094

Xu, C., Shi, X., Ji, A., Shi, L., Zhou, C., & Cui, Y. (2015). Fabrication and characteristics of reduced graphene oxide produced with different green reductants. *PLoS ONE*, *10*(12). 0144842. https://doi.org/10.1371/journal.pone.

Yamada, Y. (2020). Dimerization of doxorubicin causes its precipitation. *ACS Omega*, *5*(51), 33235–33241. https://doi.org/10.1021/acsomega.0c04925

Yan, T., Zhang, H., Huang, D., Feng, S., Fujita, M., & Gao, X. D. (2017). Chitosan-functionalized graphene oxide as a potential immunoadjuvant. *Nanomaterials*, *7*(3), 59. https://doi.org/10.3390/nano7030059

Yang, X., Zhang, X., Liu, Z., Ma, Y., Huang, Y., & Chen, Y. (2008). High-efficiency

loading and controlled release of doxorubicin hydrochloride on graphene oxide. *Journal of Physical Chemistry C*, *112*(45), 17554–17558. https://doi.org/10.1021/jp806751k

Ye, Y., Yan, W., Liu, Y., He, S., Cao, X., Xu, X., Zheng, H., & Gunasekaran, S. (2019). Electrochemical detection of salmonella using an inva genosensor on polypyrrole-reduced graphene oxide modified glassy carbon electrode and AuNPs-horseradish peroxidase-streptavidin as nanotag. *Analytica Chimica Acta*, *1074*, 80–88. https://doi.org/10.1016/j.aca.2019.05.012

Yih, J., Mubarak, N. M., Abdullah, E. C., & Nizamuddin, S. (2018). Recent trends in the synthesis of graphene and graphene oxide based nanomaterials for removal of heavy metals — A review. *Journal of Industrial and Engineering Chemistry*, *66*, 29–44. https://doi.org/10.1016/j.jiec.2018.05.028

Zhan, H., & Liang, J. F. (2016). Extreme activity of drug nanocrystals coated with a layer of non-covalent polymers from self-assembled boric acid. *Scientific Reports*, *6*, 1–11. https://doi.org/10.1038/srep38668

Zhang, B., Yang, X., Wang, Y., & Zhai, G. (2017). Heparin modified graphene oxide for pH-sensitive sustained release of doxorubicin hydrochloride. *Materials Science and Engineering C*, *75*, 198–206. https://doi.org/10.1016/j.msec.2017.02.048

Zhang, C. C., Gao, X., & Yilmaz, B. (2020). Development of ftir spectroscopy methodology for characterization of boron species in fcc catalysts. *Catalysts*, *10*(11), 1–11. https://doi.org/10.3390/catal10111327

Zhang, J., Yang, H., Shen, G., & Cheng, P. (2010). Reduction of graphene oxide via L -ascorbic acid. *Chemical Communications*, *46*(7), 1112–1114. https://doi.org/10.1039/b917705a

Zhang, M., Tao, H., Liu, Y., Yan, C., Hong, S., Masa, J., Robertson, A. W., Liu, S., Qiu, J., & Sun, Z. (2019). Ultrasound-assisted nitrogen and boron codoping of graphene oxide for efficient oxygen reduction reaction. *ACS Sustainable*

Chemistry and Engineering, *7*(3), 3434–3442. https://doi.org/10.1021/acssuschemeng.8b05654

Zhang, Q., Li, W., Kong, T., Su, R., Li, N., Song, Q., Tang, M., Liu, L., & Cheng, G. (2013). Tailoring the interlayer interaction between doxorubicin-loaded graphene oxide nanosheets by controlling the drug content. *Carbon*, *51*(1), 164–172. https://doi.org/10.1016/j.carbon.2012.08.025

Zhang, W., Liu, T., & Xu, J. (2016). Preparation and characterization of 10B boric acid with high purity for nuclear industry. *SpringerPlus*, *5*(1). pp.1-10 https://doi.org/10.1186/s40064-016-2310-6

Zheng, P., & Wu, N. (2017). Fluorescence and sensing applications of graphene oxide and graphene quantum dots: a review. *Chemistry - An Asian Journal*, *12*(18), 2343–2353. https://doi.org/10.1002/asia.201700814

Zhou, X., Zhang, J., Wu, H., Yang, H., Zhang, J., & Guo, S. (2011). Reducing graphene oxide via hydroxylamine : A simple and efficient route to graphene. *The Journal of Physical Chemistry C*, *115*(24), 11957–11961.

Zhu, L., Zhang, C., Guo, C., Wang, X., Sun, P., Zhou, D., Chen, W., & Xue, G. (2013). New insight into intermediate precursors of Brust-Schiffrin gold nanoparticles synthesis. *Journal of Physical Chemistry C*, *117*(21), 11399–11404. https://doi.org/10.1021/jp402116x

Zhu, P., Shen, M., Xiao, S., & Zhang, D. (2011). Experimental study on the reducibility of graphene oxide by hydrazine hydrate. *Physica B: Physics of Condensed Matter*, *406*(3), 498–502. https://doi.org/10.1016/j.physb.2010.11.022

Zhu, Y., Murali, S., Stoller, M. D., Velamakanni, A., Piner, R. D., & Ruoff, R. S. (2010). Microwave assisted exfoliation and reduction of graphite oxide for ultracapacitors. *Carbon*, *48*(7), 2118–2122. https://doi.org/10.1016/j.carbon.2010.02.001

Zoladek, S., Rutkowska, I. A., Blicharska, M., Miecznikowski, K., Ozimek, W., Orlowska, J., Negro, E., Noto, V. Di, & Kulesza, P. J. (2018). Evaluation of reduced-graphene-oxide-supported gold nanoparticles as catalytic system for electroreduction of oxygen in alkaline electrolyte. *Electrochimica Acta*, *233*, 113–122.

APPENDICES

A. Calibration curves

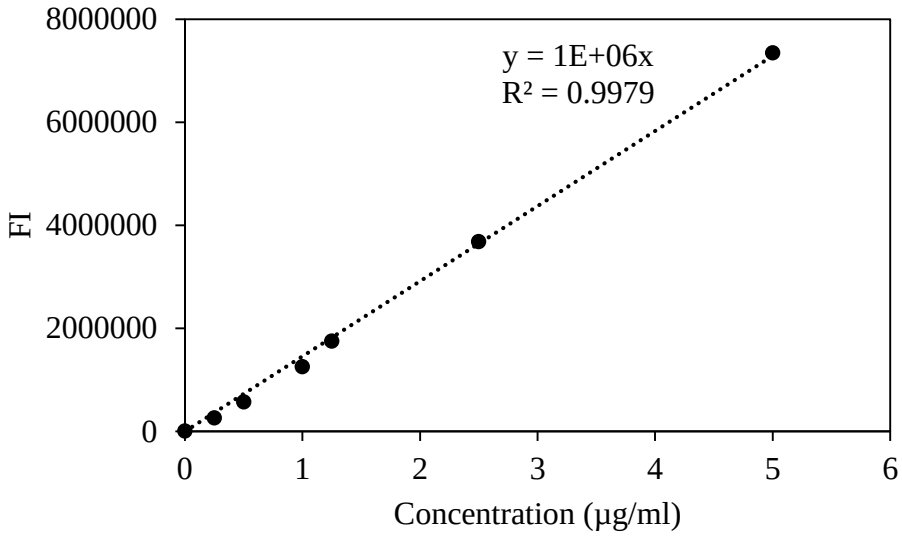

Figure A 1. 1 Calibration curve of DOX constructed with different concentrations of DOX standards prepared in PBS (pH 7.4, 1 M) with 10% DMSO.

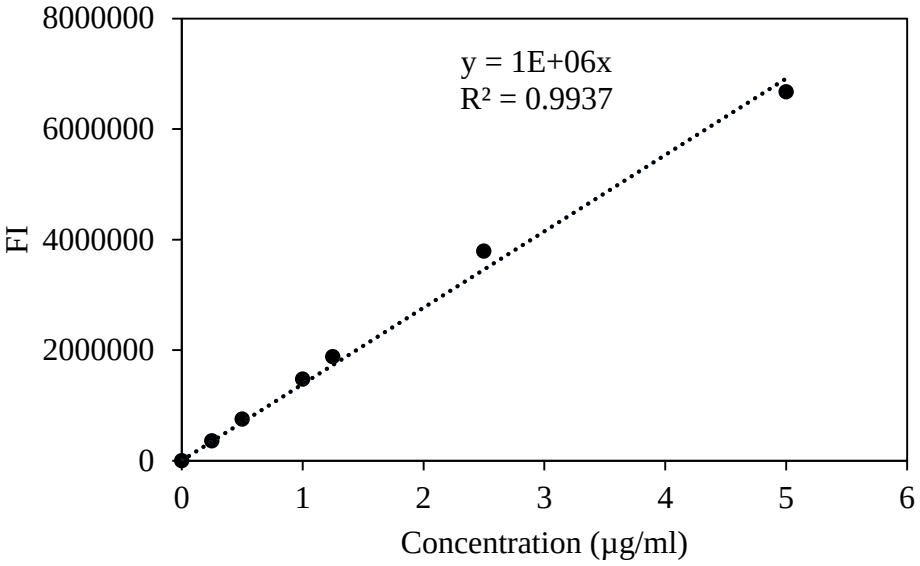

Figure A 1. 2. Calibration curve of DOX constructed with different concentrations of DOX standards prepared in citrate buffer (pH 4, 1 M) with 10% DMSO.

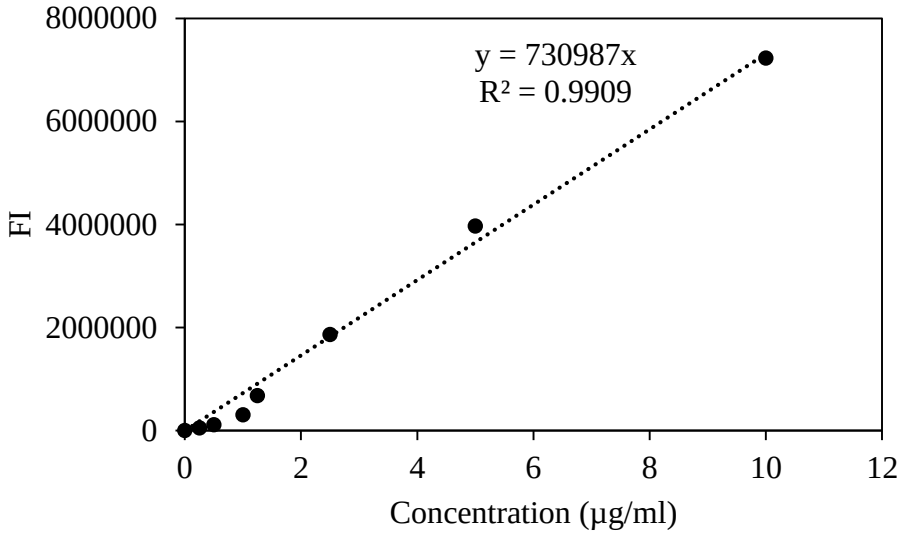

Figure A 1. 3. Calibration curve of DOX constructed with different concentrations of DOX standards prepared in PBS (pH 7.4, 1 M).

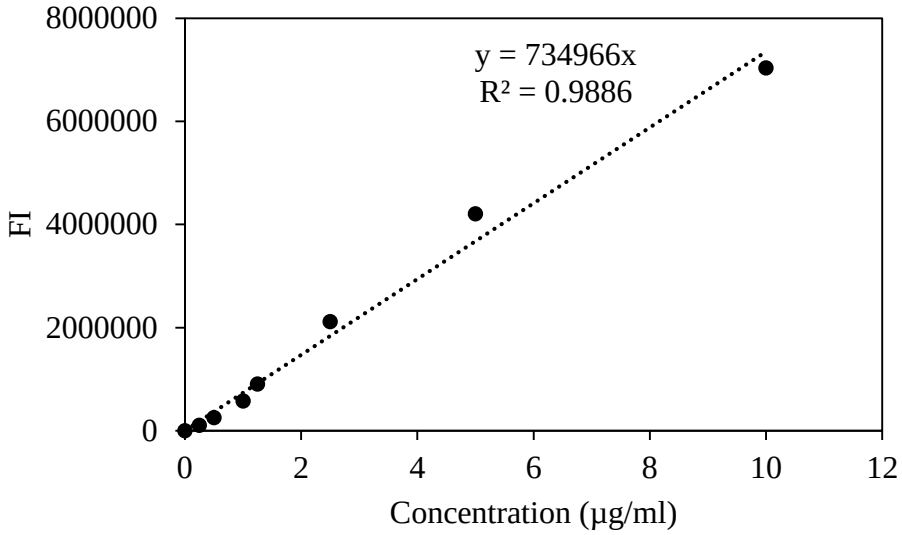

Figure A 1. 4 Calibration curve of DOX constructed with different concentrations of DOX standards prepared in citrate buffer (pH 5.5, 1 M).